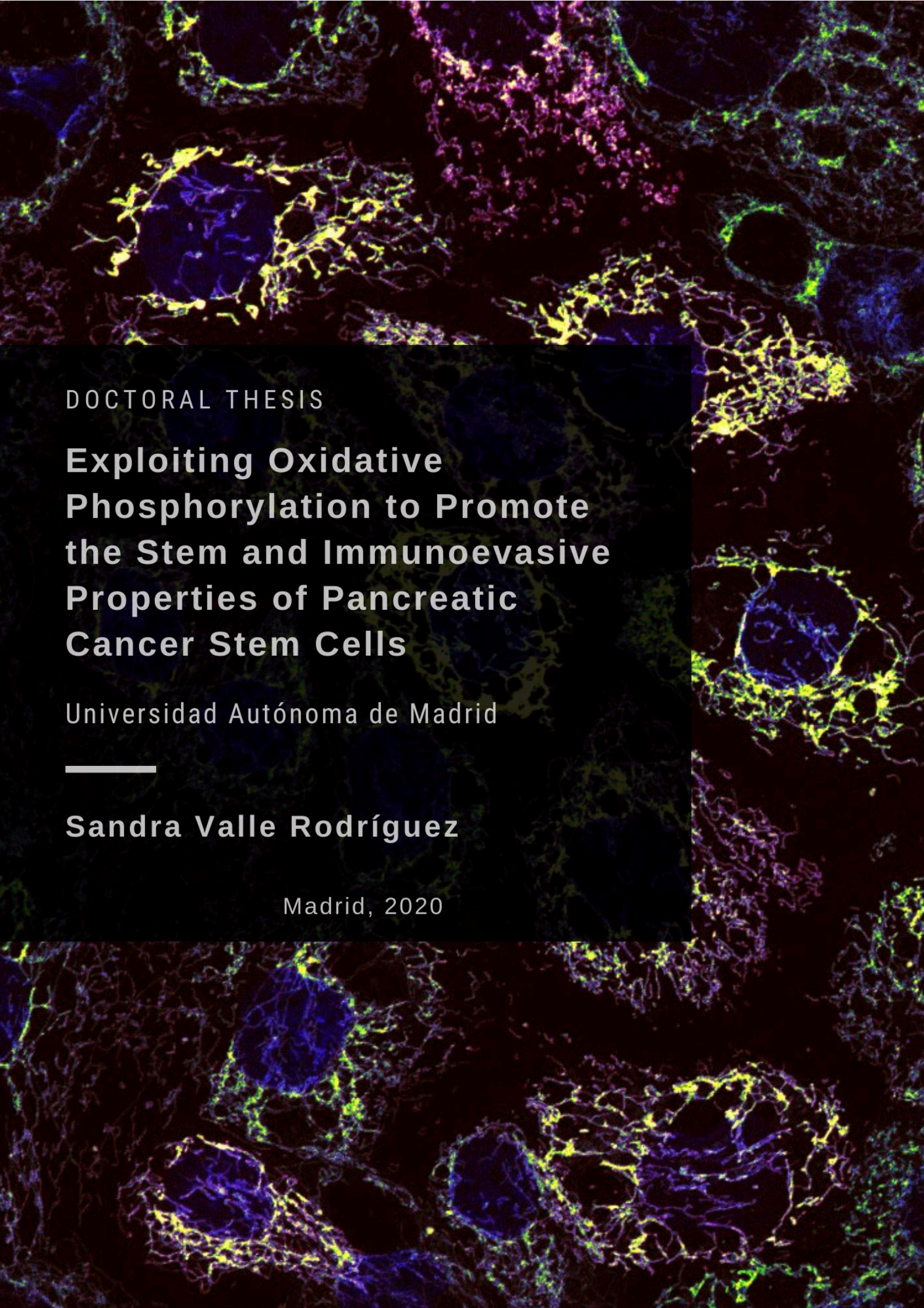

DOCTORAL THESIS

Exploiting Oxidative Phosphorylation to Promote the Stem and Immunoevasive Properties of Pancreatic Cancer Stem Cells

Universidad Autónoma de Madrid

Sandra Valle Rodríguez

Madrid, 2020

Universidad Autónoma de Madrid

Facultad de Medicina – Departamento de Bioquímica

Programa de Doctorado en Biociencias Moleculares

MEMORIA DE TESIS DOCTORAL

Exploiting Oxidative Phosphorylation to Promote Stem and Immunoevasive Properties of Pancreatic Cancer Stem Cells

Sandra Valle Rodríguez

Madrid, 2020




Universidad Autónoma de Madrid

Departamento de Bioquímica

Facultad de Medicina

Instituto de Investigaciones Biomédicas "Alberto Sols"

CSIC-UAM

Exploiting Oxidative Phosphorylation to Promote Stem and Immunoevasive Properties of Pancreatic Cancer Stem Cells

Memoria presentada para optar al título de Doctor por la graduada en Biología

Sandra Valle Rodríguez

dentro del programa de Doctorado en Biociencias Moleculares

Proyecto de Tesis Doctoral dirigido por el

Dr. Bruno Sainz Anding y el Dr. Miguel Ángel Fernández Moreno

y realizado en el Departamento de Bioquímica, Facultad de Medicina

de la Universidad Autónoma de Madrid e Instituto de Investigaciones Biomédicas

"Alberto Sols"

CSIC-UAM

Madrid, diciembre de 2019

Meraki /μεράκι/

Poner el alma, creatividad y pasión en lo que haces,

dejando un pedazo de ti siempre en tu trabajo.

AGRADECIMIENTOS

Quizás una de las cosas más difíciles para mi es lanzarme a escribir en un papel completamente en blanco. Si a esto le sumamos la especial emoción que siento al enfrentarme a este querido y, a la vez, temido apartado, la cosa se complica aún más. Creo que la mayor dificultad viene cuando sabemos que tenemos que poner el broche final a una etapa, lo cuál, a mi me cuesta especialmente. Lo que está claro es, que si he llegado a escribir este final, ha sido gracias a todas y cada una de las personas que han formado parte de mi vida durante estos 4 años. Tan sólo espero que mis palabras estén a la altura de todas ellas.

En primer lugar, me gustaría agradecer a mi director de tesis, Bruno Sainz, la oportunidad que me ha dado para poder desarrollar mi carrera como investigadora en su laboratorio. Gracias por saber ver más allá y no tratarme como un número de expediente, por haber confiado en mi, en mi poder de trabajo, por hacerme más fuerte. Gracias por creer en el proyecto, por enseñarme a hacer buena ciencia y apoyarme profesionalmente durante esta etapa maravillosa de conocimiento, lo cuál hubiese sido imposible sin tu calidad científica. Gracias, de corazón.

Gracias también a mi co-director de tesis Miguel Ángel Fernández, por ser un pilar fundamental de esta investigación, porque sin ti no hubiese sido posible realizar este proyecto. Gracias Miguel por cada meeting, por cada idea, por tu sapiencia metabólica de la que tanto he aprendido. Gracias por cada charleta a horas intempestivas en el parking, por simplemente preguntarme “¿Qué tal vas, niña?”, por tu paciencia y estar siempre disponible a cualquier duda que me surgía y cada golpecito en el moño cuando estaba absorta trabajando en el ordenador. Ha sido un placer trabajar contigo.

Agradecer de igual modo a Patricia Sancho el haberme dado la oportunidad de trabajar en su laboratorio, en el Hospital Miguel Servet de Zaragoza. Gracias por hacerme sentir como en casa tanto tú como Bea, por vuestra generosidad y atención. Ha sido una experiencia que recuerdo con especial cariño y fue en parte gracias a vosotras.

Gracias a todos mis compañeros de laboratorio del B-33 (ahora B-17) Sonia, Diego, Laura, Patri, JC, Lala y Alfonso.

A Sonia, por ser mi maestra Jedi cuando entré en el laboratorio hecha una baby Yoda inexperta, y enseñarme todas las técnicas que conocías. Por tu enorme paciencia, por mostrarnos el camino de la verdadera merienda con horchata y fartons, por ser la artífice de la mejor lista de Spotify jamás creada "Don´t worry, be guapi" y que sonara cada viernes cuando ya las fuerzas nos fallaban. Gracias por todas las risas compartidas y ponerle ritmo de heavy metal a la vida.

A Diego, por ser una de las mejores personas con las que me he cruzado durante estos años. Por cuidarme y preocuparte por mi, por tenderme siempre una mano (o dos) cuando me encontraba realmente desbordada. Por cada abrazo, mensaje o llamada. Por todos esos bollos de Inma que me alegraban el estómago y el corazón, por cada detalle, por saber siempre como sacarme una sonrisa. Gracias por cada consejo y hacerme sentir que puedo ser yo, contigo. Me siento muy afortunada de haber podido trabajar este tiempo juntos.

A Laura (mi Loga) por ser uno de mis apoyos incondicionales en el labo y también fuera de él. Gracias, porque no podría haber tenido una mejor *partner in crime* de tesis que tú. Gracias por ser luz, por compartirla con los demás y no apagar la de nadie, por ser un ejemplo de sororidad y compañerismo. Por tu capacidad de esfuerzo, constancia y trabajo. Por todas las risas (que han sido muchas) y las lágrimas (en las que siempre estabas ahí con tus abrazos curativos). Por enseñarme a bailar juntas bajo la lluvia en vez de esperar a que esta pasase. Por cada chorizo zamorano sorpresa (del duro y del blando, ojo) que hace que un *tapper* de lentejas se convierta en un auténtico manjar de dioses. Por tus increíbles *performances* de Bran Stark cuando el *winter is coming*, por hacerme los coros de diosa del *soul* cuando se apoderaba de nosotras la Whitney o la Aretha, por compartir ambas esa pasión por la comida. Gracias por ayudarme a mantener intacta la poca cordura mental que me quedaba y por todo el cariño y ánimo que me has dado y das. Te quiero, amiga. *Always and forever*.

A Patri por ser un ejemplo de valentía y fortaleza. Por ser una crack de la histología y sus derivadas tinciones. Por tener el don de hacer reír a los demás incluso en los momentos más complicados. Gracias por enseñarme a ver siempre el lado bueno de las cosas y a sonreír pese a todo.

A las nuevas incorporaciones del labo: Lala, JC y Alfonso. Gracias por vuestra ayuda y tenderme una mano sobre todo en estos últimos meses de estrés. Por descubrirme el maravilloso mundo del té desteinado y las respectivas cremitas, las monerías y los stickers de Paquita Salas. Estoy segura de que con vuestro trabajo vais a conseguir todo lo que os propongáis hacer.

A mis excompis de labo: Marta, Lourdes y Marina. Gracias por el tiempo compartido con vosotras porque pese a que por situaciones laborales ya no estemos juntas, sigo guardando una gran amistad con vosotras. A mi Martiña, por tu gran apoyo tanto dentro como fuera del labo, por tu tesón y pasión en todo lo que haces. Por enseñarme a que "las cosas se hacen con *xeito* o no se hacen, *carallo".* A mi Lour, por ser una trabajadora incansable y ofrecerme siempre tu ayuda, incluso cuando tu también estabas hasta arriba de trabajo. Por recordarme que "siempre sale el sol, chipirón" y todas las risas compartidas. A mi Marinain, porque no hay muchas alumnas como tú. Por tu alegría pegadiza y hacer que trabajar en el labo haya sido mucho más fácil.

Me gustaría agradecer también a todas las personas del departamento con las que he tenido la suerte de compartir esta etapa, especialmente a Manu, Raúl, Chema y Adri. Gracias por las charlas en los pasillos, por las reflexiones filosóficas o las listas de reggaeton compartidas en las interminables horas de cultivos, por el tráfico de macrófagos de estraperlo, por venir al labo simplemente para ver como llevaba la tesis o la vida en general, por los ánimos y por los golpecitos en la ventana recordándome que tenía una casa a la que ir. Gracias.

A todos los profesores del departamento con los que he tenido el placer de compartir docencia. Sin lugar a dudas, ha sido una de las experiencias mas enriquecedoras y bonitas de toda esta etapa, lo voy a recordar con especial cariño. Gracias a todos por haberme hecho sentir parte de cada uno de los proyectos, por tratarme como una más y por cada una de las palabras de agradecimiento y afecto. Gracias, de verdad.

Y, como no podría ser menos, me gustaría agradecer al servicio de limpieza de la facultad en especial a Rosi, Cari y Jesús, por ser unas personas maravillosas, profesionales y cercanas. Gracias a mi Rosi de España, por contagiarnos siempre con

su alegría cada vez que venía a nuestro labo, por las innumerables confidencias, por cuidar y preocuparte por “tus niñas” y apreciarnos tanto.

Ya, en el terreno más personal, no puedo dejar de agradecer a mi familia, especialmente a mis padres. Gracias por no condicionarme, por dejarme elegir en libertad y apoyarme en todo aquello que me hace feliz. Por ser un ejemplo de lucha, respeto, fuerza, generosidad y amor incondicional. Gracias mamá, por enseñarme a que sin trabajo no se consigue nada, que todo esfuerzo tiene su recompensa aunque a veces tarde más en llegar, a no rendirme. Por aguantarme cuando estoy inaguantable, por tu enorme paciencia y comprensión. Gracias papá, por tu apoyo, por dar sin esperar, por hacerme saber que siempre puedo contar contigo y por ser mi “Javify” personal sea la hora que sea para llevarme o recogerme de vuelta de un congreso. Os quiero y os lo digo poco.

A mi hermana, por compartir risas y agobios a partes iguales. Por compartir el humor absurdo que solo nosotras entendemos, por sacarnos de quicio mutuamente, por poner música siempre en casa, por ser la dueña del drama y chincharnos para acabar riéndonos antes de dormir. Porque en el fondo no podríamos vivir la una sin la otra.

A mi tío Fali, por su generosidad y estar siempre disponible para arreglarme el cuerpo y sobre todo las cervicales que no me dejaban vivir. Por las infusiones calentitas de esas tuyas que entonan el alma. Gracias.

A mis abuelos, por ser como otros padres para mí. Por ser un ejemplo de humildad y trabajo incansable pese a las dificultades. Gracias por cada abrazo, beso y apretón de manos. Por cada muestra de amor en forma de tortilla de patatas, arroz, cocido, rabo de toro y bizcocho. Gracias abuela por cuidarme y quererme tanto. Gracias abuelo por sentirte siempre tan orgulloso de mi. Por enseñarme que “contra la pereza, diligencia” y que “las cosas se hacen bien o no se hacen”. Por enseñarme a que nunca pierda la curiosidad. Me siento muy afortunada de teneros a mi lado. Os quiero.

A Álvaro porque sin ti no hubiese llegado hasta aquí. Por saber mejor que nadie todo lo que esto ha supuesto, por tu apoyo y ayuda constante, por estar ahí siempre, por ser calma, por creer en mí más de lo que yo lo hago conmigo misma y no dejar que me rinda. Por transformar mis alas. Gracias por ser el mejor compañero de ciencia y vida que podría tener, superar retos a tu lado siempre es más fácil. Te quiero.

A la familia que uno elige, a mis amigos de siempre porque, aunque nos veamos dos veces al año, es como si el tiempo no pasase. A Kevin, Raquel, Ángel, Lucía, Josu, Lander y Marina. Gracias por estar y por todos los buenos momentos compartidos.

A mi Terce, porque a pesar de que nos separen unos cuántos kilómetros siempre podemos contar el uno con el otro. Gracias por hacer más feliz la vida a los demás, por nuestros audios y conversaciones telefónicas interminables, porque siempre sabes como arrancarme una carcajada.

A mis paposos, por compartir esta bonita y sana amistad. A Rober, Javi, Pedro, Laura, Raquel, Pablo, Andrew y Baratas. Gracias por los momentos de cañas y risas, por todo el cariño y apoyo científico que siempre me dais, por querernos como somos.

A mis Maris, Marta, Alva, Ire y Andre, porque no sé que hubiese sido de mí en estos 10 años sin vosotras a mi lado. Gracias por estar siempre que os he necesitado, por estar en las buenas y sobre todo en las malas, por ser más que amigas, por ser hermanas no biológicas. Por ser mi suerte. Por ser esenciales en mi vida, por todo lo que me enseñáis y por no concebir un futuro sin vosotras. Lo sabéis todo. Gracias siempre.

Exploiting Oxidative Phosphorylation to Promote the Stem and Immunoevasive Properties of Pancreatic Cancer Stem Cells

DOCTORAL THESIS **SANDRA VALLE RODRÍGUEZ**
MADRID 2020

SUMMARY / RESUMEN

Pancreatic ductal adenocarcinoma (PDAC), the fourth leading cause of cancer death, has a 5-year survival rate of approximately 9% and is expected to become the second most lethal tumor by the year 2030. These alarming statistics can be attributed to the high metastatic and chemoresistant capacity of this tumor, and the ineffectiveness of conventional therapies to provide long-term progression-free survival (> 5 years). The latter is believed to be due, in large part, to the existence of a "stem"-like subpopulation of cells within the tumor known as cancer stem cells (CSCs), which have inherent plasticity, have been experimentally shown to be the initiators of the primary tumor, are able to evade chemotherapy, remain quiescent and metastasize to distant organs. To better understand the biology and plasticity of pancreatic CSCs, with the ultimate goal of eliminating them, we have initiated studies to dissect these cells at the molecular level.

Metabolic adaptation is believed to be one of the hallmarks of cancer cells. Interestingly, we published that against established dogma, pancreatic CSCs have a metabolism dependent on oxidative mitochondrial phosphorylation (OXPHOS) in contrast to non-CSCs, which depend on glycolytic metabolism (Warburg effect). Using this discovery to our advantage, we have developed a novel 2D *in vitro* system for long term enrichment of pancreatic CSCs that is amenable to drug screening and CSC-specific studies. Specifically, in the presence of galactose we can establish long-term 2D cultures of primary PDX-derived PDAC cultures enriched in PaCSCs. Compared to glucose, ATP yield from galactose is slower. Thus, due to ATP yield differences, non-PaCSCs cannot survive in galactose, while OXPHOS-dependent PaCSCs survive and become enriched. Moreover, under galactose condition, we show that primary PDAC cells are highly plastic, present an enrichment in CSC biomarkers and pluripotency-associated genes, enter into a slow-cycling/quiescent stage, increase mitochondrial networks and OXPHOS activity and are more invasiveness *in vivo*, the latter being due, in part, to the modulation of immune evasion markers, an aspect of PaCSCs biology that has been poorly studied to date.

In summary, this novel cell culture system could be potentially used to screen for novel CSC-specific inhibitors as well as new compounds directed towards cancer cell metabolism, an area of research that is gaining considerable attention, and based on the correlation observed with immune evasion, may synergize with immunotherapeutic approaches for improved and long-lasting antitumor outcomes.

El adenocarcinoma ductal de páncreas (PDAC), la cuarta causa principal de muerte por cáncer, tiene una tasa de supervivencia a 5 años de aproximadamente el 9% y se espera que se convierta en el segundo tumor más letal para el año 2030. Estas alarmantes estadísticas pueden atribuirse a la alta capacidad metastásica y quimiorresistencia de este tumor y la ineficacia de las terapias convencionales, las cuales no proporcionan una supervivencia a largo plazo (> 5 años). Se cree que esto último se debe a la existencia de una subpoblación de células "madre" dentro del tumor conocida como células madre de cáncer (CSCs), las cuales poseen una plasticidad intrínseca, son las iniciadoras del tumor primario, pueden evadir la quimioterapia, permanecer inactivas y metastatizar en órganos distales. Para comprender mejor la biología y la plasticidad de las CSC pancreáticas hemos iniciado estudios para diseccionar estas células a nivel molecular.

Se cree que la adaptación metabólica es una de las características de las células tumorales. En 2015 publicamos que las CSC pancreáticas tienen un metabolismo basado en la fosforilación oxidativa (OXPHOS) en comparación con las no CSCs, que dependen de un metabolismo glucolítico (efecto Warburg). Utilizando como ventaja este descubrimiento, hemos desarrollado un novedoso sistema 2D *in vitro* basado en la utilización de galactosa como fuente de carbono para el enriquecimiento a largo plazo de CSC pancreáticas, lo que nos servirá para el estudio de nuevos fármacos y características específicas de las CSC. En comparación con el uso de glucosa, la obtención de ATP a partir de galactosa es más lento. Por lo tanto, las no PaCSC no pueden sobrevivir en presencia de galactosa como única fuente de carbono, mientras que las PaCSC dependientes de OXPHOS sobreviven y se enriquece su población. Además, en condiciones de galactosa, las células son altamente plásticas, presentan un enriquecimiento en biomarcadores CSC, son más quiescentes, aumentan las redes mitocondriales, la actividad OXPHOS y son más invasivas *in vivo*, esto último debido, en parte, a la modulación de los marcadores de evasión inmune, un aspecto de la biología de las PaCSCs que ha sido poco estudiado hasta la fecha.

En resumen, este nuevo sistema podría usarse potencialmente para detectar nuevos inhibidores de CSC y compuestos dirigidos hacia el metabolismo y la inmuno-evasión de las células tumorales, un área de investigación que está recibiendo una considerable atención actualmente.

Exploiting Oxidative Phosphorylation to Promote the Stem and Immunoevasive Properties of Pancreatic Cancer Stem Cells

DOCTORAL THESIS **SANDRA VALLE RODRÍGUEZ**
MADRID 2020

TABLE OF CONTENT

ABREVIATIONS

ABCG2	ATP-binding casette sub-family G member 2
ADM	Acinar-to-ductal metaplasia
ATP	Adenosine Tri-Phosphate
ATG5	Autophagy related 5
BSA	Bovine Serum Albumin
bFGF	Basic Fibroblast Growth Factor
CAFs	Cancer Associated Fibroblasts
CD133	Prominin-1
CNT	Concentrative nucleoside transporter
CSC	Cancer Stem Cell
CSCs	Cancer Stem Cells
CXCR4	Chemokine receptor type 4
DAPI	4,6-diamidino-2-phenylindole
DilC	1,1′-Dioctadecyl-3,3,3′,3′-tetramethylindocarbocyanine
DKK-1	Dickkopf-related protein 1
DMEM/F12	Dulbecco´s Modified Eagle Medium: Nutrient Mixture F-12
DNA	Deoxyribonucleic acid
DOX	Doxorubicin
dpi	Day(s) post-injection
ECAR	Extracellular Acidification Rate
ECM	Extracellular microenvironment
EDTA	Ethylenediaminetetraacetic acid
ELDA	Extreme limiting dilution assay
ELISA	Enzyme-linked immunosorbent assay
EMT	Epithelial-to-mesenchymal transition
EMP	Epithelial-to-mesenchymal plasticity
EpCAM	Epithelial cell adhesion molecule
ETC	Electron transport chain
FACS	Fluorescent-activated cell sorting
FBS	Fetal bovine serum
Fluo+	Autofluorescent positive
Fluo-	Autofluorescent negative
FSC	Forward Scatter

Gal-CC	Galactose cultured-cells
GAPDH	Glyceraldehyde 3-phosphate dehydrogenase
GEM	Gemcitabine
GEMM	Genetically engineered mouse model
Glu-CC	Glucose cultured-cells
GM-CSF	Granulocyte-macrophage colony-stimulating factor
GnP	nab-paclitaxel plus gemcitabine
hENT	Human equilibrative nucleoside transporter
HRP	Horseradish peroxidase
H2B	Histone 2B
ICAM-1	Intercellular Adhesion Molecule 1
KRAS	V-Ki-ras2 Kirsten rat sarcoma viral oncogene homolog
LAMP-1	Lysosomal-associated membrane protein 1
LC3B I	Microtubule-associated protein light chain 3 B I
LC3B II	Microtubule-associated protein light chain 3 B II
lncRNA	Long non-coding RNAs
MET	Metformin
mRNA	Messenger ribonucleic acid
MTX	Mitoxantrone
mpi	Months post-injection
mtDNA	Mitochondrial Deoxyribonucleic acid
NAC	Neoadjuvant chemotherapy
NFκB	Nuclear factor κB
NK	Natural Killer
NOD-SCID	Non-Obese Diabetic Adenosine Deaminase Deficiency
NRF2	Nuclear factor erythroid 2-related factor 2
OCR	Oxygen Consumption Rate
OS	Overall survival
OXPHOS	Oxidative Phosphorylation
PaCSCs	Pancreatic cancer stem cells
PanIN	Pancreatic Intraepithelial Neoplasia
PBS	Phosphate buffered saline
PBS-T	Tris-buffered saline

PCR	Polymerase chain reaction
PDAC	Pancreatic ductal adenocarcinoma
PDX	Patient-derived xenograft
PGC-1α	Peroxisome proliferator-activated receptor gamma coactivator 1α
P/S	Penicillin/Streptomycin
PVDF	Polyvinylidene difluoride
qPCR	Quantitative polymerase chain reaction
ROS	Reactive oxygen species
RT-qPCR	Quantitative real time polymerase chain reaction
RIPA	Radioimmunoprecipitation assay
RNA	Ribonucleic acid
RPMI	Roswell Park Memorial Institute medium
SDS-PAGE	Sodium dodecyl sulfate polyacrylamide gel electrophoresis
Serpin-E1	Plasminogen activator inhibitor-1
SRC	Spare Respiratory Capacity
SSEA-4	Stage-specific embryonic antigen-4
TAMs	Tumor associated-macrophages
TEM	Transmission electron microscopy
TEM8	Anthrax toxin receptor 1
TFG-β	Transforming growth factor beta
TOM20	Mitochondrial import receptor
WNT	Wingless pathway
YNL	Yellow Nano-lantern
ZEB1	Zinc finger E-box-binding homeobox 1
2DG	2-Deoxy- d-glucose

INTRODUCTION

1. Pancreatic cancer

The pancreas, an essential organ for nutrient metabolism, has both endocrine and exocrine functions. The endocrine pancreas is formed by islets of Langerhans (1-2% of pancreatic mass) and mainly regulates blood sugar levels via insulin production. The exocrine pancreas, in contrast, contains acinar and ductal cells that produces the majority of digestive enzymes and constitutes >90% of the pancreatic mass[1]. Several studies indicate that acinar cells are the main source of pancreatic intraepithelial neoplasias (PanINs). PanIN lesions are characterized by an extensive architectural disorganization, accumulation of genetic alterations and are believed to be the final precursor to pancreatic ductal adenocarcinoma (PDAC) (Figure 1). Likewise, more than 85% of pancreatic cancer cases are diagnosed as PDAC[2,3].

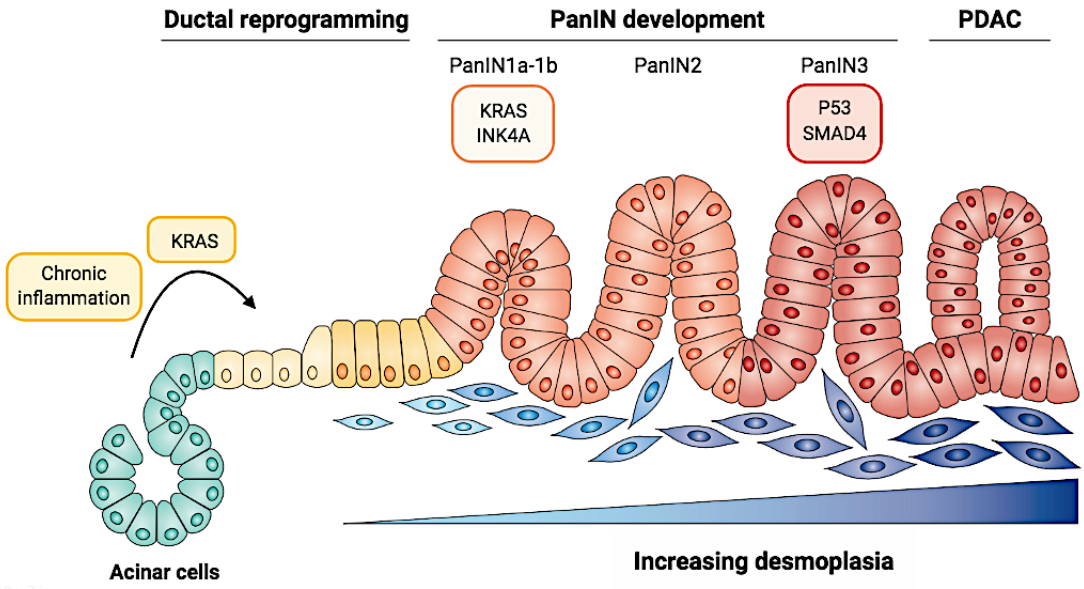

Figure 1. Schematic representation of PDAC development and the different genetic alterations during tumor progression. Pancreatic injury, loss of cell-cell and cell-matrix contacts, loss of polarity, *KRAS* hyperactivity and increased inflammatory signaling can drive acinar cells to undergo dedifferentiation and transdifferentiation to a duct-like phenotype necessary for PDAC development. *Adapted from Morris et al., 2010.*

PDAC is currently the fourth leading cause of cancer-related death in both males and females in developed countries[4]. By 2030, however, it is expected to become the second leading cause of cancer-related death trailing non-small cell lung carcinoma, although its incidence will not increase significantly to surpass the five most common cancers: lung, breast, prostate, colorectal and bladder cancer[5]. These alarming statistics are due to the fact that there are no specific symptoms that can act as predictive indicators of this

disease at an early stage. Likewise, the lack of early biomarkers and sensitive diagnostics only compounds the problem of early detection. As a consequence, the majority of pancreatic cancer patients are diagnosed when the disease is at an advanced stage and has already metastasized to distant secondary organs[3]. CA19-9 is the most common serum biomarker of disease progression used in the clinic; however, it is not recommended for general screening as this marker varies with disease stage, and it is prone to false positives[6]. For this reason, new serological markers complementing CA19-9 are urgently needed in order to detect PDAC at early stages when potentially curable surgical resection is still possible. While molecular markers could provide more specific information for patients, their development and implementation still remain a challenge and in general has been a slow process[7]. Recently, new candidate biomarkers have been identified which could complement CA19-9 for detection of PDAC at earlier stages. Addition of tissue inhibitor matrix metalloproteinase 1 (TIMP1), leucine-rich-alpha-2-glycoprotein1 (LRG1) or thrombospondin-2 (THBS2) to CA19-9 screening has been shown to significantly improve early PDAC tumor detection[8,9].

Pancreatic cancer usually presents in the head of the pancreas and extends through the surrounding tissue and metastasizes to the liver, spleen and peritoneum[10]. In general, PDAC has a slightly higher incidence in men than in women, increases with age (almost 90% of all cases are diagnosed after the age of 55 years) and predominates in certain racial groups[11]. Increased risk is likely due to a combination of both genetic and environmental factors. On the one hand, the most important genetic alteration is in the *RAS* oncogene, which is mutated in 90% of patients. Inactivating mutations in *TP53*, *CDKN2A*, *SMAD4, ARID1A, MLL3* and *TGFBR2* also play important contributing or additive effects (Figure 1). Moreover, while the majority of pancreatic cancer cases are considered as sporadic, it is estimated that approximately 15% of the PDAC cases have a familial component and carry mutations in *BRAC2*, *BRAC1, ATM, STK11, PRSS1, MLH1* and *PALB2*[2]. On the other hand, smoking, for example, has been identified as a clear risk factor, as it has been shown that smokers are up to 3 times more likely to develop pancreatic cancer. In addition, diabetes, obesity and chronic pancreatitis also confer an increased risk for the development of PDAC[12,13]. Current statistics show a progressive increase of new PDAC cases per year. More than 53,000 new cases occur annually and pancreatic cancer continues to cause 41,000 deaths each year[14].

Furthermore, only 9% of patients achieve long-term (> 5 year) survival. Surgical resection seems to be the only potentially curative therapy for patients with PDAC; however, only 15-20% of patients are eligible, and within this subset of patients, only 20% have an overall survival rate of greater than 5 years (mean from 25 to 30 months)[15,16]. Thus, while successful early detection is necessary and has been shown to be a significant contributor in altering both the incidence and death rates in other solid tumors, the fact remains that the vast majority of PDAC patients are diagnosed with advanced-stage non-resectable disease. As such, the current reference treatments 5-fluorouracil [5-FU], gemcitabine, albumin-bound paclitaxel (nab-paclitaxel) plus gemcitabine, or FOLFIRINOX (folinic acid, 5-FU, irinotecan, and oxaliplatin) only prolong the survival of patients (6-12 months), while having essentially no real impact on tumor eradication[17]. Nevertheless, substantial advances achieved in the last two decades with respect to better understanding the biology of pancreatic cancer have shed light on the cellular complexity, makeup and heterogeneity of this disease. Along these lines, it is now universally accepted that PDAC metastasis, chemoresistance, and disease relapse are driven by a subpopulation of highly plastic "stem-like" cells within the tumor known as cancer stem cells (CSCs), and from a clinical perspective, understanding how these cells function and developing inhibitors to eliminate the CSC population should lead to tumor erradication[18,19].

2. Cancer stem cells (CSCs)

Over the years, several models have been proposed to explain the heterogeneity, chemoresistance and aggressiveness of tumors. The two most widely studied models have been the clonal evolution "stochastic" and the CSC "hierarchical" models. While each model is different, we now appreciate that both models are not mutually exclusive, and both can be tied together[20,21]. The main difference between the two models is that the CSC "hierarchical" model proposes that a particular subset of tumor cells, with "stem-like" properties, are the sole drivers of tumor formation[22], metastatic dissemination, chemoresistance, and disease recurrence/relapse[23]. These cells have unlimited self-renewal capacity and can differentiate into all of the cancer cell populations present within the tumor, thus CSCs represent the cell population uniquely responsible for tumor heterogeneity. Tumor heterogeneity is a very complex process and it is still not entirely

understood. Based on the CSC model and assuming that the CSC is an "entity", it is believed that a tumor contains several CSC clones that are genetically and/or epigenetically different. Each different CSC subclone could then give rise to intermediate progenies or transitory/hybrid cells[21] that would drive the expansion of the bulk cancer cells present within the tumor; however, these progenies would lack the stem-like properties inherent to the CSC from which they were derived, such as unlimited self-renewal capacity. At any given time, and based on intratumoral or extrinsic pressures such as nutrient deprivation, hypoxia, or chemotherapy, specific CSC clones can dominate while others can essentially disappear. The existence of silent or undetectable CSC clones was demonstrated by Dieter et al.[24] in an elegant study aimed at tracking tumor-initiating cells (TICs) from human colon cancer tumors and metastases. Using a molecular tracking strategy in which sphere-derived colon cancer cells were infected with lentiviral vectors, the authors were able to amplify, by linear amplification-mediated PCR, clone-specific insertion site fusion sequences in order to trace and detect TICs. Following serial transplantation of cells from primary to tertiary mice, the authors discovered three types of TICs: extensively self-renewing longterm TICs (LT-TICs), tumor transient amplifying cells (T-TACs) and rare delayed contributing TICs (DC-TICs). While LT-TICs possessed long-term self-renewing capacity and were responsible for metastasis formation, T-TACs had limited self-renewal capacity and DC-TICs represented a silent subpopulation of cells that were active during secondary and tertiary transplantation. Thus, while tumor formation and metastases are largely driven by a specific population of TICs, rare delayed TICs also exist and can dominate under specific conditions. On the other hand, if we assume that the CSC is a "state", then daughter or progenitor cells that continue accumulating genetic changes during tumor proliferation or that alter their epigenetic programming via interactions with the tumor microenvironment (TME) could acquire a mutation or epigenetic mark that would confer them CSC characteristics[25], resulting in the generation of a new CSC clone at any given time during the life of the tumor. For the CSC model to function, however, the CSC pool must never be extinguished and functional/biological properties must exist to prevent their loss. Indeed, CSCs have the ability to renew themselves indefinitely via asymmetric and symmetric division. Asymmetric (differentiation) division gives rise to a CSC and a differentiated tumor cell, while symmetric (self-renewal) division gives rise to two identical CSCs. In both cases self-renewal capacity remains intact, which ensures the pool of CSCs and supports the

hierarchical model of tumor cell heterogeneity, with the CSC being the cell solely responsible for the formation of tumors, while non-CSCs (differentiated cancer cells) lack this capacity[26] (Figure 2A). In addition, CSCs possess other properties that ensure their survival, which include inherent resistance to chemotherapeutics, multipotency and the capacity to metastasize[27]. What continues to elude investigators is why this subpopulation of cells possess these unique properties, while non-CSCs do not. The existence of specialized cells with phenotypic plasticity is important during embryogenesis, and to some extent adult stem cells posses this behavior. In cancer, reactivation of specialized embryogenic pathways is observed, and has been shown to drive CSC genesis and tumor formation[28]. Therefore, it is believed that CSCs are epigenetically and metabolically distinct from their non-CSCs and these modifications are necessary to facilitate their phenotypic plasticity[29] (Figure 2B).

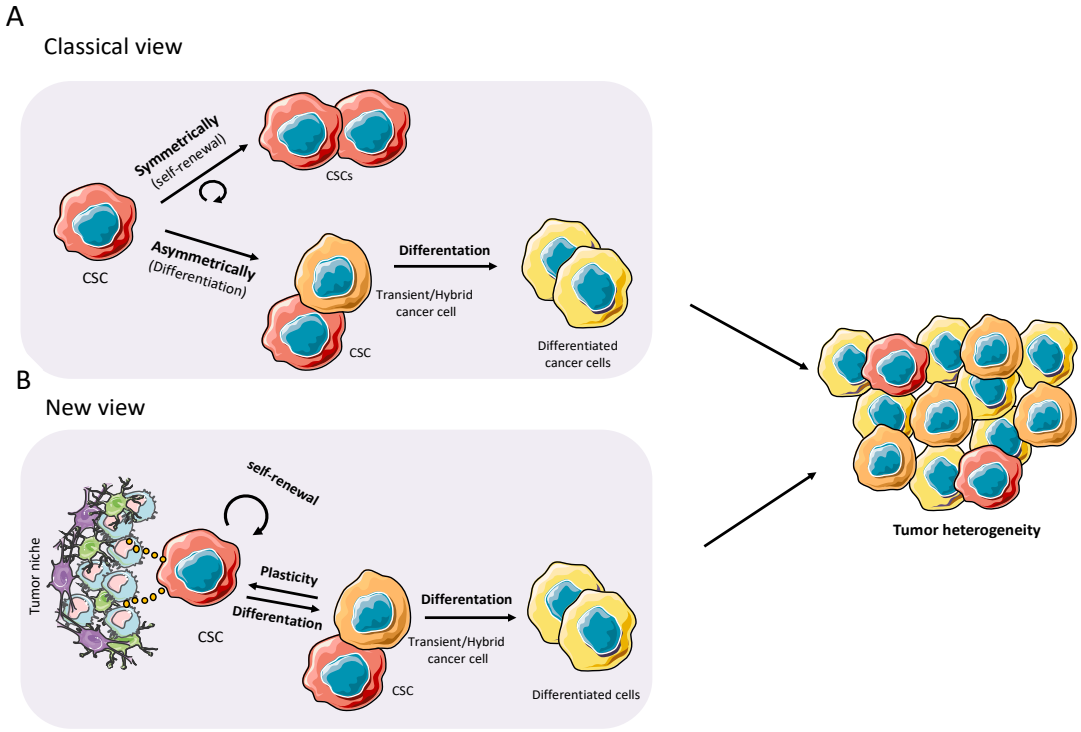

Figure 2. Models of the cancer stem cell concept to explain tumor heterogeneity. (A) Classical view shows the two pathways of CSCs differentiation: symmetrically (self-renewal) resulting in two CSCs and asymmetrically (differentiation) giving rise to a CSCs and a transient/hybrid cancer cell that gives rise to the most differentiated cells. (B) Nowadays, this classical model has suffered some modifications. CSCs receive necessary signals from the tumor niche (tumor microenvironment) modulating the path taken for their division. Due to the plasticity of the transient/hybrid daughter cells, they can also undergo reprogramming into a CSC via signals received from the tumor niche/microenvironment.

In summary, the CSC concept is well accepted and believed to be the best model to understand tumor heterogeneity and plasticity. While first was proposed more than 150 years ago[30], the CSC hypothesis would not be officially accepted until 1994, when Dick

and colleagues formally proved their existence in hematological malignancies thanks to the advent of FACS sorting combined with *in vivo* models of tumor growth in immunodeficient mice[31]. Since then, CSCs have been identified in essentially all solid tumors, including pancreatic cancer[32,33], and their existence has been directly linked to tumor progression, poor prognosis, disease recurrence and metastasis[34]. These cells are dispersed within the tumor mass and represent only a small percentage of the total number of cancer cells present within the tumor[35], making their identification, isolation and study challenging. Nonetheless, it is essential that we further develop methodologies that allow us to distinguish CSCs from other tumor cells in order to develop new therapies that can specifically target and eliminate this cellular subpopulation, and thus prevent tumor recurrence and metastatic disease.

3. Pancreatic CSC (PaCSC) characteristics

Since their discovery in 2007, PaCSCs have been identified, isolated and dissected using a variety of biomarkers. The most widely used strategy for the identification and study of CSCs is based on the use of antibodies directed against certain cell surface antigens such as CD44, TEM8, CD90, CD24, CD133, LGR5, EpCAM, and CXCR4[32,33,36,37]. Other markers have also been used to identify and isolate PaCSCs including aldehyde dehydrogenase (ALDH)[37] and autofluorescence[38]. In 2019, two new markers of PaCSCs were identified: the Anthrax Toxin Receptor 1 (ANTXR1)[39] and CD9[40]. While the use of all of these markers has increased our underlying knowledge of the biology of CSCs and has facilitated the identification of common features across many types of cancer, the molecular mechanisms driving the stem-like state of PaCSCs is still incomplete and requires further investigation. We know that at the molecular level, the PaCSC subpopulation differs from that of non-CSCs, and these differences are present at multiple levels and involve numerous biological aspects, such as genetics, epigenetics, protein modifications and signaling networks. Thus, any biological feature that makes CSCs stand out over the rest of the tumor cells, as well as from normal stem cells, could provide a potential target for either eliminating or disrupting the CSC subpopulations.

3.1. Chemoresistance

It is well known that PaCSCs have a strong and inherent chemoresistant profile. In fact, chemoresistance, together with metastatic potential and relapse, are the main clinical hallmarks of PaCSCs. When discussing the underlying mechanisms of chemoresistance, it is important to distinguish between intrinsic and acquired resistance, as the approach for targeting or disrupting each is different. While intrinsic chemoresistance relies on tumor cell and extracellular matrix interactions, acquired chemoresistance is based on either extrusion of chemotherapeutic agents out of the cells via ATP-dependent transporters or evasion of drug-induced apoptosis and/or drug-detoxifying pathways[41]. Nevertheless, as reviewed in Abdullah and Chow[42], CSCs are able to evade the cytotoxic effects of chemotherapeutic agents via diverse molecular mechanisms, such as the over-expression of ABC transporters, pro-survival B-cell lymphoma-2 (BCL-2) protein family members, ALDH1 isoforms that confer cyclophosphamide resistance, the activation of CSCs-related signaling pathways including Myc, AKT1, Wnt/β-catenin, Notch and Shh, and an enhanced DNA damage response.

ABC transporters, such as ABCG2, are known effectors of chemoresistance across multiple tumor types[43]. Overexpression of these transporters in PaCSCs creates a highly efficient efflux pump system compared to non-CSCs, resulting in prompt elimination of chemotoxic agents. Surprinsingly, ABCG2 localization and activity is not confined only to the plasma membrane. Miranda-Lorenzo et al.[38] discovered the presence of autofluorescent vesicles within the cytoplasm of PaCSCs. The authors were able to establish a direct relationship between the presence of these vesicles in PaCSCs and the maintenance of their stem-like properties, including chemoresistance. These vesicles were shown to accumulate ABCG2-dependent substrates, such as the fluorescent vitamin B2 (riboflavin). Moreover, the authors also showed that these autofluorescent vesicles could accumulate ABCG2-depedent therapeutics, such as mitoxantrone, to avoid apoptotic cell death. This finding provides not only a potential target to modulate CSC chemoresistance, but also a useful biomarker for detection and study of CSCs across different tumor entities. Another typical CSC marker that also functions as a mediator of drug resistance is aldehyde dehydrogenase 1 (ALDH1). While ALDH1 has been used as a CSC marker in several types of solid neoplasms, it has been shown to

mediate cyclophosphamide- as well as gemcitabine-resistance in PDAC[44]. For example, using gemcitabine resistance as a CSC hallmark, Duong et al.[44] showed that ALDH1 silencing reduced cancer cell proliferation and increased their sensitivity to treatment with gemcitabine. ALDH1 and autophagy have aslo recently been associated. A study by Yang et al.[45], demonstrated that the expression of the autophagy factor LC3 in PDAC tissues positively correlated with the PaCSC markers ALDH1, CD44, and CD133. Likewise, they showed that high coexpression of LC3/ALDH1 was associated with survival, and inhibition of autophagy reduced the ALDH1 PaCSC population and their resistance to gemcitabine *in vitro* and *in vivo*.

While we have made little advancements overcoming PDAC chemoresistance in the clinic, new insights into the molecular processes underlying this phenomenon are beginning to emerge as a result of intensive research. What has been discovered is that chemoresistance is much more than the overexpression of drug efflux transporters or the modulation of the cells DNA damage response, but rather many signaling pathways related to the stem-like phenotypes of CSC are also intimately linked to CSC chemoresistance. Such is the case for NFκB, Notch, AKT1, TFG-β or Wnt/β-catenin signaling pathways, all of which are both signaling pathways upregulated in CSCs and pathways that can promote chemoresistance[46–54].

3.2. Epithelial-to-Mesenchymal Transition (EMT), invasiveness and metastasis

EMT is a process whereby epithelial cells undergo numerous biological changes that confer upon them a mesenchymal phenotype. It includes the gain of migratory and invasive capacities, high resistance to apoptosis and increased secretion of extracellular matrix (ECM) components. It is mainly orchestrated by the expression of a battery of transcription factors, including *SNAIL, SLUG, ZEB1* and *TWIST* (reviewed in[55]). EMT is essential for physiological processes like embryogenesis, wound healing and tissue regeneration; however, it is also involved in pathogenic processes such as fibrosis or cancer development. As such, intensive research has focused on elucidating the drivers and molecular mechanisms of this process in cancer, especially in order to understand its role in and relationship with metastasis. In the case of PDAC, the idea that EMT is a driver of PaCSC metastasis has been well accepted for decades. However, in 2015, Zeng et al.[56] showed that *Snail1* and *Twist* deletion in the KPC (*LSL-KrasG12D/+;LSL-*

Trp53R172H/+;Pdx-1-Cre) mouse model of PDAC resulted in a significant decrease in EMT-associated gene expression, a reduction in the expression of the EMT marker αSMA in epithelial cells, and an increase in the expression of the epithelial marker E-cadherin; however, no effect on either metastasis nor invasiveness, two phenotypes strongly associated with EMT, were observed. Interestingly, the authors did discover that *Snail1* and *Twist* are critical for PDAC chemoresistance and cell proliferation. In light of these results, the authors claimed that EMT was dispensable for PDAC metastasis, a revolutionary concept at the time. In 2017, however, Krebbs et al.[57] showed that genetic depletion of *Zeb1* in the same KPC model used by Zheng and colleagues led to a decreased expression of the EMT inducer factors *Zeb2, Slug and Snail*, but not *Twist.* Moreover, *Zeb1* depletion resulted in a more differentiated state of tumor cells and an increased expression of *Gata6*, a marker of differentiation in PDAC[58]. More importantly, *Zeb1* deletion had a significant and negative effect on tumor progression, invasiveness, and metastasis, reaffirming EMT's role in PDAC metastasis. The authors therefore described "tissue-specific roles for EMT transcription factors, that may play non-redundant roles, and must be taken in consideration when dissecting EMT functioning".

EMT has been closely associated with stem-like properties, and in particular to *de novo* CSC-genesis, as it has been shown to induce stem-like properties in different cancers[59–61]. This induction has been intensively studied in breast cancer, and numerous authors have reported the activation of the CSC state via EMT. In contrast, the induction of the CSC state by EMT remains unclear and less defined in PDAC, although some recent studies would suggest a similar link between EMT and stemness, chemoresistance and metastatic capacity[62].

Whereas EMT has classically been considered the cornerstone of metastasis initiation, Mesenchymal to Epithelial Transition (MET) has been described as crucial for seeding stages. Recent studies demonstrate the existence of a hybrid epithelial/mesenchymal phenotype in cells transitioning between EMT and MET, that involves mixed epithelial and mesenchymal features (e.g. adhesiveness and motility). This phenotype seems to be linked to drug resistance and tumor-initiating potential; moreover, it allows tumor cells to collectively migrate in clusters to form metastases in a more effective way than pure EMT single cells[63]. Thus, our concept of EMT and MET as binary processes has changed, and EMT appears now as a continuum or spectrum that comprises different stages between

the pure epithelial and mesenchymal states[64]. In fact, many groups now refer to cells as epithelial (E), intermediate epithelial (iE), hybrid E/M, intermediate mesenchymal (iM) and mesenchymal (M). This new paradigm has enabled us to better understand the complex dynamics of the metastatic processes, and the recognition of the described hybrid E/M state and its properties will surely lead to a better conceptual dissection of the stages and development of metastasis. It seems clear that the tumor circulating cells (CTCs), present in the bloodstream and that mediate metastasis, should have EMT and tumor-initiating properties (i.e. CSCs traits that would allow them to successfully metastatize and rebuild the original tumor at secondary distant sites). Thus, it is not surprising to find a highly metastatic CSC sub-compartment within the CTC population[65–67] with E/M hybrid properties that set them apart from other CTCs[68].

Lastly, while the tumor itself can regulate the drivers and determinants of EMT and stem-like phenotypes, the tumor microenvironment (TME) also constitutes an important critical factor, providing cues to the CSC subpopulation to upregulate EMT and stemness. Sainz et al.[69,70], discovered a positive feedback loop by which tumor associated macrophages (TAMs) secrete free ISG15, which in turn mediates the reinforcement of the stemness, EMT phenotype and migratory capacity of PaCSCs. These changes were reflected in elevated mRNA levels of the pluripotency-associated genes *KLF4*, *SOX2* and *NANOG*, modulation of EMT-related genes including E-cadherin (*CDH1*), *ZEB1* and VIMENTIN, increased mobility assessed in migration assays, and activation of pERK1/2, involved in cell survival. In turn, CSCs were found to secrete IFNβ, inducing further expression of ISG15 by TAMs, as well as TGF-β1, Nodal and Activin that polarize macrophages towards a pro-tumor M2-like phenotype.

3.3. Plasticity

During the development of adult life, there are cellular subpopulations that have the capacity to differentiate/transition into multiple lineages, which is termed “phenotypic plasticity”. While this feature is essential during embryogenesis, it is limited in adult stem cells but can be reactivated in specific tissues such as the liver, pancreas and colon as a way of maintaining or repairing the organ. Likewise, in cancer, tumor cells reactivate plasticity as a mechanism to boost tumor progression[29]. Our understanding of normal cellular plasticity has grown over the past two decades. We now appreciate that daughter

cells, progenitor cells, transient cells and even differentiated cells can re-enter the linear and hierarchical process of cellular differentiation when necessary. This ability to re-enter what was believed to be a static uni-directional process of differentiation is known as cellular plasticity. For example, upon liver damage, terminally differentiated hepatocytes can re-enter the cell cycle to replace lost hepatocytes or liver tissue without becoming full-fledged stem cells[71]. Acinar cells of the pancreas also have the ability to transdifferentiate. Reddy et al.[72], in 1984 and Dabeva et al.[73], in 1995 showed that foci of hepatic cells can appear in the pancreas of rats treated with ciprofibrate, a peroxisome proliferator, or exposed to a low-copper diet, respectively. We now recognize that acinar cells are extremely plastic and can undergo EMT and transdifferentiate into ductal, endocrine and even adipocytes depending on specific signals and/or microenvironmental cues[74,75]. Thus, as a whole, plasticity may be more common and much more important than previously appreciated.

In the context of cancer, it is believed that the CSC is the main source of phenotypic plasticity within a tumor, and CSC phenotypic plasticity allows for the regeneration of each cellular phenotype and subtype found within the tumor[76]. For example, within identical genetic clones we can find different CSCs that differ at the phenotypic and epigenetic levels and can give rise to multiple different subpopulations within a single tumor[77,78]. Non-CSCs, such as transient cells, likely also have a certain degree of cellular plasticity and can also contribute to tumor cell and CSC "regeneration" through a differentiation process allowing them to regain a certain level of "stem cell status" (**Figure 3A**). These partially differentiated transient subpopulations that retain some stem cell characteristics are more likely to act as the cells that regenerate more undifferentiated stem cell subpopulations, rather than terminally differentiated cancer cells; however, whether terminally differentiated cancer cells have no cellular plasticity is still under debate. Nevertheless, the concept that the CSC subpopulation can be replenished by non-CSCs was experimentally proven in two recent studies targeting the $Lgr5^+$ CSC population in colon cancer organoid cultures. Specifically, Shimokawa et al.[79], eliminated the $LGR5^+$ CSC population in organoids of human colorectal cancer by inserting an inducible version of the suicide-gene caspase 9 (iCasp9) into the *LGR5* locus. Upon induction, the growth of xenografts derived from the implanted organoids was reduced. In a genetically engineered mouse model approach, Melo et al.[80] used mouse organoid

cultures engineered to express the diphtheria-toxin (DT) receptor in LGR5$^+$ cells. Upon treatment with DT, organoid-derived tumor growth was halted in a syngeneic mouse system. In both studies, however,tumors regrew and the LGR5$^+$ population re-emerged, upon removal of the inducer or DT, indicative of cellular plasticity driven by a non-CSC (or quiescent CSC) transient population.

Apart from transdifferentiation, we also appreciate and understand that cancer cell plasticity encompasses many other biological processes. For example, the capacity of a cell to alter its metabolism, resist chemotherapeutic insults and even evade the immune system by upregulating immune evasion receptors or checkpoint inhibitors can each be considered a type of cellular plasticity (**Figure 3B-C**). One of the most well-studied types of phenotypic plasticity is EMT, described above and in references[81,82]. As mentioned earlier, recent studies have broadened the concept of phenotypic plasticity by suggesting that in cancer there is a direct link between plasticity, stemness and EMT[83,84], demonstrating that cancer cells exist across a spectrum of E to M states, such as a hybrid EMT phenotype/state[84] with high phenotypic plasticity and stem cell-like properties. Thus, the idea that EMT transcription factors function predominantly to promote invasion, migration and dissemination is perhaps an archaic concept that should be reevaluated, particularly in the context of cancer. A plethora of recent studies demonstrate that EMT transcription factors affect many biological processes, including therapeutic resistance and metabolism, and it has also been shown that the EMT hybrid phenotype can act as an indicator of poor prognosis in different tumor types[85]. As mentioned above, in 2015 two independent studies challenged the idea that EMT is necessary for metastasis. Zheng et al.[56] showed that genetic elimination of the EMT transcription factors *Twist1* and *Snail1* in mouse models of PDAC had no effect on metastasis to secondary organs, but were critical for chemoresistance. Thus, EMT was determined to be dispensable for metastasis but necessary for chemoresistance.

Plasticity also plays a very important role in the process of MET. Once at the metastatic site, plasticity allows for restoration of the cellular heterogeneity and epithelial characteristics of the primary tumor[86]. Thus, regarding EMT and plasticity, the regeneration of CSCs from non-CSCs may occur more frequently than previously thought, and EMT transcription factors likely play a very important role in this interconversion. Of course, this transition severely hinders the study and isolation of these

highly plastic CSCs as their presence within a tissue and phenotypic profile are surely susceptible to environmental stimuli and may differ at any given time during the evolution of the tumor; however, new methodologies that use specific signaling mechanisms to enrich for and maintain these plastic cells in culture[87] may prove very useful for dissecting the underlying drivers of their plasticity and for therapeutic screening in drug discovery platforms.

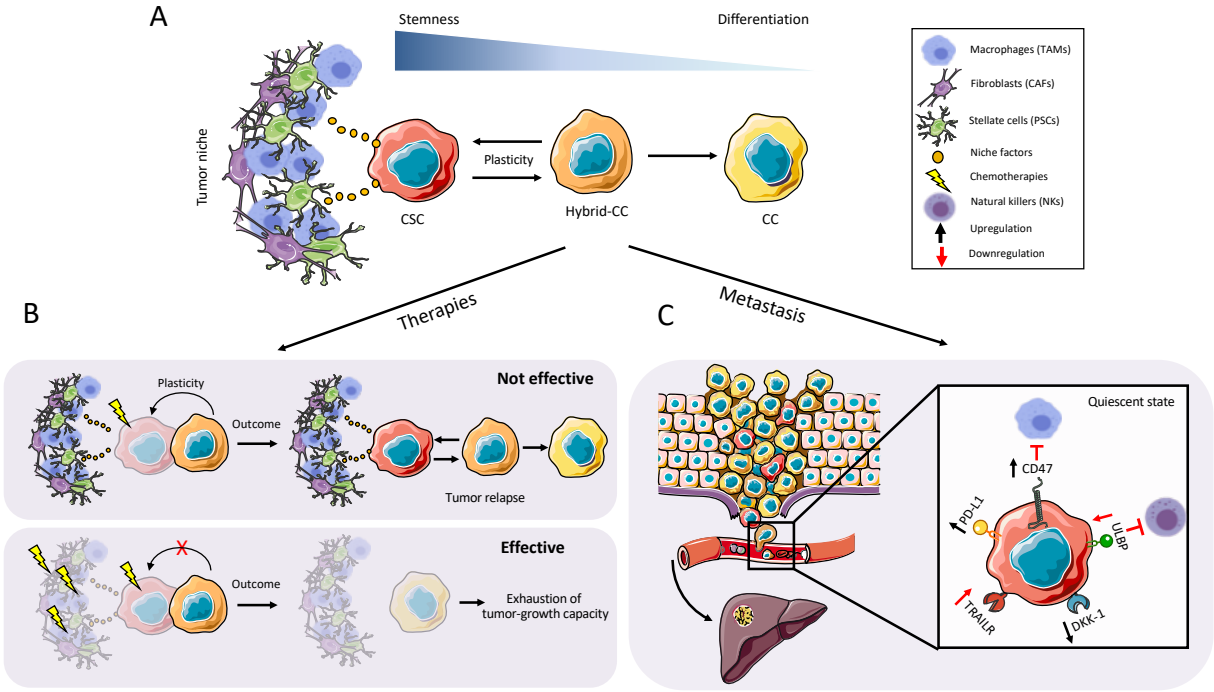

Figure 3. Redefining the roles of pancreatic cancer cells. (A) CSCs receive stimuli from the tumor niche that can influence the biology and overall status of the tumor as a whole and help CSCs maintain their stemness. In turn, CSCs can enter into an intermediate state of differentiation in which they maintain some of their stem capacity and express typical markers of differentiated tumor cells. (B) Hybrid cancer cells are able to survive under certain conditions and to regenerate tumor heterogeneity under therapeutic insult. For this reason, if combination therapies with anti-CSC/anti-tumor niche/anti-hybrid cell efficacy are used, it would be possible to eradicate the tumor in a more effective way. (C) Moreover, quiescent cancer cells are able to survive in the bloodstream and metastasize due to upregulation of immune evasion receptors/ligands (PDL-1, CD47, DKK-1) and downregulation of death receptors/ligands (TRAILR and ULBP) and enter into an immunoevasion state.

In addition, some CSC subpopulations with phenotypic plasticity may be found in a quiescence stage, that is, in a relatively inactive state[88] until they are required to rebuild into the primary tumor, or establish the secondary tumor after the metastatic process (Figure 3C). During this period, these cells can evade anti-tumor therapies or even the immune system. The ability to adopt a resting or quiescent state is a hallmark of plastic CSCs and is often responsible for disease relapse years after successful surgical intervention or tumor free survival. Thus, the identification of dormant tumor initiating cells

(DC-TICs) by Dieter et al.[24] may have actually been the identification of plastic resting CSCs. Likewise, Rhim et al.[89] showed in a mouse model of PDAC that tagged PDAC cells invaded and entered the bloodstream before tumorigenesis, and these cells exhibited EMT and stem cell properties, suggesting that quiescent plastic CSCs are already present but are resting/latent during early stages of disease development. Of course, in order to survive, these cells must also evade the immune system.

To link immune cell evasion and CSC plasticity, Malladi et al.[90] showed that "latency competent" CSCs with an inherent ability to form secondary tumors reduce the regulation of natural killer (NK) cell activator molecules when they transition into a quiescent state, through a mechanism involving autocrine inhibition of Wnt/β-catenin signaling by DKK-1, thus avoiding death by cytolysis[90]. Thus, not only do CSCs use cellular plasticity to regulate their cell proliferation to surive in a latent state for long periods of time or to evade chemotherapeutics that target proliferating cells, but they can also regulate the expression of immune evasion receptors to avoid immune cell killing and elimination. It is still to be determined the extent to which PaCSCs also possess immune cell evasion plasticity. It was recently shown by Cioffi et al.[91] that PaCSCs upregulate the macrophage "don't-eat-me signal" CD47, which affords PaCSCs protection from macrophage-mediated phagocytosis. Whether PaCSCs can also regulate the expression of T-cell checkpoint inhibitors or NK cells ligands or interacting receptors still remains to be fully elucidated. Nonetheless, not only have plastic CSCs become a very attractive target for cancer therapy, but also their presence and state within the tumor may one day be informative when evaluating patient prognosis[87].

3.4. CSC autophagy and metabolism

PDAC is characterized by a nutrient-poor and highly hypoxic microenvironment[92]. The lack of oxygen and carbon sources, such as glucose and glutamine, creates an inhospitable environment where the available supplies are incapable of covering the requirements of the tumor cells. As such, PDAC cells and PaCSCs need to adapt to their environment by activating pathways that make them resistant to these environmental challenges[93]. For example, reduction of oxygen causes stabilization of the transcription factor hypoxia-inducible factor (HIF-1)[94], which leads to tumor cells overcoming oxygen and nutrient deprivation[95,96]. In fact, HIF-1 has been shown to suppress pyruvate

dehydrogenase activity, redirecting glucose into glycolysis rather than the TCA cycle to more rapidly meet the energy requirements of the cell[97]. At the same time, hypoxia has been shown to induce a stem phenotype in many different cancers via diverse mechanisms[98–100], including activation of autophagy[101]. Autophagy is an adaptive catabolic process commonly activated in cells that enter into a resting and/or non-dividing state as a consequence of different environmental stressors such as lack of nutrients, depletion of growth factors and hypoxia[102]. In cancer, deregulated autophagy has been shown to be necessary and its inhibition can affect tumor growth and progression in different tumor types, including PDAC[103]. Autophagy mediates the recycling of the cell's own components and, therefore, provides the cell with nutrients[104] due to the formation of autophagosomes, vesicles with a double membrane that engulf intra-cellular cargo, such as protein aggregates, organelles and ribosomes, and eventually fuse with the lysosome to promote the degradation of the cargo and reuse of the broken down products[102]. Signaling of autophagy is mediated by the expression of *BECLIN1*, *ATG5* and conversion of the LC3B-I protein to LC3B-II[105]. LC3 processing results in its insertion into the extending phagophore membrane facilitating the engulfment of selective targets for degradation, followed by autophagosome:lysosome fusion and proteolytic degradation of the engulfed cargo.

Importantly, in PDAC, high levels of autophagy correlates with poor prognosis[106] and autophagy has been shown to be important for many aspects of CSCs biology, including survival, quiescence and EMT[107]. Compared to non-CSCs, CSCs contain more autophagic vesicles and express more genes related to autophagy[108]. Thus, CSCs have been reported to be in a continuous and active autophagic state and inhibition of autophagy can severely impair CSCs. For example, Yang et al.[45], showed a high correlation between autophagy and PaCSC biomarkers such as ALDH-1, CD44 and CD133 in tissues. When they blocked autophagy, they saw an important reduction in the PaCSC population suggesting that autophagy is essential for the maintenance of PaCSCs. In addition, Zhu et al.[109] described that increased autophagic flux is associated with a high expression of HIF-1 and the interaction of both factors results in a dynamic equilibrium between CSCs and non-CSCs.

Moreover, basal levels of autophagy have been shown to be necessary to maintain the pluripotency of CSCs and that this process is regulated by *NAMPT* (limiting enzyme

in the NAD^+ synthesis pathway) and the transcription factor *POU5F /OCT4*. Elimination of *NAMPT* and *POU5F1* causes a decrease in the expression of pluripotency-associated genes and upregulates markers of differentiation. Interestingly, the regulatory effects of *NAMPT* and *POU5F1* on pluripotency are accompanied by different levels of autophagy. Most importantly, any deviation from the autophagic "baseline", either increasing or decreasing, strongly impairs CSC pluripotency and promotes differentiation and/or senescence of CSCs[110]. Taken together, these results reveal a link between the NAD^+ biosynthesis pathway, the POU5F1 transcription factor and pluripotency, as well as identify autophagy as a new regulator of CSC pluripotency[111].

Apart from autophagy, under adverse and hypoxic microenvironmental conditions, metabolic reprogramming can also occur. Metabolic adaptation is believed to be one of the hallmarks of cancer cells. However, the cellular heterogeneity present in different tumors is important to highlight that different phenotypes such as hypoxic versus normoxic or quiescent versus proliferative will have different metabolic requirements, which in turn may result in different responses to metabolic therapies. Tumor cells are capable of having higher metabolic rates than their normal counterparts, utilizing glucose, glutamine, several amino acids and even fatty acids as substrates[112] (Figure 4). Thanks to their metabolic plasticity cancer cells quickly adapt to the challenges posed by the microenvironment reciprocally contributing to the heterogenous cellular metabolic landscape of the tumor niche.

Glucose is an essential nutrient for cancer cells. While cancer cells increase glucose metabolism through glycolysis (Warburg effect) to meet their energy requirements, glycolysis may not fully cover the metabolic needs of pancreatic tumors due to its low energetic efficiency. In fact, mutations in the *KRAS* gene have been shown to lead to a distinct metabolic program in PDAC cancer cells characterized by increased glycolytic flow, providing tumor cells with proliferative substrates and a sufficient energy supply. In situations where this increase in metabolic rate cannot be effective, the cell requires an adequate mitochondrial function for the energy supply necessary for its survival[113]. In this sense, CSCs seem to adapt their metabolism to microenvironmental changes by conveniently shifting energy production from one pathway to another, or by acquiring intermediate metabolic phenotypes. Despite recent efforts to unravel the metabolic characteristics of pancreatic tumors, little is known about the metabolic phenotype of

PaCSCs. Recently, Sancho et al.[114], observed that unlike their differentiated cellular progeny, PaCSCs are highly dependent on mitochondrial oxidative phosphorylation (OXPHOS). The OXPHOS system (four complexes of the Respiratory Chain and the ATP synthase or Complex V) constitutes the main source of energy in differentiated cells in adult tissues[115], and interestingly this pathway seems to be the preferred mechanism for energy production in CSCs in various types of tumors, including PDAC[116]. This dependence is mediated by the *PGC-1α* transcription factor, which plays an important role in cellular metabolism energy regulation. In turn, *PGC-1α* is regulated by the expression of the *c-MYC* oncogene, which is expressed at low to undetectable levels in PaCSCs[114] (Figure 4).

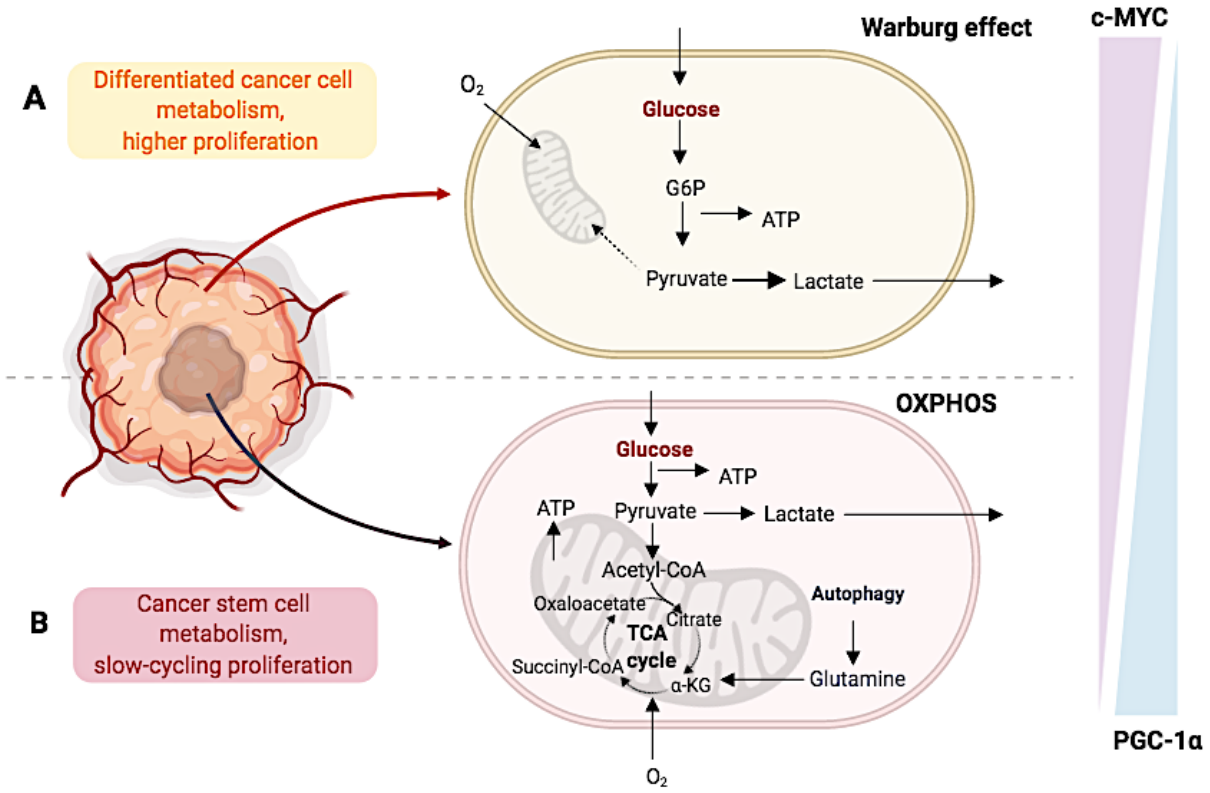

Figure 4. Metabolic profiles between different tumor cell populations within PDAC. (A) Differentiated tumor cells (non-CSCs) rely on the Warburg effect (aerobic glycolysis) for obtaining energy. (B) CSCs have a mitochondrial oxidative phosphorylation-dependent (OXPHOS) phenotype for obtaining energy. These metabolic differences are controlled by the transcription factor PGC-1α, which is negatively regulated by the expression of c-MYC in PDAC.

Although the OXPHOS system involves a significantly greater number of biochemical reactions, it is almost 20 times more efficient in terms of generation of ATP per unit of glucose. It is hypothesized that the dependence of PaCSCs on OXPHOS may reflect an adaptation of these cells to the nutrient-poor microenvironment of pancreatic tumors[108]. Moreover, CSCs, which base their metabolism on OXPHOS, have increased

mitochondrial mass and membrane potential, and higher mitochondrial ROS, all of which may confer upon PaCSC a more invasive and metastatic potential. Since CSCs are virtually dependent on OXPHOS function, mitochondria may be an excellent target for therapeutic purposes. In fact, several investigations have achieved a greater sensitivity to different chemotherapeutics if they are combined with mitochondrial inhibitors such as metformin[117]. This combination approach is important, as using mitochondrial inhibitors such as metformin alone can lead to resistance driven by inherent CSC metabolic plasticity adaptation processes[114]. Interestingly, Krebs et al.[118] also showed that *Zeb1* is involved in the metabolic plasticity of PDAC cells derived from KPC mice. While the levels of *Zeb1* specifically in PaCSCs were not analyzed, this multifunctional EMT transcription may also be involved in PaCSCs OXPHOS.

4. Tumor microenvironment of PDAC

Cancer cells represent a minority of the total PDAC tumor mass (5-10%). The rest of the tumor is formed by other cellular and non-cellular components of great relevance that make up the tumor microenvironment and that are key for tumor development. One of the main defining characteristics of PDAC is its desmoplastic microenvironment, which is composed of a very dense fibrotic and collagen-rich stroma. In fact, approximately 90% of the whole PDAC tumor mass is composed of stromal cells / components. Moreover, PDAC is known to create an immune-suppressive microenvironment that results in immune evasion from the host's antitumor immune system, leading to rapid cancer progression. Recent studies have shown that the tumor microenvironment of pancreatic cancer, including cancer-associated fibroblasts (CAFs), stellate cells, extracellular matrix (ECM), various immune cell types, and cytokines released by these cells, participates in controlling tumor growth, invasion, and metastasis via a dynamic crosstalk with cancer cells[119–121]. All these components fulfill different roles within the tumor and could confer chemoresistance in PDAC[122,123].

The extracellular matrix consists of a variety of materials such as collagen, integrin, laminin, fibronectin, glycosaminoglycan and matrix metalloproteinase (MMP). When the dysregulation of integrin subunits occurs in the basement membrane in pancreatic cancer tissue, PDAC tumor cells can escape and start invading surrounding organs[124].

CAFs are a major component of the PDAC stroma, derived from different kinds of progenitor cells such as fibroblasts, pancreatic stellate cells, and epithelial, endothelial, and mesenchymal stem cells[121]. CAFs are activated by TGF-β, a cytokine that regulates tumor growth, differentiation, and immune cell function and plays an important tumor-suppressive role, but enhances tumor growth as cancer progresses. Specific to the stroma, TGF-β can enhance the ability of CAFs to form abundant filopodia, which allows CAFs to migrate into cancer cell nests and are stimulated by C-C motif chemokine ligand 2 (CCL2)[125–127]. In the context of tumor development, CAFs induce desmoplasia through the secretion of collagen types I and III, fibronectin, proteoglycans and glycosaminoglycans, leading to increased mechanical pressure in the extracellular matrix, which may promote cancer-cell migration, invasion, angiogenesis, and metastasis[124].

Importantly, myeloid cells are the main immune cell type found in the PDAC stroma. The most important myeloid cells within the tumor are tumor-associated macrophages (TAMs), which have diverse immunosuppresive and pro-tumorigenic functions. For example, TAMs can contribute to local immunosuppression limiting $CD8^+$ T-cell activation and proliferation thanks to the production of ROS and nitric which modified T-cell receptor[128]. In addition, TAMs are able to secrete glycoproteins that help to stimulate CAFs migration, facilitating successful PDAC cell metastasis[129]. At the functional level, TAM-secreted growth factors, chemokines and cytokines (IL-17, IL-6, IL-8, TNFα, TGF-β) can also orchestrate numerous events critical for tumor progression and metastasis[130]. Specific to PDAC, TAM-secreted peptides can activate pancreatic CSCs, promoting tumor growth, EMT and metastasis[69,131]. Likewise, recent evidence now also implicates TAMs as critical players in tumor cell chemoresistance[132–136] and CTC dissemination[137,138].

In contrast to the location of the other cells that make up the TME, T-cell populations are found at the periphery of the tumor and within the tumor niche. Likewise, a recent study showed that the infiltration of $CD4^+$ and $CD8^+$ T-cells conferred a survival advantage for PDAC patients compared to PDAC patients who did not present T-cell infiltration[139]. The reason why T-cells are found to a lesser extent inside the PDAC tumor is uncertain. It may be that T-cells are excluded from tumors due to the extensive fibrotic stroma that may act as a physical barrier, or because of an early established immunosuppressive microenvironment that impedes their entry[140]. PD-L1 is the main ligand for PD-1, which is crucial for suppressing T-cell proliferation, migration and secretion of cytotoxic mediators,

and thus blocks the antitumor immune responses by binding to PD-1. Several studies have evaluated the expression of PD-L1 on the surface of tumor cells, suggesting that high PD-L1 expression correlates to poor prognosis in PDAC[141–144], as has been seen in other tumor types.

Due to the relevance of the different cells that make up PDAC, the relationship between PaCSCs and stromal cells could be important in processes such as tumor development and metastasis. In this sense, it has been suggested that CSCs can evade immune detection and immune cell-mediated elimination[145]. CSC immune-suppressive mechanisms are critical for CSCs to evade immune cell elimination, inevitably promoting the expansion of pro-tumorigenic immune cells (e.g. TAMs), which in turn regulate CSC maintenance and differentiation to sustain tumor establishment, growth and metastasis[145,146]. Moreover, accumulating evidence indicates that T-cell and NK cell activation co-stimulatory molecules are expressed at low levels, whereas T-cell and macrophages inhibitory molecules including PD-L1 and CD47, respectively, are expressed at high levels on CSCs[147,148]. While these studies highlight the urgent need to understand the interplay between CSCs and the immune system, this interaction is complex and is only partially deciphered in PDAC to date. In fact, even though immunotherapy has revolutionized cancer treatment, PDAC does not respond to immune checkpoint blockade. This may be due to a low mutations burden, the inherent immune-evasive profile of CSCs, with a subsequent paucity in T-cell infiltration and the development of an immune-supressive tumor microenvironment[149,150].

In conclusion, in order to advance our understanding of the biology of CSCs and to develop new CSC-centered clinical treatments, it is necessary to expand the study on the response of CSCs to therapies in the context of their niche, the inherent plasticity and chemoresistance of CSCs, process related to autophagy, EMT and quiescence/slow-proliferation and their metabolism. All of these characteristics are complementary and thus cannot be studied separately since they are all necessary to understand what CSCs truly are. Therefore, the complete study of all these characteristics would undoubtedly help to effectively eliminate the CSC subpopulation and improve therapies against PDAC.

HYPOTHESIS & OBJECTIVES

Considering that inherent PDAC properties such as aggressiveness, chemoresistance and metastasis are believed to be due, in large part, to the existence of a "stem"-like subpopulation of cells within the tumor known as cancer stem cells (CSCs), and taking advantage of the metabolic profile differences found between PaCSCs and differentiated non-PaCSCs (i.e. OXPHOS versus glycolysis, respectively), the starting hypothesis on which the present doctoral thesis has been developed is the following:

PaCSCs can be efficiently isolated and studied by exploiting their metabolic requirements and limitations. Thus, the culture of PDAC cells under conditions that require mitochondrial metabolism (e.g. OXPHOS) will allow for a sustained enrichment in OXPHOS-dependent PaCSCs, which we propose to use as a platform to better understand the biology and plasticity of PaCSCs, with the ultimate goal of identifying new potential therapeutic targets to eliminate these cells.

Based on this hypothesis, the main objective of this doctoral thesis was to establish a long-term culture enriched in OXPHOS-dependent PaCSCs that would lend itself to evaluating different molecular and biological features related to the stem properties of CSCs, including plasticity, EMT, tumorigenesis, metabolism and immune evasion. In order to achieve this general objective, the following specific objectives were proposed:

1. Evaluate the metabolic profile, specifically the mitochondrial state, of PaCSC and non-PaCSC populations derived from patient-derived xenograft models.
2. Establish an optimal *in vitro* culture system for the long-term enrichment and maintenance of OXPHOS-dependent PaCSCs by modulating the carbon source available *in vitro* (glucose versus galactose).
3. Assess the biological and physiological relevance of the aforementioned culture system by analyzing key phenotypes, different markers, receptors and pathways related to stem hallmarks/properties, including:
    a. Stemness
    b. Mitochondrial metabolism (OXPHOS)
    c. Autophagy
    d. Cell cycle and quiescence
    e. Chemoresistance
    f. Immunoevasion and metastasis

MATERIALS & METHODS

1. Cell culture

1.1. Primary Human PDAC culture cells

During this research work, four primary cell cultures established from Patient-Derived Xenografts (PDX) provided by the research group of Dr. Manuel Hidalgo under a Material Transfer Agreement with the Spanish National Cancer Centre (CNIO), Madrid, Spain (Reference number. I409181220BSMH). The four primary PDX cultures established (PANC185, PANC185scd-single cell derived-, PANCA6L and PACN286) have been previously described (ref). Briefly, for their establishment, PDX-derived tumor tissue fragments were minced, enzymatically digested with collagenase (STEMCELL Technologies, Vancouver, Canada) for 60 minutes at 37°C, and after centrifugation for 5 minutes at 1,200 rpm the pellets were resuspended and cultured in RPMI 1640 medium (Gibco, Thermo Fisher Scientific, Waltham, Massachusetts, USA), 10% fetal bovine serum (FBS), and 50 units/ ml penicillin/streptomycin. From this moment on, the cells were kept in culture at a temperature of 37°C in an atmosphere with 5% of CO_2 and 90% of relative humidity.

For the maintenance of cell stocks, cells were seeded in 75 cm^2 (T75) flasks and maintained for a maximum of 15 passages in culture. For experiments, cells were seeded in 100mm tissue-culture dishes or 12 or 24 multi-well plates. The experiments were carried out when the cells reached a confluence level of 60-70%. The manipulation of the cells in culture was carried out inside a sterile vertical laminar flow hood. Cells were authenticated by microsatellite assessment and routinely tested for mycoplasma contamination.

1.2. Establishment of OXPHOS-competent enriched cultures (Gal-CC) and OXPHOS-independent cultures (Glu-CC)

PDAC primary cultures (PANC185, PANC185scd, PANCA6L and PANC286) were trypsinized and seeded at a concentration of 800,000 cells in 100mm tissue-culture dishes with RPMI medium supplemented with 10% fetal bovine serum (FBS) and 50 units/mL of penicillin and streptomycin at a temperature of 37°C in an atmosphere with

5% of CO_2 and 90% of relative humidity. After 24 hours, cells were either cultured with 1) DMEM medium (Dulbecco´s Modified Eagle Medium) (Gibco, Thermo Fisher Scientific, Waltham, Massachusetts, USA), with glucose 0.9 g/L, 10% FBS and 50 units/mL of penicillin and streptomycin [Glucose-cultured cells (Glu-CC): OXPHOS-independent conditions], or 2) DMEM medium (Dulbecco´s Modified Eagle Medium) (Gibco, Thermo Fisher Scientific, Waltham, Massachusetts, USA) with galactose 0.9 g/L, 10% FBS and 50 units/mL of penicillin and streptomycin [Galactose-cultured cells (Gal-CC): OXPHOS-competent enriched conditions]. Media for both conditions were changed every 2-3 days, over a period 14 days. During this time, cells were collected for further processing and analysis, as described later.

1.3. Sphere formation assay

Spheres from primary PDAC cells cultures in glucose and galactose conditions were generated and expanded in DMEM-F12 medium (Invitrogen, Carlsbad, California, USA) supplemented with B-27 (Gibco, Thermo Fisher Scientific, Waltham, Massachusetts, USA) and bFGF (heparin binding growth factor) (PeproTech EC, London, UK). One-thousand cells/ml/well were seeded in ultra-low attachment 24-well plates (Corning, New York, USA) as described previously[151]. For serial passaging, spheres were harvested at day 7 using a 40 µm cell strainer, dissociated into single cells with trypsin, and then re-grown in the same conditions for 7 additional days (14 days total). The number of spheres was determined by microscopy using an inverted EVOS FL microscope (Thermo Fisher Scientific, Waltham, Massachusetts, USA) using a 10X objective with phase contrast. The data were analyzed with Prism 8 program (GraphPad Software, La Jolla, California, USA) to determine significance.

1.4. Lentivirus production and cell transduction

Lentiviral particles were produced by co-transfection of 293T cells (Invitrogen, Carlsbad, California, USA) with the indicated plasmids using the polyethylenimine (PEI)-based transfection method (Sigma Aldrich, St. Louis, Missouri, USA). Briefly, $5x10^6$ HEK293T cells were co-transfected with 1µg packaging plasmid psPAX2, 1µg envelope plasmid VSVG and 2µg of H2B-mCherry or the NANOG reporter lentiviral vector

backbone (the sequence of the construct has been previously described in the publication by Hotta et al.)[152]. After 8 hours, the transfection medium was changed and recombinant lentiviruses were harvested 48 and 72 hours later. The virus particles containing supernatant were filtered through 0.45µM PVDF membrane filters, aliquoted and stored at -80°C until needed. For lentivirus transduction, primary PDAC culture cells were seeded in 6-multiwell plates at a concentration of 3 to $5x10^4$ cells/well. One mL of virus was directly overlaid on cells and Polybrene (Sigma Aldrich, St. Louis, Misouri, USA) was added at a final concentration of 8µg/ml. After 16 hours, medium was changed. Stably transduced cells were obtained after mCherry-H2B-positive or YFP-positive cell sorting using a FACS Vantage SE Flow Cytometer (BD Bioscience, San Jose, California, USA) with BD FACSDiVa software (University of Virginia, USA). After sorting, cells were cultured in RPMI 1640 medium (Gibco, Thermo Fisher Scientific, Waltham, Massachusetts, USA), 10% fetal bovine serum (FBS), and 50 units/ ml penicillin/streptomycin at a temperature of 37°C in an atmosphere with 5% of CO_2 and 90% of relative humidity until their use in subsequent experiments.

1.5. Measurement of mitochondrial metabolism by Seahorse analyzer

Oxygen consumption rate (OCR) measurements were performed with a XF extracellular flux analyzer (Seahorse Bioscience, North Billerica, Massachusetts, USA). Briefly, Gal-CC or Glu-CC were seeded at a density of $1x10^5$ cells per well in a XF24 cell culture microplate. DMEM (4.5 g/L glucose, +L-Glutamine, -Pyruvate, pH 7.6 at RT) supplemented with 10% heat inactivated FBS (Gibco, Thermo Fisher Scientific, Waltham, Massachusetts, USA) and 1% Pen/Strep was used for cell culturing. On the day of the assay (24 hours after seeding), medium was exchanged to non-carbonated Seahorse measurement medium and the XF24 plate was transferred to a temperature-controlled (37°C) XF24 Extracellular Flux analyzer and equilibrated for 10 minutes. To determine the basal respiration, four assay cycles (1 minute mix, 2 minutes wait and 3 minutes measuring period) were used. Oligomycin (4µM) was added by automatic pneumatic injection to inhibit ATP synthase and thus approximate the proportion of respiration used to drive ATP synthesis versus proton leak-linked respiration. Oligomycin was followed by an injection of FCCP (carbonyl cyanide p-trifluoromethoxyphenylhydrazone) (0.5µM) to completely dissipate proton motive force and maximally stimulate mitochondrial

respiration, thus determining spare respiratory capacity and substrate oxidation capacity. An injection of rotenone (4μM) and antimycin A (2μM) was used to correct for the non-mitochondrial respiration rate (three assay cycles), which was subtracted from all the other rates. Coupling efficiency was calculated as the oligomycin-sensitive fraction of mitochondrial respiratory activity, estimating the proportion of basal respiration used to drive ATP synthesis. To determine extracellular acidification rate (ECAR) for glycolysis, experiments were terminated by injection of 2-DG (2-deoxy-D-glucose, 100 mM), correcting for non-glycolytic acidification. Injection of 2-DG enables the calculation of glycolytic acidification. OCR was plotted against ECAR to illustrate oxidative versus glycolytic metabolism in cancer cells. Raw data was normalized to protein content (μg). The data were analyzed with Prism 8 program (GraphPad Software, La Jolla, California, USA) to determine significance.

1.6. Quiescence-associated PKH26 dye assay

Primary PDAC culture cells were labeled with PKH26 red fluorescent cell membrane labeling dye (Sigma Aldrich, St. Louis, Missouri, USA) according to the manufacturer's instructions and seeded in glucose and galactose media. At indicated days post staining, for a total of 14 days, cells were trypsinized, washed and the percentage of PKH26 positive cells was determined using an Attune NxT Acoustic Cytometer and detected with laser YL1 (PE) (Thermo Fisher Scientific, Waltham, Massachusetts, USA). DAPI (Sigma Aldrich, St. Louis, Missouri, USA) was used to exclude dead cells with the laser VL1. Data were analyzed with FlowJo 9.3 software (Tree Star Inc., Ashland, Orlando, USA). The data were analyzed with Prism 8 program (GraphPad Software, La Jolla, California, USA) to determine significance.

1.7. Senescence-associated β-galactosidase enzyme assay

After 14 days, Glu-CC and Gal-CC were labeled using the β-galactosidase kit (Sigma Aldrich, St. Louis, Missouri, USA) according to the manufacturer's instructions. Glu-CC and Gal-CC were washed with 1X PBS (Gibco, Thermo Fisher Scientific, Waltham, Massachusetts, USA) and fixed with fixation buffer for 7 minutes at room temperature. After incubation, cells were washed and incubated with the staining solution overnight at

37°C. After overnight incubation, cells were harvested and β-galactosidase positive cells were determined using Axiovert 135 TV optical microscope (ZEISS, Germany) and ImageJ 2.0.0 software (NIH, USA) was used for the quantification of positive β-galactosidase area. The data were analyzed with Prism 8 program (GraphPad Software, La Jolla, California, USA) to determine significance.

1.8. Chemorresistance assays

PDAC cells were seeded in 12-well plates at a concentration of 10^4 cells/well. Following 14 days of culture with glucose or galactose, Gal-CC or Glu-CC were treated with 1µg/mL of Gemcitabine (GEM), 3µM of Mitoxantrone (MTX) or 1µM of Doxorubicin (DXR) for 2 days. After 2 days, drugs were removed and Glu-CC and Gal-CC were allowed to recover for 3 days in RPMI 1640 medium (Gibco, Thermo Fisher Scientific, Waltham, Massachusetts, USA). For metabolic drug assays, Glu-CC and Gal-CC were treated with 5µM of Menadione, 10nM of Rotenone, 100µM of Resveratrol, 3mM of Metformin and 5mM of 2DG for 3 days. Following treatments, the supernatants were collected and the ToxiLight™ bioassay kit (Cat no. LT07-217, Lonza, Switzerland) was used to evaluate the toxicity using a bioluminescence GLOMAX Luminometer (Promega). The data were normalized to the control without treatments. The data were analyzed with Prism 8 program (GraphPad Software, La Jolla, California, USA) to determine significance.

1.9. Isolation of Macrophages and T-cells from human blood samples

Blood samples were obtained from healthy donors via the Biobank of the Hospital Ramón y Cajal-IRYCIS (ISCIII Biobank Register No. B.0000678), Madrid, Spain, integrated in the Spanish National Biobanks Network. Samples were obtained with informed consent and with approval from of the Ethics Committee of each respective hospital and according to Declaration of Helsinki principles. Blood samples were diluted with 1X PBS (Gibco, Thermo Fisher Scientific, Waltham, Massachusetts, USA) and Ficoll (Merck, Darmstadt, Germany) was used to isolate Peripheral Blood Mononuclear Cells (PBMC). Blood samples were centrifuged at 400 G for 45 minutes. Afterwards, PBMC were collected and divided to three 6-well culture plates (per donor) with RPMI 1640

media (Gibco, Thermo Fisher Scientific, Waltham, Massachusetts, USA) containing 10% FBS and 50 units/ ml penicillin/streptomycin. After 24 hours, monocytes adhered to the plate surface were separated from the T lymphocytes that remain in suspension, the latter of which were seeded in T75 flasks for their subsequent activation and growth. For the activation of T-cells, PHA-P (Sigma Aldrich, St. Louis, Missouri, USA) was used at a concentration of 5 µg/mL for 48 hours to induce the expression of IL-2. After 48 hours, T-cells were centrifuged and re-seeded into T-75 flasks with RPMI 1640 media containing 10% FBS and 50 units/ ml penicillin/streptomycin and 20ng/mL of human IL-2 recombinant (Gibco, Thermo Fisher Scientific, Waltham, Massachusetts, USA). These steps were repeated every 3 days for 7 days. After 7 days of activation, T-cells were used to perform the subsequent experiments. Both immune cell types were kept in culture at a temperature of 37°C in an atmosphere with 5% of CO_2 and 90% of relative humidity to further assays.

1.10. Macrophages immunoevasion assay

Five days after isolation of macrophages from blood of healthy donors, macrophages were labelled with DilC, a red membrane dye, according to the manufacturer's instructions (Thermo Fisher Scientific, Waltham, Massachusetts, USA). Glu-CC and Gal-CC were harvested and labelled with PKH67 green fluorescent cell membrane labeling dye (Sigma Aldrich, St. Louis, Missouri, USA) according to the manufacturer's instructions. Labelled cells (PKH67) were seeded together with labelled macrophages (DilC) during 72 hours. Afterwards, macrophage-mediated phagocytosis ($DilC^+PKH67^+$ population) was assessed using an Attune NxT Acoustic Cytometer and detected with laser BL1 (DilC) and RL1 (APC; PKH67) (Thermo Fisher Scientific, Waltham, Massachusetts, USA). Data was analyzed with FlowJo 9.2 software (TreeStar, Ashland, OR). The data were analyzed with Prism 8 program (GraphPad Software, La Jolla, California, USA) to determine significance.

1.11. T-cells immunoevasion assay

Seven days after isolation, expansion and activation of T-cells from blood of healthy donors, Glu-CC and Gal-CC were harvested and co-seeded with activated T-cells during

10 days. Afterwards, T-cells were removed by filtration and the extent of cytotoxicity was determined with the ToxiLight™ bioassay kit (Lonza, Switzerland) using a bioluminescence GLOMAX Luminometer (Promega). The data were analyzed with Prism 8 program (GraphPad Software, La Jolla, California, USA) to determine significance.

2. Flow cytometry

2.1. Flow cytometry analysis

For cell surface antibody marker expression, cells were tripsinized and blocked with Flebogamma at a concentration of 50µg/mL (GRIFOLS, Barcelona, Spain) for 15 minutes at 4°C, washed, marked with antibody for 30 minutes at 4°C in darkness, washed and resuspended in 600µL of Flow Buffer [1X Phosphate buffered saline (PBS); 3% FBS (v/v); 3mM EDTA (v/v)] before analysis with a 4-laser Attune NxT Acoustic Cytometer (Thermo Fisher Scientific, Waltham, Massachusetts, USA). Refer to antibodies listed in Table 1 for working concentrations.

For the detection of PARKIN (intracellular) by cytometry, cells were fixed with 4% paraformaldehyde (PFA) in 1X PBS (Gibco, Thermo Fisher Scientific, Waltham, Massachusetts, USA) for 10 minutes, washed and permeabilized for 15 minutes with 1X Triton. For Annexin-V staining, supernatant floating cells and attached cells were pooled and resuspended in 1X Annexin-V staining buffer containing Annexin-V-FITC diluted 1:20 (Biotium, Freemont, California, USA) and incubated for 20 minutes at room temperature prior to flow cytometric analysis. For intracellular autofluorescent biomarker detection cells were excited with blue laser 488nm and selected as intersection with the filters 530/40 (FIT-C) and 580/30 (PE).

For Mitochondria markers, Glu-CC and Gal-CC were stained with Mitotracker Deep Red (Cat no. M22426), CM-H2XRos (Cat no. M7513), MitoTracker® Red CMXRos (Cat no. M7512), Mitotracker Green FM (Cat no. M7514) and NAO (Cat no. A1372) (all from Invitrogen) in the absence of FBS for 30min at 37°C, at concentrations of 2nM, 100nM and 10nM respectively, and 0,1µM for Mitotracker Green FM and NAO. Fluorescence was detected using the filters RL1 (APC), YL1 (PE) and BL1 (FITC). MitoSOX (Cat no.

M36008, Invitrogen) was used at 5μM for 30 min at 37°C and detected with laser YL1 (PE). MitoBlue (kindly provided by Dr. JL Mascareñas, Universidad de Santiago de Compostela) was used at 10μM for 20 min at 37°C and detected with laser VL2. Data were analyzed with FlowJo 9.3 software (Tree Star Inc., Ashland, OR.).

For lentiviral-transduced mCherry-H2B-positive or YFP-positive (NANOG) cells, Glu-CC and Gal-CC were analyzed with laser YL1 (PE) for mCherry-H2B and BL1 (with excitation at 508nm and emission at 527nm) for YFP fluorescent.

For all assays, 2mg/ml DAPI (Sigma Aldrich, St. Louis, Missouri, USA) was used to exclude dead cells with laser VL1 (with excitation at 405nm and emission at 450nm). Data were analyzed with FlowJo 9.3 software (Tree Star Inc., Ashland, Orlando, USA). The data were analyzed with Prism 8 program (GraphPad Software, La Jolla, California, USA) to determine significance.

2.2. Fluorescence-Associated Cell Sorting (FACS)

For cell sorting, PDAC cells were tripsinized and blocked with Flebogamma at a concentration of 50μg/mL (GRIFOLS, Barcelona, Spain) for 15 minutes at 4°C, washed, marked with antibody for 30 minutes at 4°C in darkness, washed and filtered through 0.45μM filters and resuspended in 2mL Sorting Buffer [1X PBS; 0,1% FBS (v/v); 3mM EDTA (v/v)]. A FACS Vantage SE Flow Cytometer (BD Bioscience, San Jose, California, USA) was used and events were analyzed using the BD FACSDiVa software (University of Virginia, USA). After sorting, cells were cultured in RPMI 1640 medium (Gibco, Thermo Fisher Scientific, Waltham, Massachusetts, USA) containing 10% fetal bovine serum (FBS) and 50 units/ ml penicillin/streptomycin at a temperature of 37°C in an atmosphere with 5% of CO_2 and 90% of relative humidity until their use in subsequent experiments.

DAPI was used at a concentration of 2mg/ml (Sigma Aldrich, St. Louis, Missouri, USA) to exclude dead cells with laser VL1 (with excitation at 405nm and emission at 450nm). Data were analyzed with FlowJo 9.3 software (Tree Star Inc., Ashland, Orlando, USA). The data were analyzed with Prism 8 program (GraphPad Software, La Jolla, California, USA) to determine significance.

Table 1. Antibodies for FACS, Sorting, Western Blot and Immunofluorescence

1ª Abs-Epitope	Source	Dilution	Application	Manufacturer
α-hu-CD133/1-APC	Mouse monoclonal	1:10	FC	Miltenyi Biotec
α-hu-CD24-PEVio700	Mouse monoclonal	1:10	FC	Miltenyi Biotec
α-hu-CXCR4-PE	Mouse monoclonal	1:10	FC	Miltenyi Biotec
α-hu-TEM8	Mouse monoclonal	1:50	FC	Abcam
α-hu-β-catenin	Rabbit monoclonal	1:100	WB/IF	BDbioscience
α-hu-PD-L1-Alexa700	Mouse monoclonal	1:10	FC	BioLegend
α-hu-CD47-APC	Mouse monoclonal	2,5:50	FC	Miltenyi Biotec
α-hu-CD155-APC	Mouse monoclonal	1:10	FC	Miltenyi Biotec
α-hu-CD206-FITC	Mouse monoclonal	2,5:50	FC	Miltenyi Biotec
α-hu-ULBP2/5/6	Mouse monoclonal	1:50	FC	R&D systems
α-hu-CD90-APC	Mouse monoclonal	2,5:50	FC	Life Technologies
α-β-ACTIN	Mouse monoclonal	1:5000	WB	ThermoFisher
α-GAPDH	Mouse monoclonal	1:5000	WB	ThermoFisher
α-hu-LC3BI/II	Rabbit monoclonal	1:500/1:100	WB/IF	Sigma Aldrich
α-hu-LAMP-1 (H43A)	Mouse monoclonal	1:100	IF	Santa Cruz
α-hu-PARKIN	Rabbit monoclonal	1:500/1:200	FC/IF	ThermoFisher
α-hu-SSEA4-APC	Mouse monoclonal	1:50	FC	BioLegend
α-hu-CD44-PE	Mouse monoclonal	1:50	FC	Becton Dickinson
TOM20	Mouse monoclonal	1:200	IF	Santa Cruz
α-ms-CD45-FITC	Rat monoclonal	1:100	FC	BDbioscience
α-ms-CD11b-PerCP Cy5.5	Rat monoclonal	1:200	FC	TONBO
α-ms-F4-80-PE	Recomb-human	1:100	FC	Miltenyi Biotec
2ª Abs-Epitope	**Source**	**Dilution**	**Application**	**Manufacturer**
Anti-mouse-HRP	Sheep	1:5,000	WB	Amersham
Anti-rabbit-HRP	Donkey	1:5,000	WB	Amersham
Anti-mouse Alexa 647	Goat	1:500	IF	Invitrogen
Anti-rabbit Alexa 555	Goat	1:500	IF	Invitrogen

2.3. Cell cycle analysis

One million cells were seeded in 100mm tissue-culture dishes and after 24 hours their cell cycles were synchronized using serum free medium (-FBS). Twenty-four hours later, treatments with glucose and galactose media were started and cell cycle was determined 14 days later. Cells were trypsinized and fixed in cold 70% ethanol and stored at -20°C. After 24 hours, cells were incubated with 100ug/ml RNAase A (Sigma Aldrich, St. Louis, Missouri, USA) in 1X PBS (Gibco, Thermo Fisher Scientific, Waltham, Massachusetts, USA) during 30 minutes at 37°C and then stained with 50 µg/ml of propidium iodide (PI) solution (Sigma Aldrich, St. Louis, Missouri, USA) and stored overnight at 4°C. Approximately 20,000 cells/sample were analyzed using the Attune NxT Acoustic Cytometer (ThermoFisher Scientific, Waltham, Massachusetts, USA) with laser YL2 (excitation at 561nm and emission at 615nm). The percentage of cells in each phase of the cell cycle was determined using FlowJo 9.3 software (Tree Star Inc., Ashland, Orlando, USA). The graphic data were analyzed with Prism 8 program (GraphPad Software, La Jolla, California, USA).

3. Western Blot

3.1. Western Blot analysis

Glu-CC and Gal-CC were harvested in RIPA buffer (Sigma Aldrich, St. Louis, Missouri, USA) supplemented with protease inhibitor cocktail (Roche Applied Science, Indianapolis, USA). They were incubated for 30 minutes on ice in a rotating platform and subsequently centrifuged for 30 minutes at 14,000 rpm and 4°C. The supernatant with the cell lysate was collected and the protein concentration was quantified using the BCA protein reagent kit (Pierce, Thermo Fisher Scientific, Waltham, Massachusetts, USA). The optical density was determined by a Synergy™ HT Multi-Mode Microplate Reader (BioTek, Winooski, Vermont, USA). After quantification, 50µg of protein extract were resolved by SDS-PAGE and transferred to PVDF membranes (Amersham Pharmacia, Piscataway, New Jersey, USA). Membranes were sequentially blocked with Blocking Buffer containing 1X PBS, 5% Bovine Serum Albumin (BSA) (w/v) and 0.1% Tween20 (v/v), incubated with a 1:1000 dilution of indicated antibodies (Table 1) overnight at 4ºC.

After overnight incubation, membranes were washed 3 times with 1X PBS-T containing 0.05% Tween20 (v/v), incubated with horseradish peroxidase-conjugated goat anti-rabbit or goat anti-mouse antibody (secondary antibodies) (Sigma Aldrich, St. Louis, Misouri, USA), and washed again to remove unbound antibody. Bound antibody complexes were detected with SuperSignal chemiluminescent substrate (Amersham Pharmacia, Piscataway, New Jersey, USA) using the MyECL Imager (Thermo Fisher Scientific, Waltham, Massachusetts, USA). For densitometry analysis, Western Blot images were analyzed using PhotoShop CS (Adobe Systems, USA). The data were normalized to the indicated housekeeping protein. The data were analyzed with Prism 8 program (GraphPad Software, La Jolla, California, USA) to determine significance.

3.2. Autophagy flux assay

For autophagy flux analysis, Glu-CC and Gal-CC were treated with the lysosomotropic reagent Bafilomycin A1 at a concentration of 150nM (Calbiochem, Thermo Fisher Scientific, Waltham, Massachusetts, USA) for 5 hours. After treatment, Glu-CC and Gal-CC were harvested and analyzed by Western Blot as described above. For densitometry, Western Blot images were analyzed using PhotoShop CS (Adobe Systems, USA). Autophagy flux compares the LC3B-II (Sigma Aldrich, St. Louis, Missouri, USA) levels with and without the autophagy inhibitor and is calculated as the ratio of LC3B-II in the presence and absence of the autophagy inhibitor compared to the control condition (Gal-CC vs- Glu-CC). The data were normalized to the indicated housekeeping protein. The data were analyzed with Prism 8 program (GraphPad Software, La Jolla, California, USA) to determine significance.

3.3. Cytokine array

Changes in protein levels related to immune evasion processes were determined thanks to changes in the levels of cytokines released into the culture medium by Glu-CC and Gal-CC cells. For this, we used the Proteome Profiler Human Cytokine Array Kit (R&D Systems, Minneapolis, MN, USA). For the sample processing and testing, the reagents and instructions provided in the kit were followed. Cytokine array images were obtained using the MyECL Imager (Thermo Fisher Scientific, Waltham, Massachusetts, USA). For

densitometry analysis, cytokine array images were analyzed using PhotoShop CS (Adobe Systems, USA). Data were normalized to the indicated array positive control. The data were analyzed with Prism 8 program (GraphPad Software, La Jolla, California, USA) to determine significance.

4. RNA extraction and RT-qPCR

RNA was isolated by using the standard protocol of the guanidine thiocyanate (GTC). One microgram of purified RNA was used for the synthesis of cDNA using the Thermo Scientific Maxima First Strand cDNA Synthesis Kit (Thermo Fisher Scientific, Waltham, Massachusetts, USA) according to manufacturer´s instructions, followed by RT-qPCR analysis using SYBR green and a StepOne Plus real-time thermo-cycler (Applied Biosystems, Foster City, California, USA). The reaction consisted of an initial denaturation step of 10 minutes at 95°C followed by 40 cycles of denaturation (15 seconds at 95°C) and annealing (1 minute at 60°C). Finally, the results obtained for each gene were normalized with β-actin housekeeping mRNA levels corresponding to each sample. For primers used see Table 2. The data were analyzed with Prism 8 program (GraphPad Software, La Jolla, California, USA) to determine significance.

Table 2. Primer sequences

Gene	Application	Primer sense	Primer antisense
β-Actin	RTqPCR	GCGAGCACACGAGCCTCGCC	CATCATCCATGGTGAGCTGGCGG
Klf4	RTqPCR	ACCCACACAGGTGAGAAACC	ATGTGTAAGGCGAGGTGGTC
MT-RNR1	qPCR	CCACGGGAAACAGCAGTGAT	CTATTGACTTGGGTTAATCGTGTG
Oct3/4	RTqPCR	CTTGCTGCAGAAGTGGGTGGA	CTGCAGTGTGGGTTTCGGGCA
Sox2	RTqPCR	AGAACCCCAAGATGCACAAC	CGGGGCCGGTATTTATAATC
Slug	RTqPCR	GGGGAGAAGCCTTTTTCTTG	TCCTCATGTTTGTGCAGGAG
Snail	RTqPCR	CTCCCTGTCAGATGAGGAC	CCAGGCTGAGGTATTCCTTG
Vimentin	RTqPCR	GAGAACTTTGCCGTTGAAGC	GCTTCCTGTAGGTGGCAATC
Zeb1	RTqPCR	CCAGGTGTAAGCGCAGAAA	CCACAATATGCAGTTTGTCTTCA
PGC1α	RTqPCR	TGACTGGCGTCATTCAGGAG	CCAGAGCAGCACACTCGAT
ABCG2	RTqPCR	CCGCTGGAATGCAAAATAG	CCATACGAACAGCTCCACA
Nanog	RTqPCR	TGAACCTCAGCTACAAACAGG	AACTGCATGCATGCAGGACTGCA
Sox9	RTqPCR	ACGCACATCTCCCCCAACGC	GCATTGCCCCGAGTGCTCGCC
DKK-1	RTqPCR	GCCAGTGAGCGCCACCTTGA	GCACCCGTACGGCTCCTAGTTG
Cdh1	RTqPCR	TGCCCAGAAAATGAAAAAGGC	GTGTATGTGGCAATGCGTTC
NRF2	RTqPCR	AGGAGGAGGAAGTGGAGGGA	ACATTCAGCTGGCGCGTAGGTT
NFκB	RTqPCR	CTCGCCACCCGGCTTCAGAAT	AAGGTATGGGCCATCTGTTGGCA
ATG5	RTqPCR	AAGCAACTCTGGATGGGATTG	AAAGGTCTTTCAGTCGTTGTCTGA
NDUFA9	RTqPCR	AGTGGAGCGGATGCACATCAC	GACGGTCTTGGCCGGCTTCA
MT-COI	RTqPCR	CTCTTCGTCTGATCCGTCCT	ATTCCGAAGCCTGGTAGGAT
MT-RNR2	RTqPCR	CCCGATGGTGCAGCCGCTATT	TCATTTACGGGGGAAGGCGCT
PARKIN	RTqPCR	CCGGCTGACCAGTTGCGTGT	GTCACAATTCTGCACAGTCCAGTC
GARS	RTqPCR	GCACACACTGTCTCTGCCTG	CCGAATGATGAAGGAGGAAG
MKLN1	RTqPCR	GTTCTCCTTGTGAAATCCGC	TTCTTGCATGAGCAAACTGG
SFPQ	RTqPCR	TCGTACTGTTAGGCCCTTGG	AACCTTGCATGAAGAGCACC
HOTAIR	RTqPCR	GGCGGATGCAAGTTAATAAAA	TACGCCTGAGTGTTCACGAG
MSI-1	RTqPCR	CTTCGGCCAGTTCGGGGAGG	TGACGAAGCCGAAACCCCTGG

5. Lactate production assay

Culture medium from Glu-CC and Gal-CC were collected to evaluate the changes in the levels of lactate production. The analysis was performed using the Lactate Assay Kit (Sigma Aldrich, St. Louis, Missouri, USA) according to the manufacturer's instructions. The optical density was determined using a Synergy™ HT Multi-Mode Microplate Reader (BioTek, Winooski, Vermont, USA) at a wavelength set to 570nm. The data were analyzed with Prism 8 program (GraphPad Software, La Jolla, California, USA) to determine significance.

6. ATP determination assay

Lysate pellets of cells from Glu-CC and Gal-CC were collected to evaluate the changes in the levels of ATP. The analysis was performed using the Molecular Probes ATP Determination Kit (Thermo Fisher Scientific, Waltham, Massachusetts, USA) according to the manufacturer's instructions. Bioluminiscence was determined using a Synergy™ HT Multi-Mode Microplate Reader (BioTek, Winooski, Vermont, USA). The data were analyzed with Prism 8 program (GraphPad Software, La Jolla, California, USA) to determine significance.

7. TFGβ secretion assay

Culture medium from Glu-CC and Gal-CC were collected to evaluate the changes in the levels of TGFβ secretion. The analysis was performed using the Human TGFβ-1 Immunoassay Quantikine ELISA Kit (R&D Systems, Minneapolis, MN, USA) according to the manufacturer's instructions. The optical density was determined using a Synergy™ HT Multi-Mode Microplate Reader (BioTek, Winooski, Vermont, USA) at a wavelength set to 450nm. The data were analyzed with Prism 8 program (GraphPad Software, La Jolla, California, USA) to determine significance.

8. Imaging analysis

8.1. Electron microscopy

Primary PDAC culture cells or Glu-CC and Gal-CC were centrifuged and pellets were fixed with 0.1M cacodylate buffer with a pH of 7.4 at room temperature for 2 hours. After incubation, cells were post-fixed in 1% osmium tetroxide and potassium ferricyanide (0.8%) in 1X PBS (Gibco, Thermo Fisher Scientific, Waltham, Massachusetts, USA) for 1 hour at room temperature, dehydrated and included in Epon resin. Next, ultrafine sections were obtained on which a double contrast was made with uranyl acetate and lead citrate. The samples were processed by the UAM Electron Microscopy unit. Pictures were taken with a JEM-1010 transmission electron microscope (JEOL, USA). Finally, pictures were

analyzed by ImageJ 2.0.0 software (NIH, USA). The data were analyzed with Prism 8 program (GraphPad Software, La Jolla, California, USA) to determine significance.

8.2. Confocal microscopy

Post-FACS sorted and non-sorted Glu-CC and Gal-CC were seeded in 24-well culture dishes (Corning, New York, USA) and incubated at a temperature of 37°C in an atmosphere with 5% of CO_2 and 90% of relative humidity. The mitochondrial probes MitoTracker DeepRed and MitoTracker CMXRos were used at 2nM and 10nM, respectively for 30 minutes at 37°C (all from Invitrogen, Carlsbad, California, USA). Following two washes with 1X PBS (Gibco, Thermo Fisher Scientific, Waltham, Massachusetts, USA), and 5 minutes incubation with DAPI (2mg/mL, Sigma Aldrich, St. Louis, Missouri, USA), MitoTracker DeepRed was excited at 644 nm and the fluorescence emitted was detected at 665 nm (far red fluorescence) and assigned red fluorescence. MitoTracker CMXRos was excited at 579 nm and the fluorescence emitted was detected at 599 nm and assigned green fluorescence. For immunofluorescence assays, cells were fixed with 4% PFA in 1X PBS (Gibco, Thermo Fisher Scientific, Waltham, Massachusetts, USA) for 20 minutes at room temperature, washed with 1X PBS, permeabilized with 1X Triton™ X-100 for 15 minutes, blocked with 1% BSA in 1X PBS for 1 hour at room temperature and then incubated with specific antibodies (Table 1) in a solution of 1% BSA in 1X PBS. ProLong® Gold Antifade Reagent with DAPI (Thermo Fisher Scientific, Waltham, Massachusetts, USA) was then added to mark cell nuclei. All images were collected with a laser scanning confocal microscope Zeiss 710 (ZEISS, Oberkochen, Germany) and analyzed using the software Leica 2009 (Leica, Wetzlar, Germany). The analysis of fluorescent areas was quantified by ImageJ 2.0.0 software (NIH, USA). The data were analyzed with Prism 8 software (GraphPad Software, La Jolla, California, USA) to determine significance.

8.3. Optical microscopy

All the samples processed for optical microscopy were visualized and photographed with an Axiovert 135 TV microscope (ZEISS, Germany), equipped with an Olympus DP50 digital camera and a fluorescence lamp. The images were obtained with the program

ViewFinderTM 7.1 (Better Light, USA) and processed with the program PhotoShop CS (Adobe systems, USA) and ImageJ 2.0.0 software (NIH, USA).

8.4. Real-time proliferation assay

Glu-CC and Gal-CC were seeded in a 96-well plate at a concentration of 500 cells/well. After 24 hours, cells were cultured with glucose or galactose-containing media for an additional 72 hours at a temperature of 37°C in an atmosphere with 5% of CO_2 and 90% of relative humidity. The real-time analysis of proliferation and autofluorescence was performed by IncuCyte® ZOOM System (ESSEN BioScience, USA) taking images every 30 minutes for 48 hours. The results were analyzed with the IncuCyte Zoom 2015A software (ESSEN BioScience, USA). The data were analyzed with Prism 8 software (GraphPad Software, La Jolla, California, USA) to determine significance.

9. *In vivo* assays

9.1. Zebrafish maintenance and xenograft assays

Zebrafish embryos were obtained from adult zebrafish matings (*Danio rerio*, wild-type), maintained in 30L tanks with a ratio of 1 fish per liter of water, with 14:10 day/night cycle and a temperature of 28,5ºC according to the published procedures[153]. All the procedures used in the experiments, fish care and treatment were performed in agreement with the Animal Care and Use Committee of the University of Santiago de Compostela and the standard protocols of Spain (Directive 2012-63-UE). At the final point of the experiments, zebrafish embryos were euthanized by tricaine overdose.

Zebrafish embryos were collected at 0 hours post-fertilization (hpf) and incubated until 48hpf at 28.5ºC. At 48hpf, hatched embryos were anesthetized with 0.003% of tricaine (Sigma Aldrich, St. Louis, Missouri, USA). PANC185scd and PANCA6L mCherry-H2B labelled cells cultured with glucose and galactose media were trypsinized, resuspended and concentrated in an eppendorf at a rate of one million cells per tube of each condition. After that, all of the cells were resuspended in 10µL of 1X PBS (Gibco,

Thermo Fisher Scientific, Waltham, Massachusetts, USA) with 2% of PVP (Polyvinylpyrrolidone) to avoid cellular aggregation.

Borosilicate needles (1 mm O.D. x 0.75 mm I.D.; World Precision Instruments) were used to perform the xenograft assays in the zebrafish embryos. Between 100 and 150 cells were injected into the circulation of each fish (Duct of Cuvier) using a microinjector (IM-31 Electric Microinjector, Narishige) with an output pressure of 34kPA and 30ms of injection time per injection. Following this, the injected embryos were incubated at a temperature of 34ºC for 6 days post injection (dpi) in 30mL Petri dishes for each condition with SDTW (salt dechlorinate tap water). Imaging of the injected embryos was performed using a fluorescence stereomicroscope (AZ-100, Nikon) at 1, 4 and 6 days post-injection (dpi) in order to measure the proliferation of the Glu-CC and Gal-CC of PANC185scd and PANCA6L mCherry-H2B injected cells inside the zebrafish circulation in each of the conditions assayed.

The image analysis of the injected embryos was carried out using Quantifish software (University College London, London, UK) in order to obtain the proliferation ratio of the cells in the region of the caudal hematopoietic tissue (CHT) of the embryos, where the cells proliferate and metastasize. This program measures, in each of the images provided, the intensity of the fluorescence and the area of the positive pixel above a certain threshold of the cells. With these parameters, a value of integrated density is obtained allowing one to compare different times between images and reaching a proliferation ratio. The statistical data were analyzed with Prism 8 program (GraphPad Software, La Jolla, California, USA).

9.2. ELDA tumorigenicity assay

For tumorigenicity assays, serial dilutions of PANCA6L mCherry-H2B Glu-CC and Gal-CC resuspended in Matrigel™ (BD Biosciences, San Jose, California, USA) were subcutaneously injected into 4- to 5-week-old female nude mice (Hsd:Athymic Nude-Foxn1nu/Foxn1+; Envigo) and tracked for 3 months for tumor formation. All animal experiments were conducted in accordance with FELASA guidelines and approved protocols. Mice were housed according to institutional guidelines and all experimental

procedures were performed in compliance with the institutional guidelines for the welfare of experimental animals approved by the Universidad Autónoma de Madrid Ethics Committee (CEI 60-1057-A068) and la Comunidad de Madrid (PROEX 335/14) and in accordance with the guidelines for Ethical Conduct in the Care and Use of Animals as stated in The International Guiding Principles for Biomedical Research involving Animals, developed by the Council for International Organizations of Medical Sciences (CIOMS). After 3 months of tumor growth, mice were sacrificed and tumors were digested with collagenase (STEMCELL Technologies, Vancouver, Canada) to evaluate the percentage of mCherry-H2B-positive cells and the percentage of CD133 positive cells inside the mCherry-H2B positive cell population within each tumor by flow cytometry as described before. Data were analyzed with FlowJo 9.3 software (Tree Star Inc., Ashland, Orlando, USA). Moreover, the CSC frequency was calculated using the ELDA: Extreme Limiting Dilution Analysis software (Walter and Eliza Hall, Institute of Medical Research, Australia). The data were analyzed with Prism 8 program (GraphPad Software, La Jolla, California, USA) to determine significance.

9.3. Tail vein injection for invasion assay

Eight-week-old NOD-SCID mice (Instituto de Investigaciones Biomédicas "Alberto Sols" CSIC-UAM) were injected intravenously via the tail vein with either $5x10^5$ mCherry-H2B-labelled PANC185scd and PANCA6L Glu-CC or Gal-CC (resuspended in 0.9% physiological saline solution) using a 27G needle. The mice were sacrificed 10 days post-injection (dpi) or 3 months post-injection. Indicated organs were collected, digested and stained with antibodies to detect tumor-associated macrophages population (TAMs) (CD45+CD11b+F4-80+) (**Table 1**) by flow cytometry. In parallel, the percentage of mCherry-H2B positive cells present in each organ was also analyzed. Both TAMs and mCherry-H2B positive populations were determined by FACS using an Attune NxT Acoustic Cytometer (ThermoFisher Scientific, Waltham, Massachusetts, USA). DAPI (Sigma Aldrich, St. Louis, Missouri, USA) was used to exclude dead cells with laser VL1. Data were analyzed with FlowJo 9.3 software (Tree Star Inc., Ashland, Orlando, USA). Moreover, before digestion, Glu-CC and Gal-CC organs of 3 months post-injection mice were also analyzed *ex vivo* by IVIS-Lumina II (Caliper Life Sciences, Hopkinton, Massachusetts, USA) and analyzed using the software Living image 3.2 (Perkin Elmer,

Waltham, Massachusetts, USA). The data were analyzed with Prism 8 program (GraphPad Software, La Jolla, California, USA) to determine significance.

10. Statistical analysis

The majority of the data obtained in the assays were analyzed using the Holm-Sidak t-test statistical test. The 2-way ANOVA statistical test was used for the data obtained from the immunoevasion experiment of macrophages from healthy donors. For the data obtained from *in vivo* experiments in zebra fish, the unpaired t-test statistical test was used. For all analyzes, the level of significance was set at $p < 0.05$ and the differences between groups were labeled such as $p < 0.05$=*, $p < 0.01$=** and $p < 0.001$=***. Statistical analysis was performed using the GraphPad Prism 8 program (GraphPad Software, La Jolla, California, USA).

RESULTS

1. Pancreatic Cancer Stem Cells (PaCSCs) have increased mitochondrial function

One of the major challenges faced when studying CSCs is the inability to maintain a long-term adherent culture enriched in CSCs. While 3D non-adherent spheres allow for CSC enrichment, spheres are not highly adaptable to various methodologies and screening platforms due to their 3D nature and the need to passage them once they reach critical mass. Attempts to establish 2D cultures enriched in CSCs using FACS have also proven ineffective as marker-enriched CSCs quickly undergo both symmetric and asymmetric division to re-establish the heterogeneity of the culture that was present prior to sorting. Thus, as seen in **Figure 5** primary PDAC cultures of PANC185 cells were sorted using the classical PaCSC biomarker CD133 and Autofluorescence (Fluo)[154,155] and re-seeded in normal culture conditions. We evaluated the percentage of both PaCSC biomarkers in different time intervals post-sorting by flow cytometry. Interestingly, after 24 hours of post-sorting cells, the percentages of $CD133^+$ and $Fluo^+$ cells were less than 20% and, at 48 hours post-sorting cells the percentage of both PaCSC biomarkers was less than 10% (**Figure 5**). Thus, the enrichment in CSCs in 2D cell cultures is not stable and marker-enriched CSCs quickly return (~48-72 hours) to their pre-sort distribution (~1-5%).

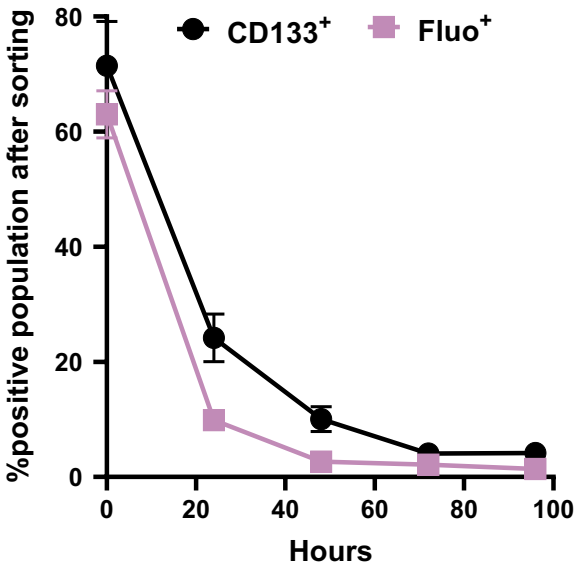

Figure 5. Primary PDAC cultures of PANC185 cells were sorted using the PaCSC markers CD133 or autofluorescence (Fluo), and the percentage of $CD133^+$ (black) or $Fluo^+$ (violet) cells was re-determined by flow cytometry at the indicated hours post-sorting.

Therefore, the medium-long term study of a culture enriched in CSCs is not feasible with the current available systems, and for that reason we decided to further dissect CSCs to discover other properties that could facilitate a long-term CSC-enriched 2D culture. Likewise, it is known that pancreatic CSCs do not follow the traditional dogma of tumor cell energy requirements. While the energy requirements of highly proliferative non-CSCs are predominantly met by glycolysis (Warburg effect), pancreatic CSCs behave more like differentiated less proliferative cells (e.g. quiescent), satisfying their high-energy requirements via mitochondrial respiration. For this reason, in order to find a metabolic property to achieve a long-term CSC-enriched 2D culture, primary PDAC cultures (PANC185 and PANC354) were sorted using PaCSC biomarker CD133 and divided into CD133 positive ($CD133^+$) cell population (PaCSCs) and CD133 negative ($CD133^-$) cell population (non-PaCSCs). Subsequently, we carried out a transmission electron microscopy (TEM)-based morphological and structural analysis of the mitochondria of these two populations and observed in a stack of images of both populations, that $CD133^+$ cells contained more differentiated mitochondria compared to $CD133^-$ cells, the latter of which contained swollen mitochondria with less pronounced cristae (red arrows, **Figure 6 left**) that appeared to be eliminated by autophagy (white arrows, **Figure 6 left**) whereas in $CD133^+$ population of cells, these autophagic structures were less frequent.

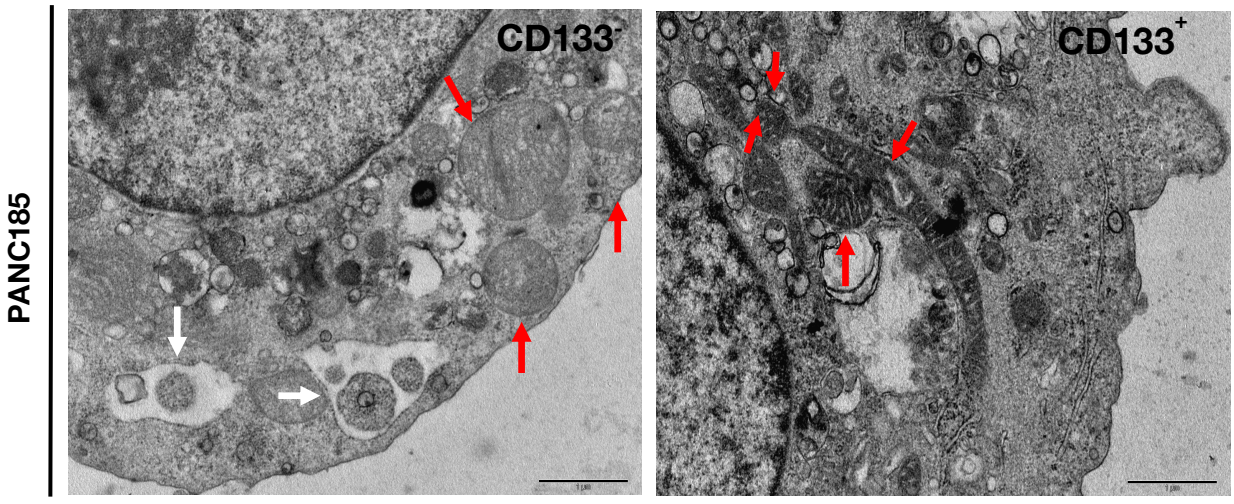

Figure 6. PANC185 cells were stained with an anti-CD133-APC antibody and sorted to divide the cell population into $CD133^-$ cells (non-CSCs=left) and $CD133^+$ cells (CSCs=right). Transmission electron micrographs were acquired and shown are representative images. Mitochondria (red arrows) are better defined in the $CD133^+$ population compared to $CD133^-$, which present autophagosomes (white arrows) in their cytoplasm.

Based on the results mentioned above, PANC185 and PANCA6L cells were sorted for two PaCSCs biomarkers: CD133 and Autofluorescence (Fluo), and an equal number of sorted cells were divided into double positive ($CD133^{+}Fluo^{+}$ cells, PaCSCs) or double negative populations ($CD133^{-}Fluo^{-}$ cells, non-PaCSCs) and were re-seeded in normal culture conditions for 7 days. Later, we analyzed the mitochondrial status by immunofluorescence with different mitochondrial markers. Markers of mitochondrial mass (Mitotracker-DeepRed FM) and mitochondrial membrane potential (MitoTracker-CMXRos) were analyzed by confocal microscopy. Microscopic analysis showed that $CD133^{+}Fluo^{+}$ cells contained more mitochondrial mass (Mitotracker-DeepRed FM=red) and these mitochondria had a higher membrane potential (Mitrotracker-CMXRos=green) compared to $CD133^{-}Fluo^{-}$ cells **(Figure 7A).** Moreover, the percentage of positive fluorescent area for MitoTraker DeepRed and MitoTraker CMXRos was quantified, and a significant increase in MitoTracker DeepRed of about 3-4-fold and a significant increase in MitoTracker CMXRos of about 2-3-fold was determined in the $CD133^{+}Fluo^{+}$ population in both primary cultures compared to $CD133^{-}Fluo^{-}$ cells **(Figures 7B-C).** In addition, as an indirect measure of mitochondrial mass/quantity, the levels of the mitochondria 12S ribosomal RNA gene (MT-RNR1) were also measured, and qPCR analysis revealed a significant increase of about 2-fold in the number of mtDNA copy numbers in $CD133^{+}Fluo^{+}$ population compared to $CD133^{-}Fluo^{-}$ population **(Figure 7D).** Moreover, at 7 days post-sorting, the number of DAPI-positive nuclei was significantly higher in the $CD133^{+}Fluo^{+}$-sorted population compared to $CD133^{-}Fluo^{-}$ in both primary cultures **(Figure 7E),** suggesting that cells positively enriched in CSCs have increased proliferation compared to negatively-enriched cells[156155,157,158] which is likely linked to reestablishing the heterogeneity of the culture that was present prior to sorting, as seen in **Figure 5.**

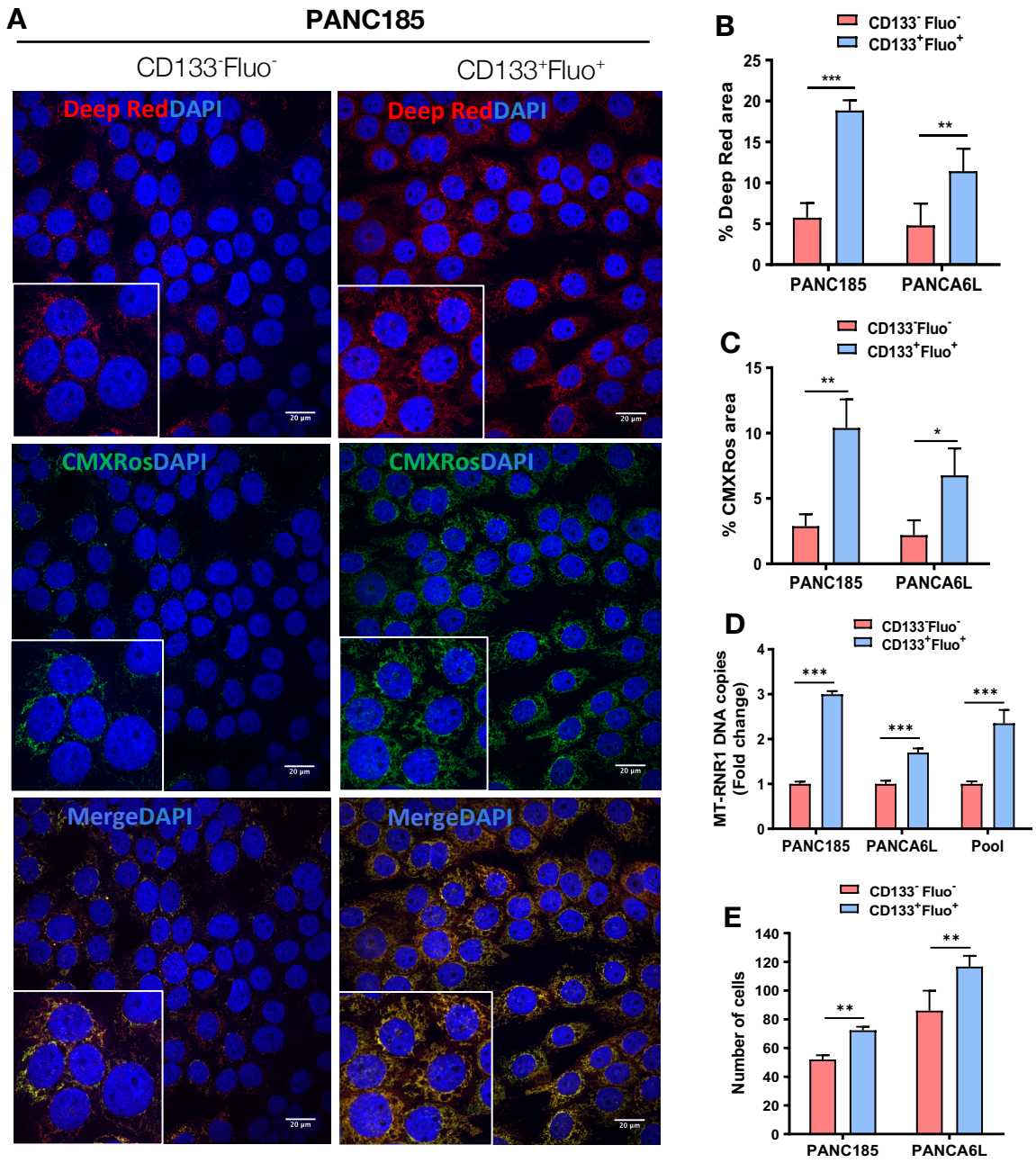

Figure 7. (A) PDAC primary cultures were sorted based on two different CSC biomarkers, CD133 and autofluorescence (Fluo), and nuclear marker (DAPI) to obtain the two cell populations: $CD133^{+}Fluo^{+}$ cells (CSCs) and $CD133^{-}Fluo^{-}$ cells (non-CSCs). After re-seeding, both populations were marked with mitochondrial markers MitoTracker-DeepRed FM (red) and MitoTracker-CMXRos (green) and DAPI (nuclear marker, blue). Shown are representative fluorescent images obtained by confocal microscopy analysis for PANC185. (B-C) Quantification of the percentage of fluorescent area for the (B) MitoTracker-DeepRed FM mitochondrial biomarker or the (C) Mitotracker-CMXRos mitochondrial membrane potential marker in PANC185 and PANCA6L, in two cell populations: $CD133^{+}Fluo^{+}$ cells (blue) and $CD133^{-}Fluo^{-}$ cells (red), using ImageJ (n= 6 samples per group). (D) Quantification of the levels of the mitochondrial 12S ribosomal RNA gene (MT-RNR1) by qPCR in $CD133^{+}Fluo^{+}$ cells and $CD133^{-}Fluo^{-}$ cells in PANC185 and PANCA6L (n= 3 samples/tumor). Data are normalized to β-Actin expression and presented as fold-change for each tumor and pooled data. $CD133^{-}Fluo^{-}$ was set as 1.0. (E) Quantification of the number of DAPI-positive nuclei in $CD133^{+}Fluo^{+}$-sorted and $CD133^{-}Fluo$-sorted in PANC185 and PANCA6L cultures, determined using ImageJ (n= 6 samples per group). Holm-Sidak t-test statistical analysis: (*) = $p< 0.05$; (**) = $p<0.01$; (***) = $p<0.001$.

These data confirmed previous published studies showing that CSCs have a more active mitochondrial state[156,159–161], which we reasoned could be exploited to establish a long-term CSC-enriched 2D culture. Thus, we set out to develop a novel *in vitro* system based on the apparent metabolic differences that exist between PaCSCs and non-PaCSCs. Such a strict metabolically-based CSC-enrichment system has never been described to date, and if successful could shed light on PaCSC properties, including plasticity. Towards this end, we modulated the carbon source in our culture medium, using either Glucose (Glu) or Galactose (Gal). The galactose condition would favor cells (PaCSCs) that have a mitochondrial-dependent metabolism (OXPHOS) compared to those cells (non-PaCSCs) that strictly use glucose as a source for glycolysis even in presence of oxygen (Warburg effect). Compared to glucose, proliferative substrates and ATP production from galactose is slower due to the fact that the conversion of galactose to glucose 6-phosphate (G6P) requires several more limiting enzymatic steps (Leloir pathway)[162]. Thus, cells that are exclusively dependent on glycolysis (non-PaCSCs) cannot survive in the presence of galactose due to the differences in ATP yield, while cells that do not have such strict ATP requirements, have functional mitochondria and can obtain ATP/fuel molecule production via OXPHOS (PaCSCs) will survive, proliferate and become enriched (Figure 8).

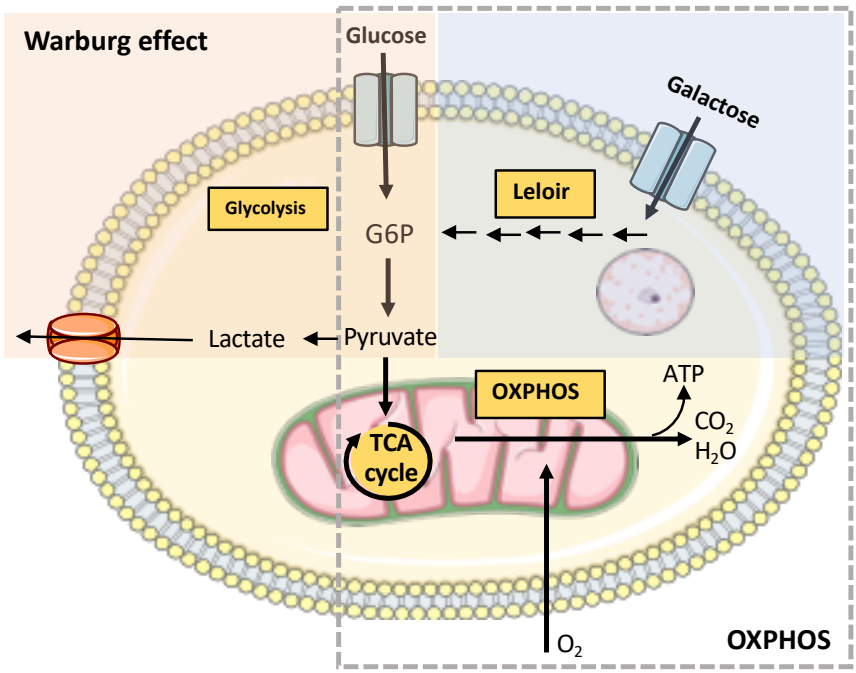

Figure 8. Schematic representation of metabolic processes under OXPHOS-competent enriched cultures (galactose-respiration) and OXPHOS-independent cultures (glucose-glycolysis).

2. Galactose system promotes enrichment in PaCSCs population

To develop our novel *in vitro* system based on the apparent metabolic differences that exist between PaCSCs and non-PaCSCs, we first tested media with and without serum and with different sources of carbon (Figures 9A-B). After 14 days in culture, we analyzed the percentage of late apoptosis (AnnexinV$^+$DAPI$^+$) (Figure 9A) and the levels of Autofluorescence (Figure 9B) to determine the condition where the ratio of CSC enrichment (i.e. percentage of autofluorescent cells) divide by the percentage of apoptotic cells was optimal in all the primary PDAC cultures (PANC185, PANC185scd, PANCA6L and PANC286), which will be used later to perform the rest of the experiments. The negative control (Ctr-/-) represents the cell culture media condition without a carbon source and serum. All data were compared to the control basal late apoptosis levels (AnnexinV$^+$/DAPI$^+$) in standard conditions (medium + 10% FBS and 4.5 g/L of glucose), which is represented by a red line in the graphs. The best results were obtained when primary PDAC cultures were cultured in the presence of serum (FBS+), and a clear difference in CSC enrichment was observed between Glucose and Galactose (Glu FBS+ and Gal FBS+). For this reason, from here on, PDAC primary cells were cultured in the presence of Glucose (Glucose-cultured cells, Glu-CC) or Galactose (Galactose-cultured cells, Gal-CC) with FBS.

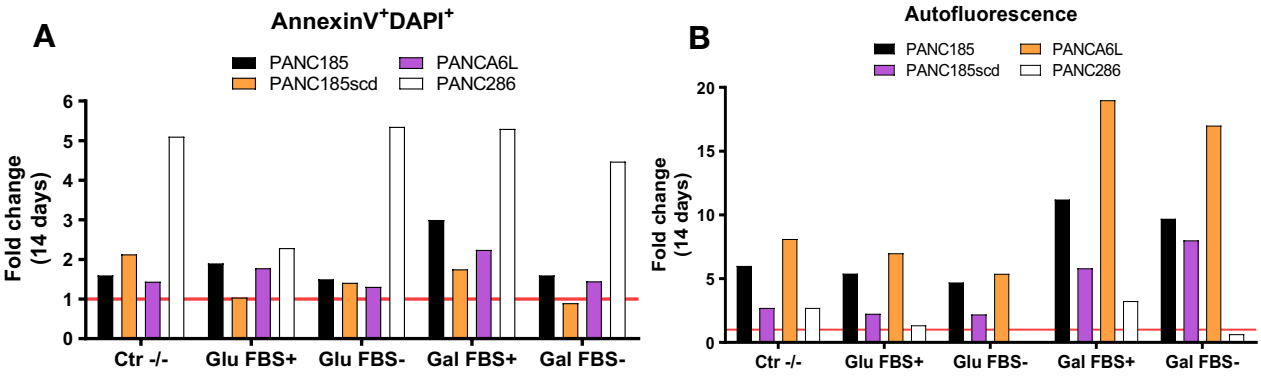

Figure 9. (A) Analysis of the effects of media with and without serum and with different sources of carbon. Fold change in the levels of AnnexinV/$^+$DAPI$^+$ populations in PDAC primary cultures with the different indicated culture media at 14d. The red line, set at 1.0, represents basal AnnexinV$^+$/DAPI$^+$ late apoptosis in standard conditions (medium + 10% FBS and 4.5 g/L Glu). (B) Fold change in the levels of the CSC autofluorescent-positive populations in PDAC primary cultures with the different indicated culture media at 14d. The red line, set at 1.0, represents basal autofluorescence in standard conditions (medium + 10% FBS and 4.5 g/L Glu). The best balance between (B) PaCSC enrichment (i.e. percentage of autofluorescent cells) and (A) the percentage of apoptotic cells was selected for all further experiments.

Firstly, to confirm the enrichment in CSCs in glucose and galactose conditions, we used a large panel of PaCSC biomarkers[39,154] with general flow cytometry gating strategies (**Figure 10A**) in the four primary PDAC cultures that were mentioned above. We observed and quantified that Autofluorescence, CD133 and CD24 significantly increased by more than 2-fold and CXCR4 and TEM8 significantly increased by 3-fold in Gal-CC compared to Glu-CC (**Figures 10A-B**), suggesting that in Gal-CC, there was a significant enrichment in PaCSCs population compared to Glu-CC.

In addition, because not all PDAC primary cultures are the same or have the same characteristics, we analyzed two additional PaCSC biomarkers such as CD90 and SSEA-4, present only on PANC286 and PANC185scd, respectively. The results were quantified and showed that CD90 significantly increased by more than 4-fold and, SSEA-4 significantly increased by more than 2-fold in Gal-CC compared to Glu-CC (**Figures 10C-D**).

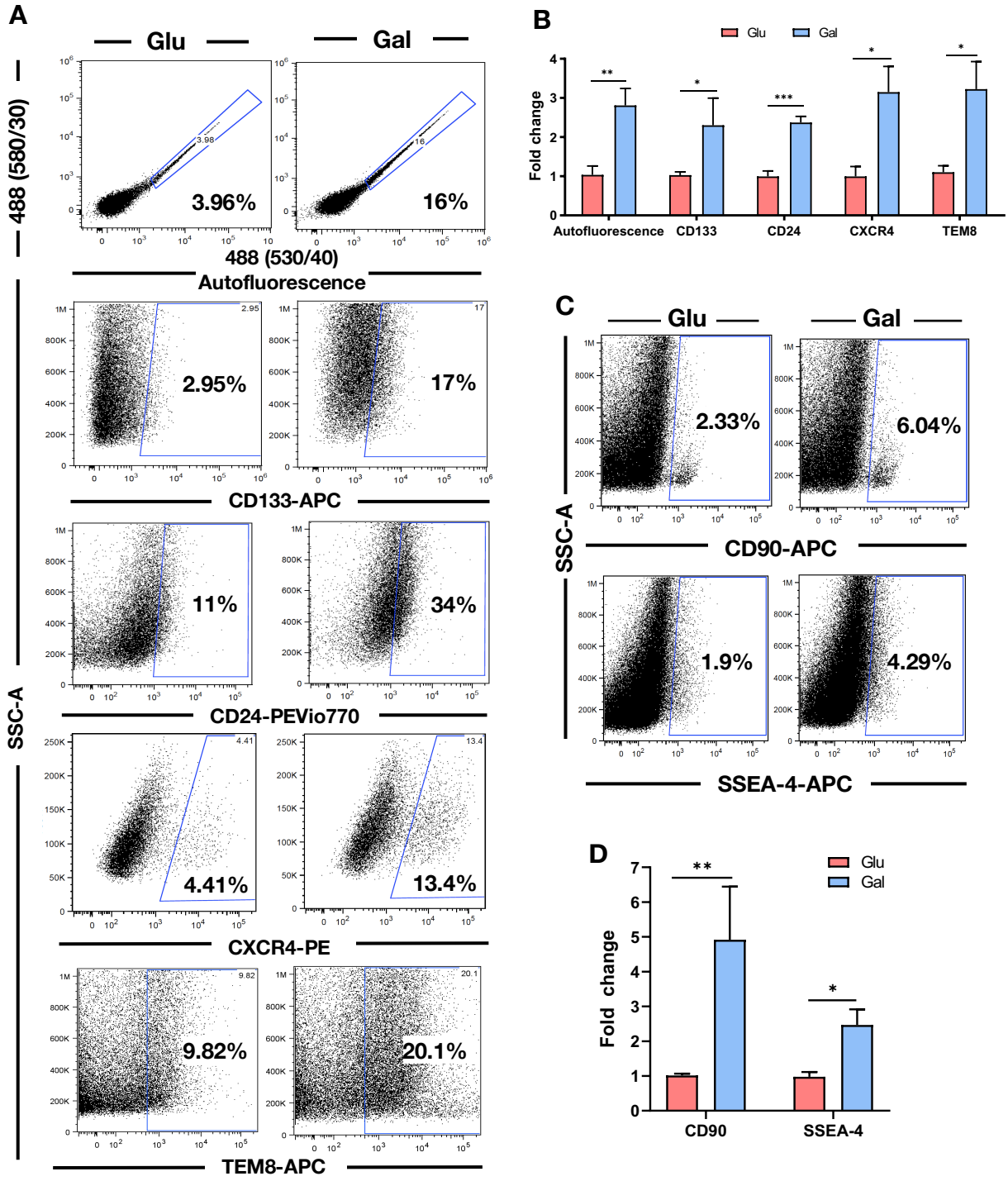

Figure 10. (A) Representative flow cytometric dot plots of the expression of different CSCs biomarkers (Autofluorescence, CD133, CD24, CXCR4 and TEM8) in Glu-CC and Gal-CC. (B) Quantification of the levels of the different CSCs biomarkers in Glu-CC and Gal-CC for 4 different tumors (n=2-3 biological replicates per tumor). Data are presented as fold-change. Glu was set as 1.0. (C) Representative FACS Dot Plots of different CSC biomarkers (CD90 and SSEA-4) in PANC286 and PANC185scd, respectively, comparing Glu-CC to Gal-CC. (D) Fold change quantification of the levels of the different CSC biomarkers comparing Glu-CC to Gal-CC (n=10 samples per group). Holm-Sidak t-test statistical analysis: (*) = p< 0.05; (**) = p<0.01; (***) = p<0.001

We next evaluated the proliferative capacity of Glu-CC and Gal-CC as we had observed lower number of cells in Gal-CC compared to Glu-CC. We used the IncuCyte Zoom System to perform a real-time analysis to assess CSC enrichment as a function of proliferation. Twenty-four hours after seeding Glu-CC and Gal-CC, the IncuCyte Zoom System acquired images over 3 days every 30 minutes using two different microscopic conditions: Phase contrast to evaluate cellular proliferation and fluorescence to evaluate PaCSCs enrichment using the Autofluorescence biomarker. After 48 hours, the analysis showed less proliferation (**Figure 11A**) but at the same time an enrichment in Autofluorescence (**Figure 11B**) in Gal-CC compared to Glu-CC during 3 days of culture in restrictive metabolic conditions.

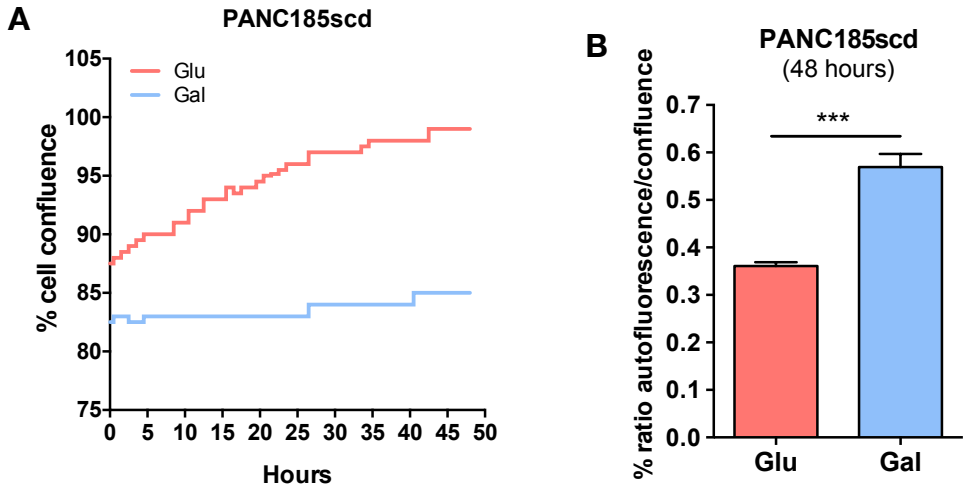

Figure 11. (**A**) Real-time quantification of percentage of cell confluence by IncuCyte Zoom System comparing Glu-CC to Gal-CC in different time intervals. (**B**) Quantification of percentage of autofluorescence/confluence ratio by IncuCyte Zoom System at 40 hours comparing Glu-CC to Gal-CC. Holm-Sidak t-test statistical analysis: (*) = p< 0.05; (**) = p<0.01; (***) = p<0.001

In addition, to assess self-renewal capacity, one of the most important functional features of CSCs, we performed a sphere formation assay to evaluate the capacity of these cells to proliferate *in vitro* in anchorage-independent conditions. In line with the observed enrichment in CSCs (**Figures 10-11**), the number of spheres were significantly higher in Gal-CC compared to Glu-CC in 1st and 2nd generation spheres (**Figure 12A**), which indicated a higher self-renewal capacity. Moreover, microscopy images were taken to evaluate the structural morphology of the spheres. Interestingly, spheres in Glu-CC were bigger than spheres in Gal-CC (**Figure 12B**). These differences found in the spheres could suggest that Glu-CC spheres were made up of a higher percentage of differentiated tumor cells (non-CSCs) with a higher proliferation rate giving rise to larger spheres,

whereas the Gal-CC spheres were made up of a more undifferentiated tumor cell population (CSCs) with a lower proliferation more quiescent state.

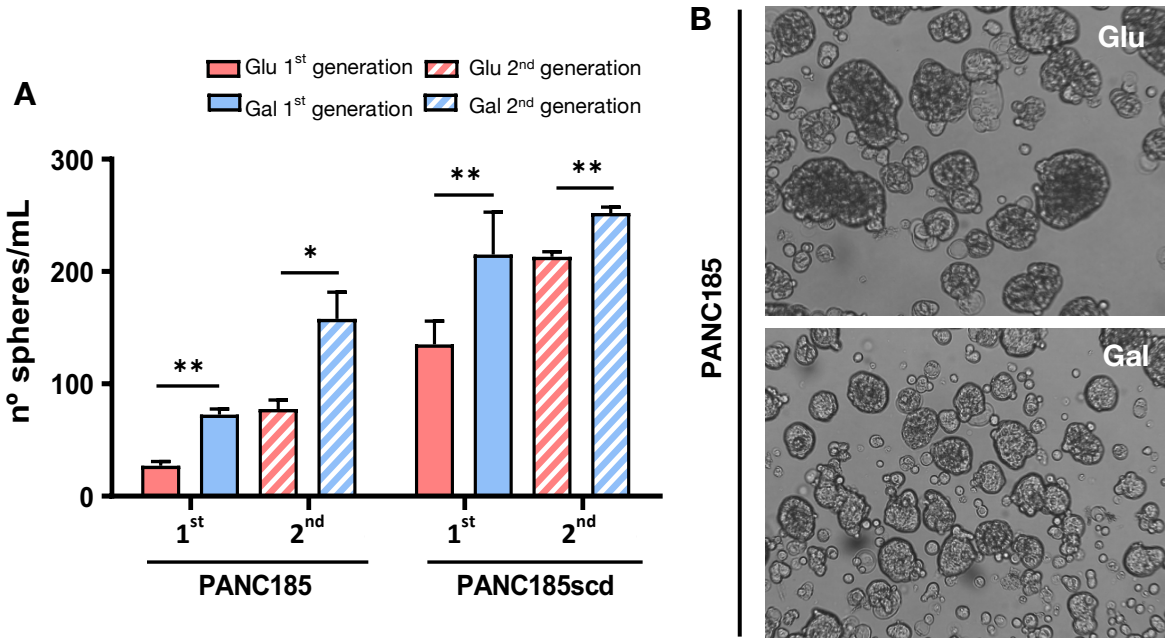

Figure 12. (A) Sphere forming capacity (number of spheres per mL) for PANC185 and PANC185scd at 7 and 14 days for Glu-CC and Gal-CC (n=6 samples per group). (B) Representative PANC185 sphere images for Glu-CC and Gal-CC at 14 days. Holm-Sidak t-test statistical analysis: (*) = p< 0.05; (**) = p<0.01; (***) = p<0.001

In order to confirm if the Gal-CC spheres were indeed contained a higher percentage of CSCs compared to Glu-CC spheres, as hypothesized above, we dissociated the spheres and analyzed different CSC biomarkers by flow cytometry. We confirmed that the observed increase in self-renewal capacity of Gal-CC was due to an enrichment in the percentage of CSCs in spheres by showing that the percentage of autofluorescent-positive (Figure 13A) and $CD133^{+}CXCR4^{+}$ double-positive (Figure 13B) cells were significantly higher in Gal-CC (more than 3-fold) compared to Glu-CC in 1st and 2nd generation spheres.

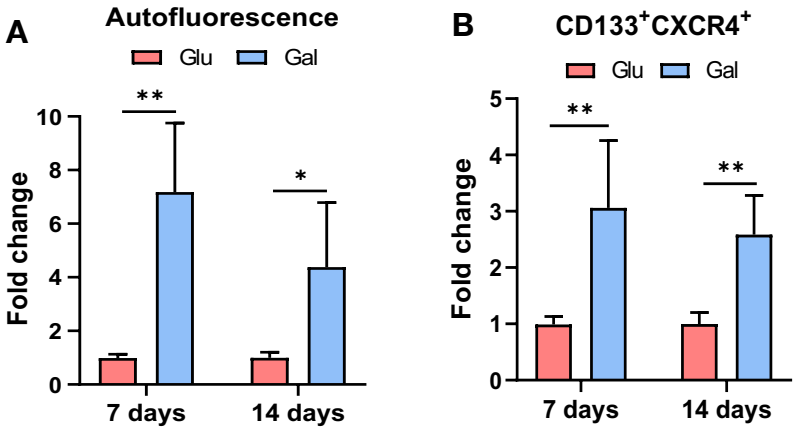

Figure 13. (A-B) Flow cytometric quantification of (A) Autofluorescent-positive and (B) $CD133^{+}CXCR4^{+}$ double positive population of cells detected in Glu-CC and Gal-CC spheres at 7 and 14 day. Data are presented as fold-change. Glu was set as 1.0. Holm-Sidak t-test statistical analysis: (*) = p< 0.05; (**) = p<0.01; (***) = p<0.001

In addition, at the transcriptional level, genes related to pluripotency (*OCT3/4, KLF4 and NANOG*) and stemness (*SOX2 and SOX9*) were evaluated by RT-qPCR in Glu-CC and Gal-CC. All transcripts analyzed significantly increased between 2-3-fold in Gal-CC compared to Glu-CC (Figure 14A). Moreover, thanks to Dr. Patrick Hermann and the members of his laboratory at the University of Ulm, NANOG expression was validated using a PANC185 NANOG-Yellow Nano-lantern (YNL) reporter system. Specifically, PANC185 cells infected with lentiviruses that carries a NANOG promoter-YNL reporter gene were cultured with glucose or galactose. After 14 days, the activity of NANOG was evaluated by flow cytometry, in which YNL expression (indicative of human NANOG promoter activity) was significantly higher in Gal-CC compared to Glu-CC (Figure 14B).

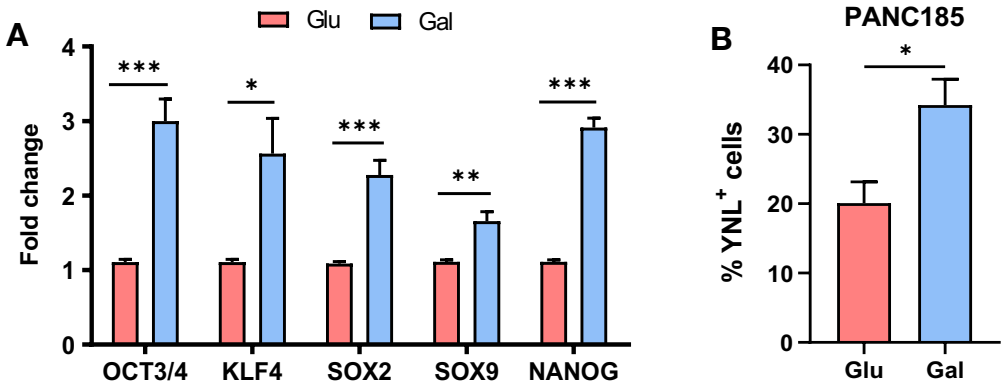

Figure 14. (A) RT-qPCR analysis of relative mRNA expression levels of different pluripotency/stemness genes in Glu-CC and Gal-CC for 4 different tumors. mRNA expression levels for each target gene are normalized to β-actin levels (n=2-3 biological replicates per tumor, 2 technical replicates). Data are presented as fold-change. Glu was set as 1.0. (B) Flow cytometric quantification of Nanog reporter YFP+ PANC185 cells in Glu-CC and Gal-CC at 14 days. Holm-Sidak t-test statistical analysis: (*) = p< 0.05; (**) = p<0.01; (***) = p<0.001

Continuing in this line, recent evidence suggests that different types of non-coding RNAs (ncRNA), such as long non-coding RNAs (lncRNAs), play a role in regulating CSC growth and replication by modulating transcription factors and downstream signaling pathways activated in CSCs[163]. Likewise, lncRNAs can act as both tumor suppressors or promoters during cancer growth and metastasis[164–166]. For these reasons, we evaluated the expression levels of a subset of lncRNAs essentials in the different tumor processes mentioned before and observed a significant increase, between 2-3-fold, in their expression in Gal-CC compared to Glu-CC (**Figure 15**).

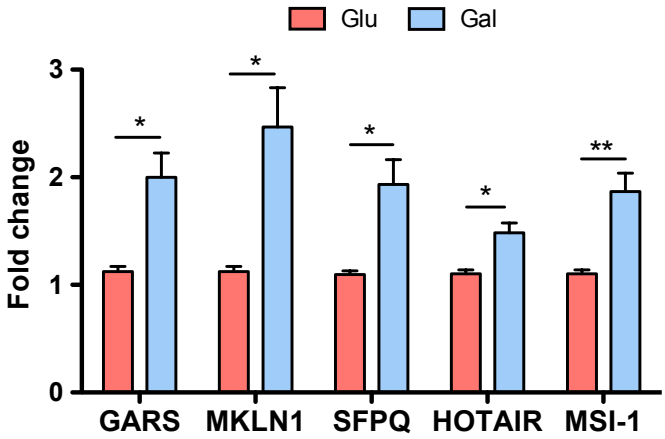

Figure 15. RT-qPCR analysis of relative mRNA expression levels of LncRNA genes in Glu-CC and Gal-CC. mRNA expression levels for each target gene are normalized to β-actin levels (n=2-3 biological replicates per tumor, 2 technical replicates). Data are presented as fold-change. Glu was set as 1.0. Holm-Sidak t-test statistical analysis: (*) = p< 0.05; (**) = p<0.01; (***) = p<0.001

Furthermore, as tumorigenesis is a hallmark of CSCs, *in vivo* Extreme Limiting Dilution Assays (ELDA) were performed to assess the tumorigenic potential and CSC frequency of PDAC cells cultured in Glu-CC or Gal-CC. The nuclear Histone H2B of PANCA6L was marked with mCherry (red) via lentiviral infection of these cells with an mCherry-H2B vector. Following infection, cells were sorted to obtain only a PANCA6L mCherry-H2B positive population to maintain in culture for future experiments. PANCA6L mCherry-H2B positive Glu-CC and Gal-CC were injected subcutaneously in Athymic nude mice at different dilutions of cells per injection (50000-10000-5000-1000). After 3 months, tumor data were analyzed. Interestingly, the size and weight of tumors derived from Glu-CC were not significantly greater than those derived from Gal-CC in all the dilutions that we evaluated (**Figures 16A-B**). Likewise, the tumors were digested to analyze by flow cytometry the percentage of mCherry-H2B positive (mCherry-H2B^{+}) cells inside tumors derived from Glu-CC and Gal-CC. The results showed that the percentage of mCherry-

H2B positive cells was very similar in tumors derived from Glu-CC and Gal-CC across all cell dilutions injected (**Figure 16C**). However, the tumor incidence derived from Gal-CC was significantly higher compared to those derived from Glu-CC at all dilutions tested (**Figure 16D**). Moreover, we analyzed the percentage of CD133 positive ($CD133^+$) cells inside the mCherry-H2B positive cell population within each tumor by flow cytometry. The percentage of CD133 positive cells was significantly higher in the vast majority of tumors derived from Gal-CC compared to tumors derived from Glu-CC (**Figure 16E**), indicating an expansion of the CSC compartment within the tumors. To validate this conclusion, the CSC frequency was calculated using the ELDA software (**Figure 16F**), and the frequency of CSCs was significantly higher in Gal-CC (1/14,741) compared to Glu-CC (1/75,781).

Taken together, the sum of these data indicates that there exists an enrichment in CSCs population, both at the molecular and functional level, when cells are cultured in conditions that demand OXPHOS (Gal-CC) compared to conditions that favor glycolytic metabolism (Glu-CC).

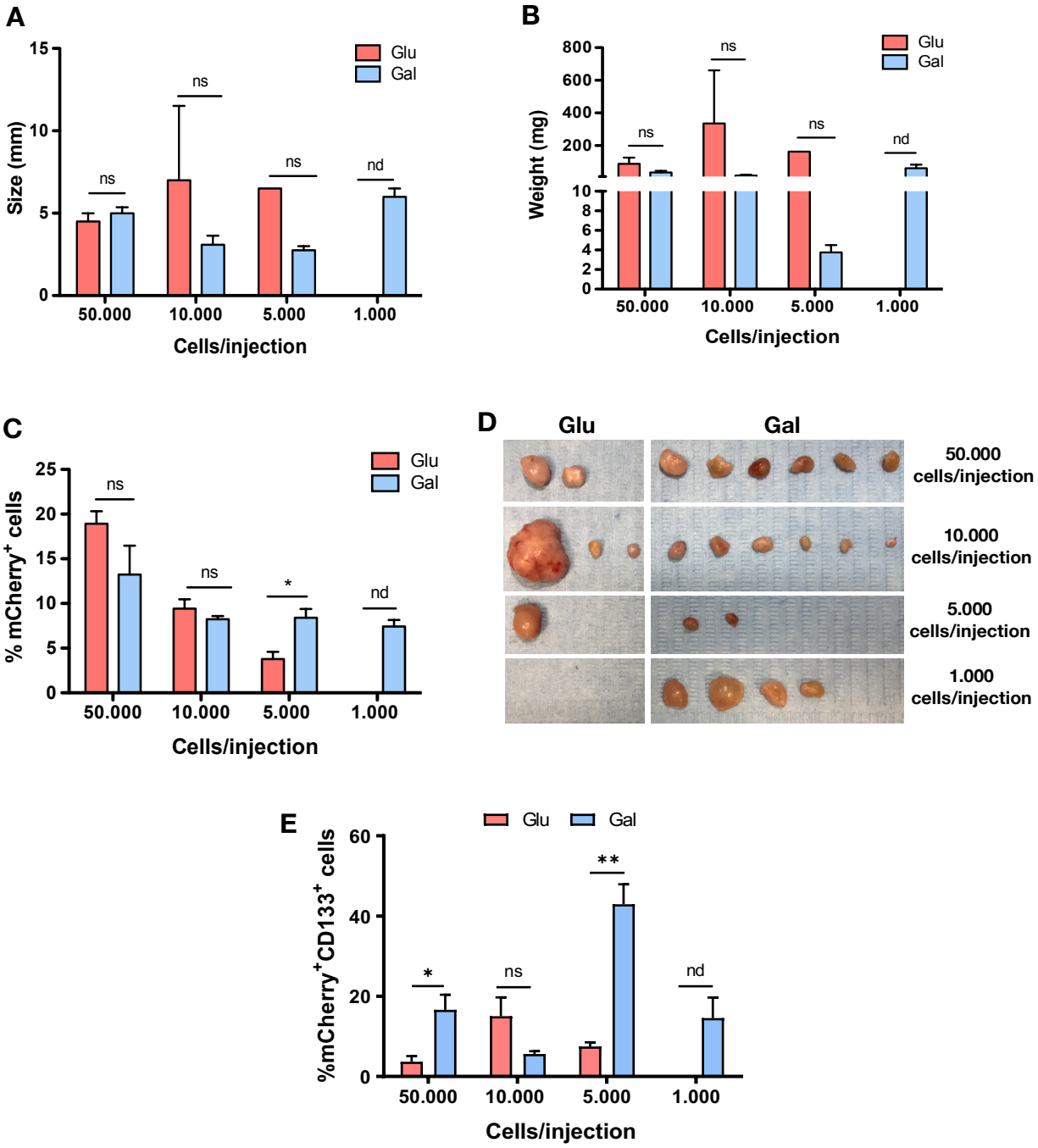

F

Nº of cells injected		50.000	10.000	5.000	1.000	Freq	Freq (%)	P value
PANCA6L mCherry-H2B	Glu	2/8	3/8	1/8	0/8	1/75781	0,000013	0,000287
	Gal	6/8	6/8	2/8	4/8	1/14741	0,000068	

Figure 16. (A) Average tumor size, (B) weights and (C) quantification by FACS of the percentage of mCherry$^+$ cells after digestion of Glu-CC and Gal-CC tumors. (D) Images of tumors obtained at the time of sacrifice for an extreme limiting dilution assay (ELDA) with 1×10^3 to 5×10^4 mCherry-H2B PANCA6L Glu-CC and Gal-CC. (E) Flow cytometric quantification of the percentage of double-positive mCherry$^+$CD133$^+$ cells after digestion of Glu-CC and Gal-CC tumors. (F) Number of tumors obtained, the frequency (Freq) and percent (%) of CSCs present in the Glu-CC and Gal-CC tumors as a function of the dilutions tested. CSCs frequencies were calculated using the Extreme Limiting Dilution Analysis software. Holm-Sidak t-test statistical analysis: (*) = $p< 0.05$; (**) = $p<0.01$; (***) = $p<0.001$; (ns)= not significant; (nd)= not determined.

3. PDAC cells increase mitochondrial-dependent metabolism (OXPHOS) in the presence of galactose as unique carbon source

Once greater enrichment of CSCs, in galactose conditions compared to glucose conditions, was verified we needed to confirm whether cells cultured in the presence of galactose have increased mitochondrial metabolism compared to those cultured in glucose. For this reason, we performed different experiments to evaluate the OXPHOS metabolism of Glu-CC and Gal-CC.

Firstly, markers of mitochondrial mass (MitoTracker DeepRed FM and MitoTracker MitoBlue), membrane potential (MitoTracker-CMXRos and MitoTracker CMH2XRos) and reactive oxygen species (ROS) (MitoSOX™) were analyzed by flow cytometry in the 4 primary PDAC cultures (**Figure 17A**). Of the mitochondrial and ROS markers analyzed, all of them significantly increased about 2-fold in Gal-CC compared to Glu-CC (**Figure 17B**), suggesting increased OXPHOS (defined by electron-transport-chain + ATPsynthase) and ROS production. Since some of the aforementioned probes depend on membrane potential, we additionally tested MitoTracker Green and Nonyl Acridine Orange (NAO), and a similar significant increase in mitochondrial mass was observed (**Figures 17C-D**). To functionally validate these findings, we measured the Oxygen Consumption Rates (OCR) of PANC185 Glu-CC and Gal-CC (**Figure 18A**) in the presence or absence of distinct inhibitors of mitochondrial function. Baseline OCR was significantly higher in Gal-CC compared to Glu-CC, and both the maximal respiration and the Spare Respiratory Capacity (SRC), which are essential for cells to respond to acute stress, increased significantly in Gal-CC compared to Glu-CC (**Figures 18A-B**). Therefore, these results indicated that OXPHOS metabolism increases in Gal-CC compared to Glu-CC. Moreover, proton leak was also significantly higher in Glu-CC, indicating decreased mitochondrial efficiency (**Figure 18B**).

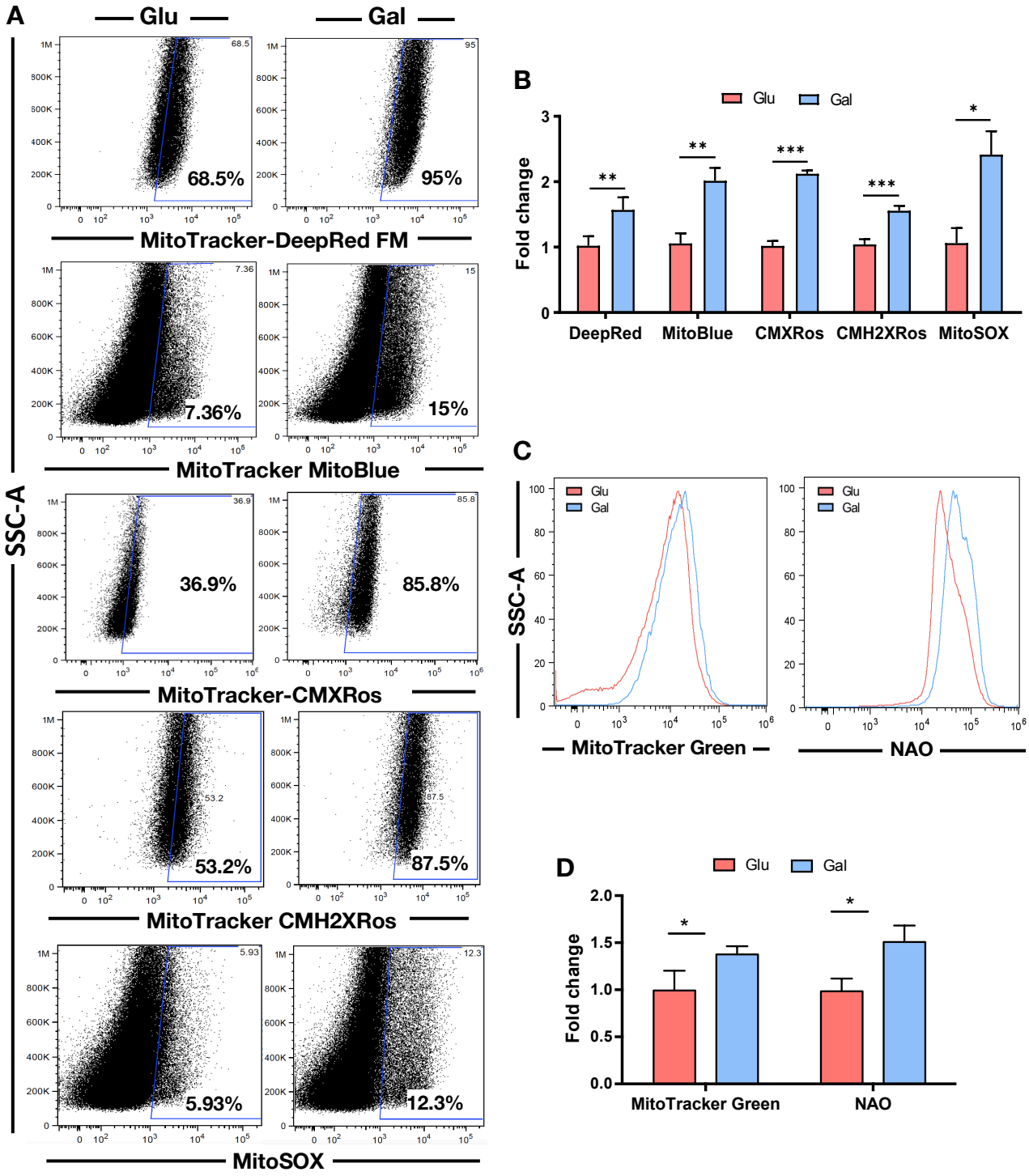

Figure 17. (A) Representative flow cytometric dot plots of the expression of different mitochondrial markers (MitoTracker-DeepRed FM, MitoTracker MitoBlue, Mitotracker-CMXRos, MitoTracker CMH2XRos) and ROS marker (MitoSOX) in Glu-CC and Gal-CC. (B) Quantification of the levels of the different markers in Glu-CC and Gal-CC (n=2-3 biological replicates per tumor). Data are presented as fold-change. Glu was set as 1.0. (C) Representative flow cytometric dot plots of the expression of different mitochondrial markers MitoTracker Green FM and Nonyl Acridine Orange (NAO) in Gluc-CC and Gal-CC. (D) Quantification of the levels of the mitochondrial markers in Gluc-CC and Gal-CC (n=2-3 biological replicates per tumor). Data are presented as fold-change. Glu was set as 1.0. Holm-Sidak t-test statistical analysis: (*) = p< 0.05; (**) = p<0.01; (***) = p<0.001; (ns)= not significant.

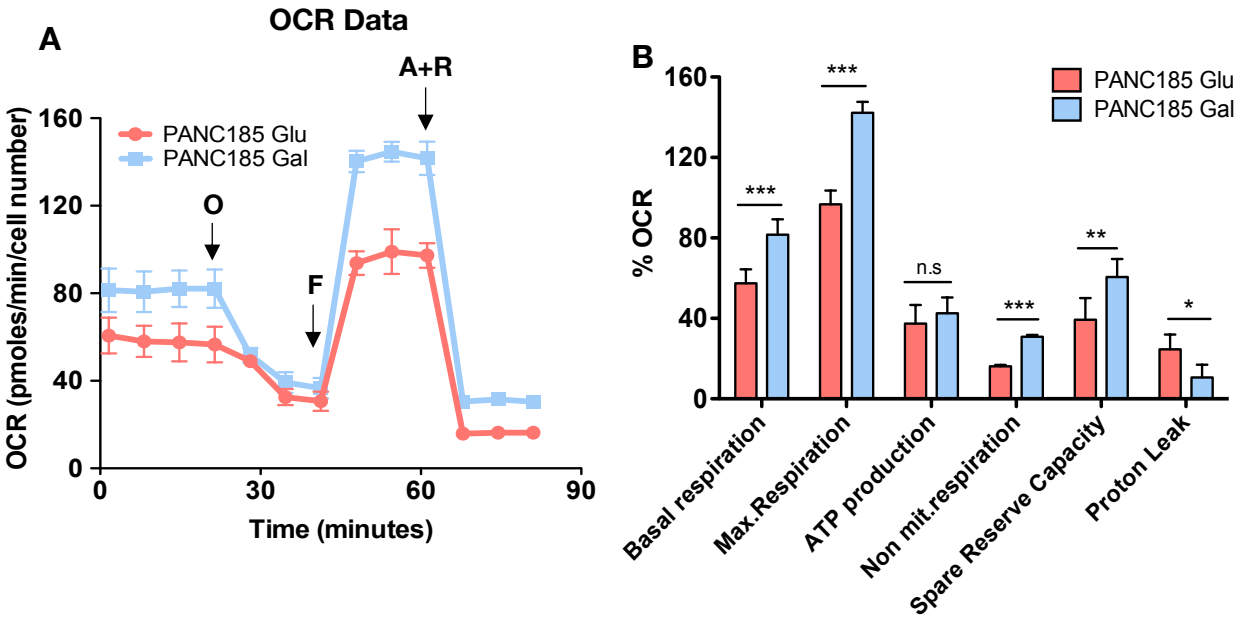

Figure 18. (**A**) Representative Oxygen Consumption Rate (OCR) plot, normalized to cell number, for PANC185 Glu-CC and Gal-CC, which were treated with distinct inhibitors of mitochondrial function: O (oligomycin), F (FCCP), A (antimycinA) and R (rotenone). Continuous OCR values (pmoles/min/cell) are shown. (**B**) Measured and calculated parameters of OCR generated from 3 samples per group. Holm-Sidak t-test statistical analysis: (*) = p< 0.05; (**) = p<0.01; (***) = p<0.001; (ns)= not significant.

As expected, Extracellular Acidification Rate (ECAR) revealed more acidification by glucose fermentation (glycolysis) in Glu-CC compared to Gal-CC (**Figure 19A**), highlighting that Gal-CC prefer OXPHOS metabolism over glycolysis. To confirm this data, and in collaboration with the laboratory of Dr. Patricia Sancho at Hospital Miguel Servet in Zaragoza, we performed a lactate production analysis for both culture conditions. As expected, Glu-CC presented significantly higher lactate production compared to Gal-CC in all primary PDAC tumors (**Figure 19B**). However, at the level of ATP, no significant differences were observed in total ATP levels between Glu-CC and Gal-CC at the time point examined (**Figure 19C**), which reflects differences in either the kinetics of ATP production and/or consumption or glycolytic rate compensations between Glu-CC and Gal-CC[167].

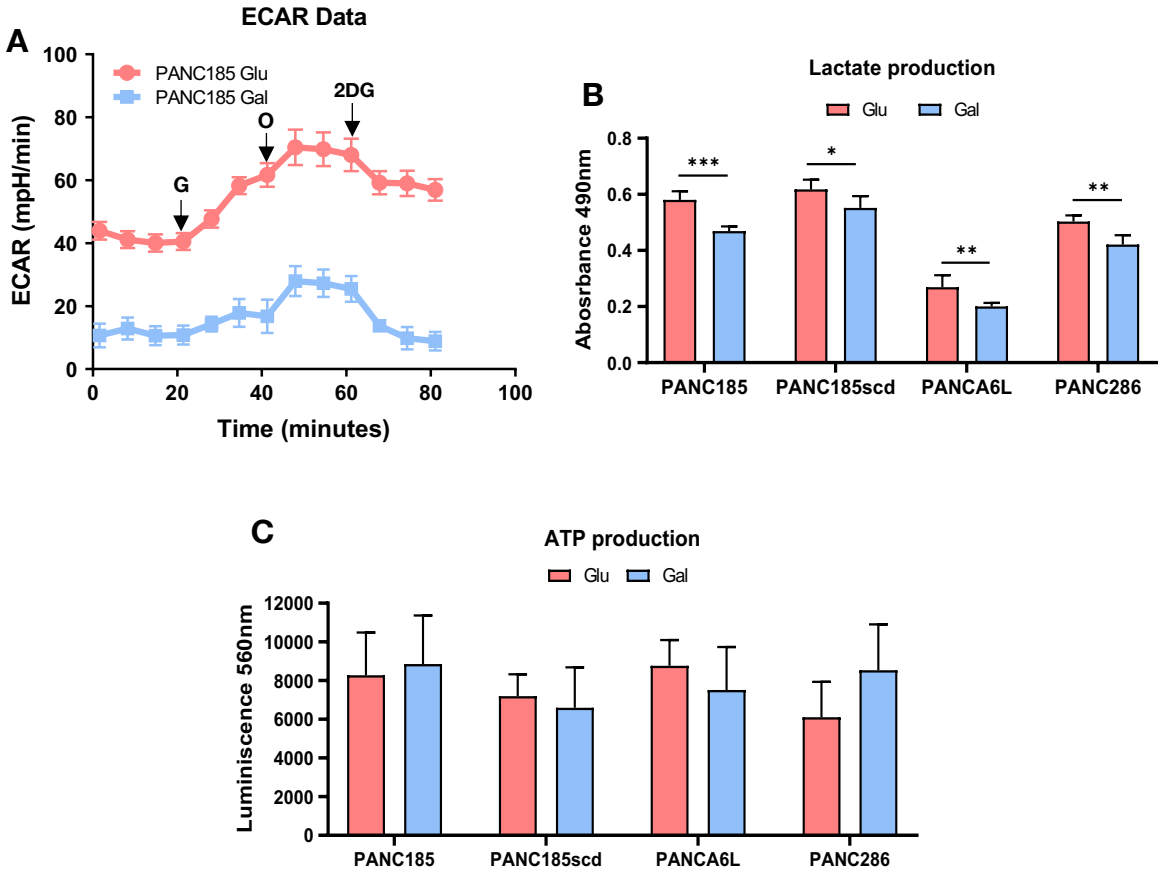

Figure 19. (**A**) Extracellular acidification rate (ECAR) measurements in Glu-CC and Gal-CC subjected to sequential injections of glucose (G), Oligomycin (O) and 2-deoxyglucose (2DG). (**B**) Quantification of the levels of lactate production by absorbance spectrophotometry, using an ELISA as per the manufacturer's instructions, normalized to total protein content in Glu-CC and Gal-CC (n=6 samples per group). (**C**) Quantification of the levels of ATP production by luminescence spectrophotometry, normalized to total protein content in Glu-CC and Gal-CC (n=6 samples per group). Holm-Sidak t-test statistical analysis: (*) = $p< 0.05$; (**) = $p<0.01$; (***) = $p<0.001$; (ns)= not significant.

Moreover, at transcriptional level, we evaluated genes related to mitochondrial activity (PGC-1α), electron transport chain complexes (NDUFA9-Complex I and MT-COI-Complex IV) and mitochondrial 16S ribosomal RNA gene (MT-RNR2) by RT-qPCR in Glu-CC and Gal-CC. All the transcripts evaluated significantly increased about 2-fold in Gal-CC compared to Glu-CC in all primary PDAC cultures (**Figure 20A**). Importantly the levels of PGC-1α, a key regulator of energy metabolism that stimulates mitochondrial biogenesis, promotes OXPHOS metabolism and is overexpressed in PaCSCs[168], was expressed to significantly higher levels in Gal-CC compared to Glu-CC. Moreover, NRF2 and PARKIN, related to the regulation of antioxidant proteins[169] and recycling of mitochondria via the coordinated process of mito-fusion, mito-fision and mitophagy[170] respectively, were also significantly increased in Gal-CC compared to Glu-CC (**Figure**

20A). Lastly, analysis of mtDNA by qPCR analysis of the gene MT-RNR1 revealed increased mitochondrial DNA copy numbers in Gal-CC compared to Glu-CC (Figure 20B), consistent with more mitochondrial biogenesis.

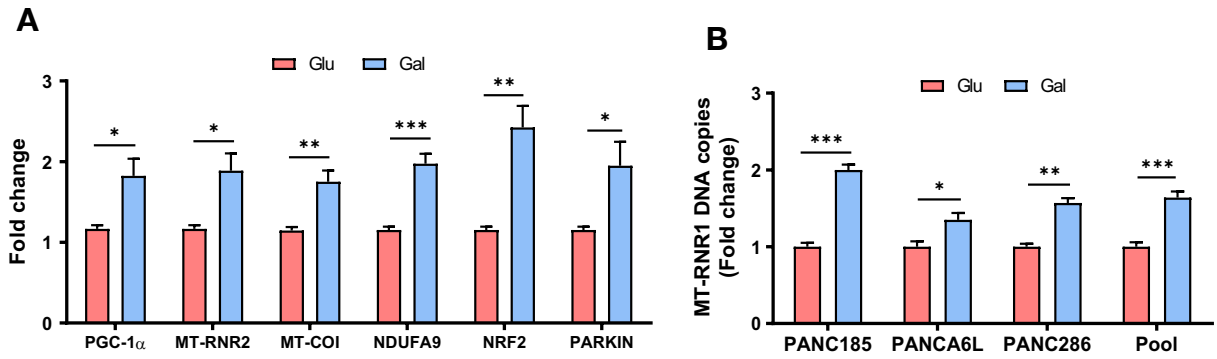

Figure 20. (A). RT-qPCR analysis of relative mRNA expression levels of different genes related to mitochondrial activity and electron transport chain complexes and ROS neutralization in Glu-CC and Gal-CC. mRNA expression levels for each target gene are normalized to β-actin levels (n=2-3 biological replicates per tumor, 2 technical replicates). Data are presented as fold-change. Glu was set as 1.0. (B) Quantification of the levels of DNA of the mitochondrial 12S ribosomal gene (MT-RNR1) by qPCR in Glu-CC and Gal-CC for each PDAC culture and Pooled samples. Data are normalized to β-Actin expression. Data are presented as fold-change. Glu was set as 1.0. Holm-Sidak t-test statistical analysis: (*) = p< 0.05; (**) = p<0.01; (***) = p<0.001.

To complement these analyses, immunofluorescence was performed in order to visualize the distribution of mitochondrial markers in PANC185 and PANCA6L inside the cells in Glu-CC and Gal-CC. We observed a significant increase in the percentage of MitoTracker-DeepRed (red) and MitoTracker-CMXRos (green) fluorescent area in Gal-CC compared to Glu-CC (Figures 21A-C). Interestingly, we could observe that the cells on the borders of the clones in Gal-CC showed more intense staining of the indicated mitochondrial markers (Figure 21D), which could suggest that these peripheral cancer cells could be helping the cancer cell population at the level of migration, as migratory cancer cells have a greater energy demand[171,172].

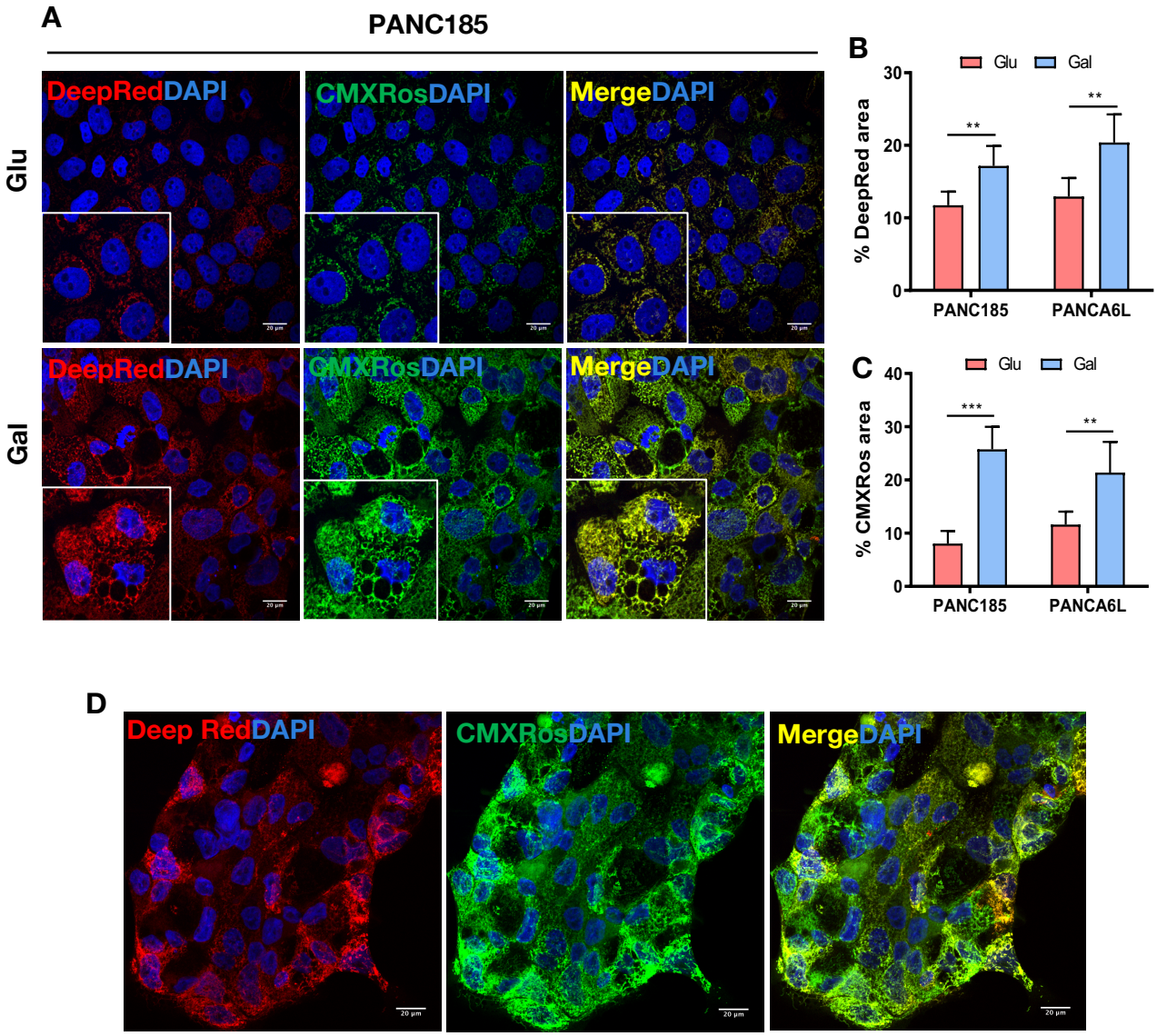

Figure 21. (A). Representative fluorescent images of Mitotracker DeepRedFM (red), CMXRos (green) and DAPI (blue) staining in PANC185 Glu-CC and Gal-CC. (B-C) Quantification of the percentage of fluorescent area for (B) MitoTracker-DeepRed FM mitochondrial biomarker or the (C) CMXRos mitochondrial membrane potential marker in PANC185 and PANCA6L Glu-CC and Gal-CC, using ImageJ. (n= 6 samples per group). (D) Representative fluorescent images of Mitotracker DeepRedFM (red), CMXRos (green) and DAPI (blue) staining in PANC185 Gal-CC. Holm-Sidak t-test statistical analysis: (*) = p< 0.05; (**) = p<0.01; (***) = p<0.001.

In addition, when we used markers of mitochondrial mass (TOM20), the mitochondria of Gal-CC were visually denser (Figure 22A), and immunofluorescence analysis revealed a significant increase in TOM20 staining, approximately 2-fold in Gal-CC compared to Glu-CC (Figure 22B), which was also used to show that the mitochondrial network in Gal-CC was more extensive compared to Glu-CC, as analyzed using ImageJ (Figure 22D). For optimal maintenance of mitochondrial metabolism and greater mitochondrial activity, the coordinated process of mito-fusion, mito-fision and mitophagy must be active in order

to eliminate aged and dysfunctional mitochondria. This process is governed by several proteins including PARKIN, a mitochondrial E3-ligase which acts in a quality control manner to ubiquitinate and induce the removal of damaged mitochondria or excess mitochondria from the cell via a process known as mitophagy[170,173]. We observed greater expression of PARKIN by immunofluorescence (**Figures 22A, C**) and by flow cytometry (**Figures 22E-F**) in Gal-CC compared to Glu-CC, indicative of active mitochondrial recycling.

Together, these data suggested that Gal-CC not only contain more mitochondria, but the mitochondria of Gal-CC are more functional and their maintenance/recycling may be more effective compared to Glu-CC, which are more glycolytic and less dependent on functional mitochondria.

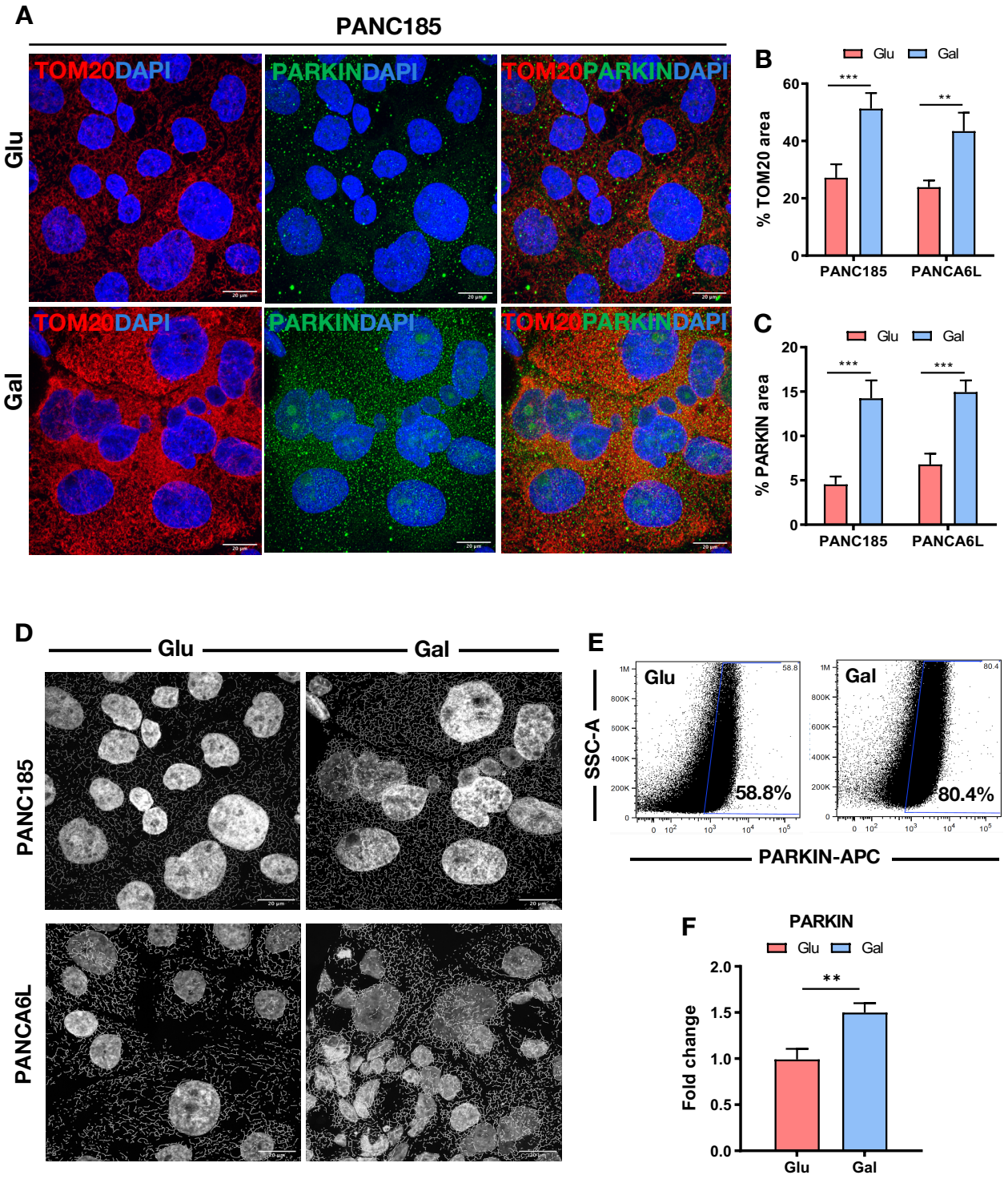

Figure 22. (A) Representative immunofluorescent images of TOM20 (red), PARKIN (green) and DAPI (blue) staining in PANC185 Glu-CC and Gal-CC. (B-C) Quantification of the percentage of fluorescent area for the (B) TOM20 mitochondrial marker or (C) PARKIN in PANC185 and PANCA6L Glu-CC and Gal-CC, using ImageJ (n= 6 samples per group). (D) Mitochondrial network visualized using an anti-TOM20 Ab, and displayed as a skeleton network using ImageJ skeleton filter, comparing Glu-CC with Gal-CC from PANc185 and PANCA6L. (E) Representative flow cytometric dot plots of intracellular PARKIN staining in PANC185 Glu-CC and Gal-CC. (F) Quantification of the levels of Parkin in Glu-CC and Gal-CC (n=4 samples per group). Data are presented as fold-change. Glu was set as 1.0. Holm-Sidak t-test statistical analysis: (*) = p< 0.05; (**) = p<0.01; (***) = p<0.001.

4. Mitochondrial-dependent metabolism (OXPHOS) causes an increase in autophagy

Once we confirmed that Gal-CC enriches for CSC with more mitochondria and enhanced mitochondrial function (increased OXPHOS), we next directed our attention to the levels of autophagy in Gal-CC versus Glu-CC based on morphological difference observed and as described below.

Autophagy is another described CSC feature[174,175]. Several publications have investigated autophagy in the context of cancer, and it has been suggested that CSCs have more autophagic flux to help them to better survive under stressful conditions (e.g. lack of nutrients, hypoxia and chemotherapeutics) inside the tumor[176–180]. In this sense, by brightfield microscopy, we observed that there were morphological differences between Glu-CC and Gal-CC in all our primary PDAC cultures (Figure 23). While Glu-CC grew as large homogeneous monolayers, Gal-CC grew forming smaller and more compact clones. Moreover, we observed significantly more vacuolar bodies in the cytoplasm of Gal-CC whereas in Glu-CC these structures seemed to be less abundant (Figure 23).

PANC185

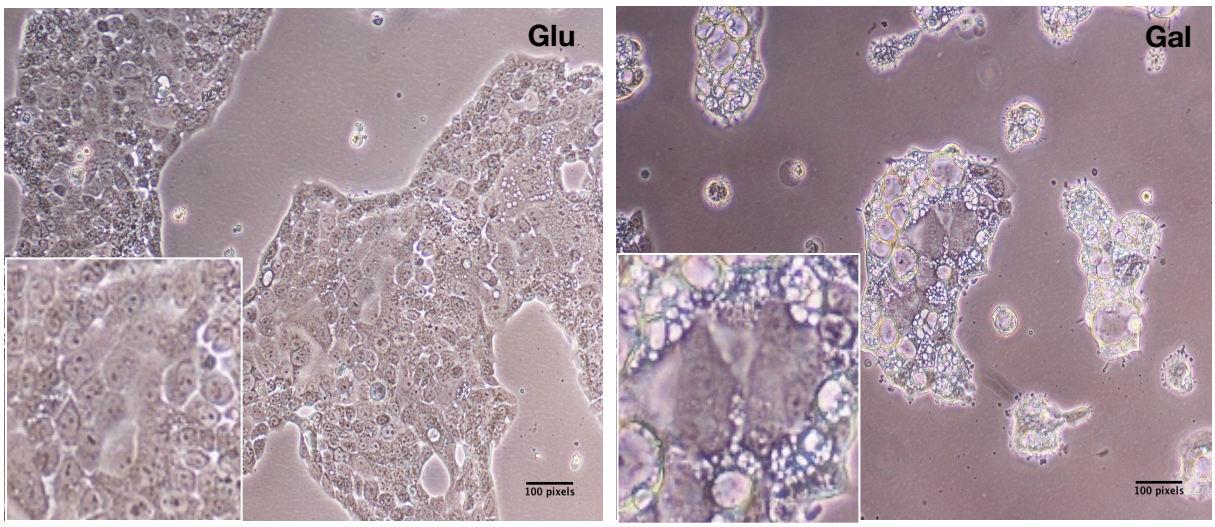

Figure 23. Representative brightfield images of 14 days of PANC185 Glu-CC and Gal-CC, taken by optical microscopy with objective 4x.

For these reasons, we evaluated these vacuolar bodies by TEM. TEM analysis confirmed an enrichment in cellular structures reminiscent of autophagic vesicles in Gal-

CC (Figures 24A-B, red arrows and blue and orange squares). We quantified the number of autophagic vesicles from a stack of TEM images and determined that the number was significantly greater (2-fold) in Gal-CC compared to Glu-CC (Figure 24C).

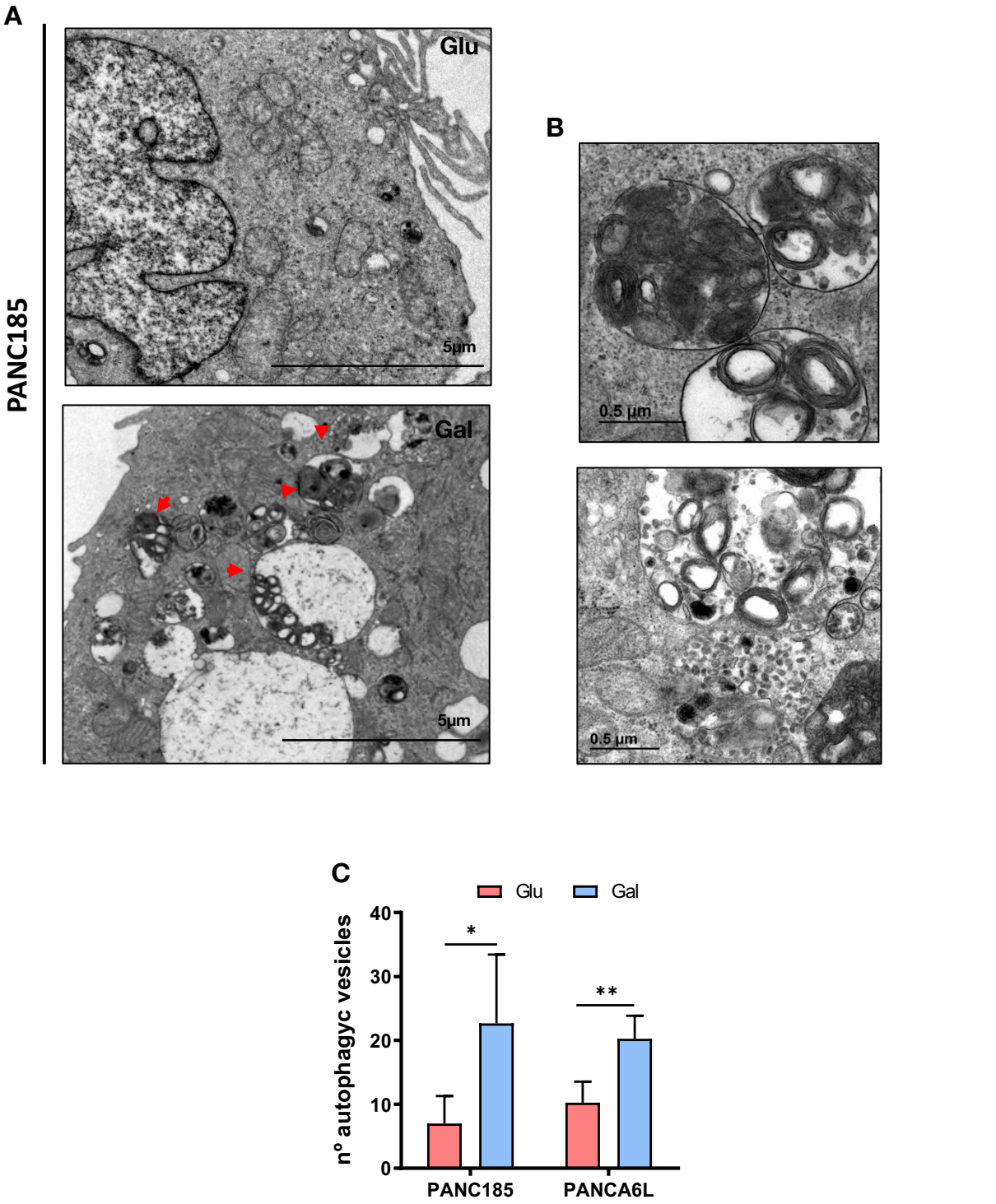

Figure 24. (A). Representative transmission electron micrographs of 14 days PANC185 Glu-CC or Gal-CC with 12k magnification. (B) Representative autophagic structures from Gal-CC with 50k magnification. (C) Number of autophagic vesicles in the TEM images of 14 days PANC185 and PANCA6L Glu-CC and Gal-CC were quantified by ImageJ (n= 6 random areas per culture). Holm-Sidak t-test statistical analysis: (*) = p< 0.05; (**) = p<0.01; (***) = p<0.001.

We next performed an immunofluorescence analysis of LC3B I-II and LAMP-1, both of which are essential proteins related to the autophagy process (**Figure 25A**). The quantification of the percentage of fluorescent area of both proteins revealed that Gal-CC had a significant higher percentage of LC3B I-II and LAMP-1 fluorescent area compared to Glu-CC (**Figures 25B-C**) in both PANC185 and PANCA6L, suggesting increased autophagy and lysosome number.

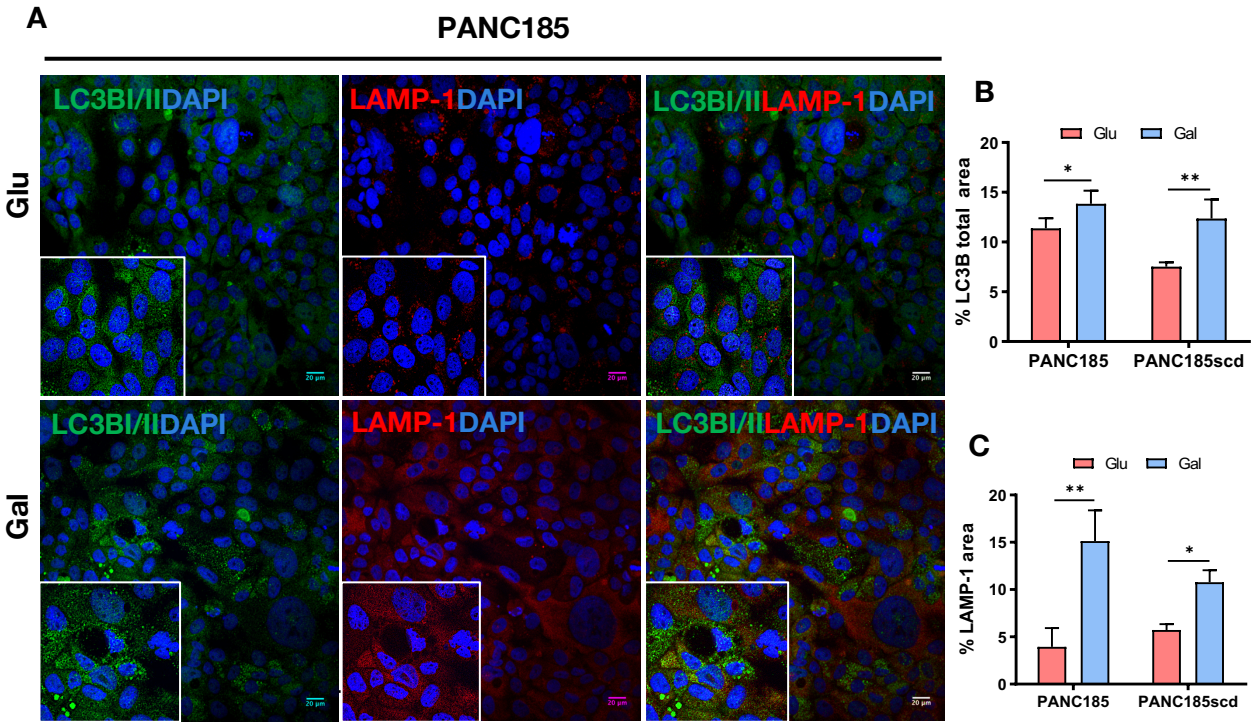

Figure 25. (**A**). Representative immunofluorescence images of PANC185 Glu-CC and Gal-CC stained with anti-LC3BI/II (green), anti-LAMP-1 (red) and DAPI (blue). (**B**) Quantification of the levels of the percentage of fluorescence area with ImageJ for LC3BI/II comparing Glu-CC and Gal-CC. (n= 6 samples per group). (**C**) Quantification of the percentage of fluorescent area for LAMP-1 in PANC185 and PANCA6L Glu-CC and Gal-CC, using ImageJ (n= 6 samples per group). Holm-Sidak t-test statistical analysis: (*) = p< 0.05; (**) = p<0.01; (***) = p<0.001.

To confirm these results, we analyzed the basal levels of LC3B I and LC3B II by Western Blot analysis (**Figure 26A**) and observed that the levels of LC3B II increased in each PDAC culture when cultured in the presence of galactose compared to glucose (**Figure 26B**). At the transcriptional level, we evaluated the expression of a key regulator of autophagy, ATG5. ATG5 was significantly increased by more than 2-fold in the majority of primary PDAC cultures in Gal-CC compared to Glu-CC (**Figure 26C**).

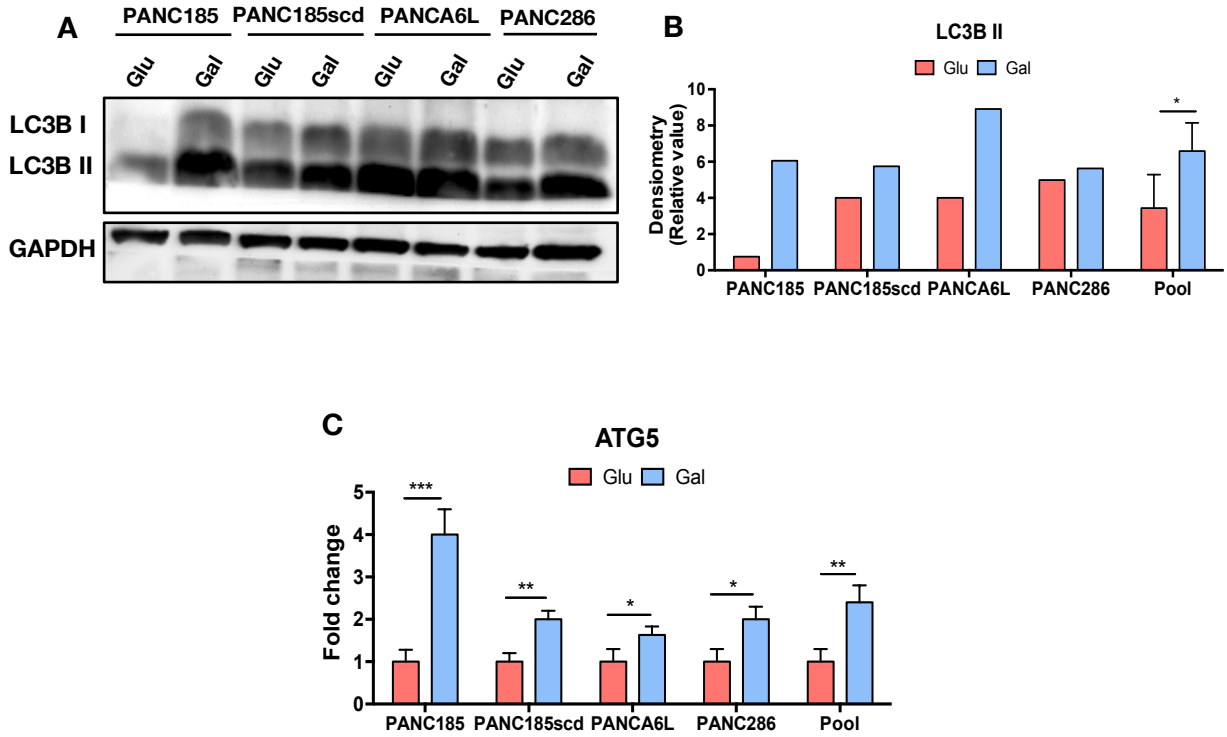

Figure 26. (A) WB analysis of LC3BI/II in Glu-CC and Gal-CC PDAC cultures. GAPDH was used as loading control. (B) Densitometric quantification of LC3BII expression in (A), normalized to GAPDH levels and expressed as relative values for each tumor or Pooled samples. (C) RT-qPCR analysis of relative mRNA expression levels of ATG5 in Glu-CC and Gal-CC PDAC cultures. mRNA expression levels for each target gene are normalized to β-actin levels (n=3 biological replicates per tumor, 2 technical replicates). Data are presented as fold-change. Glu was set as 1.0. Holm-Sidak t-test statistical analysis: (*) = p< 0.05; (**) = p<0.01; (***) = p<0.001.

Finally, we evaluated the autophagy flux to definitively show an increase in autophagy in Gal-CC compared to Glu-CC. Both PANC185 and PACN185scd were treated with Bafilomycin A1 (Baf) in Glu-CC and Gal-CC. Bafilomycin A1 is a known inhibitor of the late phase of autophagy, which prevents the maturation of autophagic vacuoles by inhibiting fusion between autophagosomes and lysosomes[181]. After 6 hours post-treatment, the levels of LC3B I and LC3B II were evaluated by WB analysis in PANC185 (Figure 27A) and PANC185scd (Figure 27B), and a significant increase in the autophagic flux was calculated for PDAC cells cultured in galactose compared to glucose (Figure 27C). To calculate the autophagic flux, the following formula was used:

- (Glu+Baf) – Glu = X
- (Gal+Baf) – Gal =Y

→ X / Y =

- > 1 = more flux Gal-CC vs. Glu-CC
- ≤ 1 = equal/less flux Gal-CC vs. Glu-CC

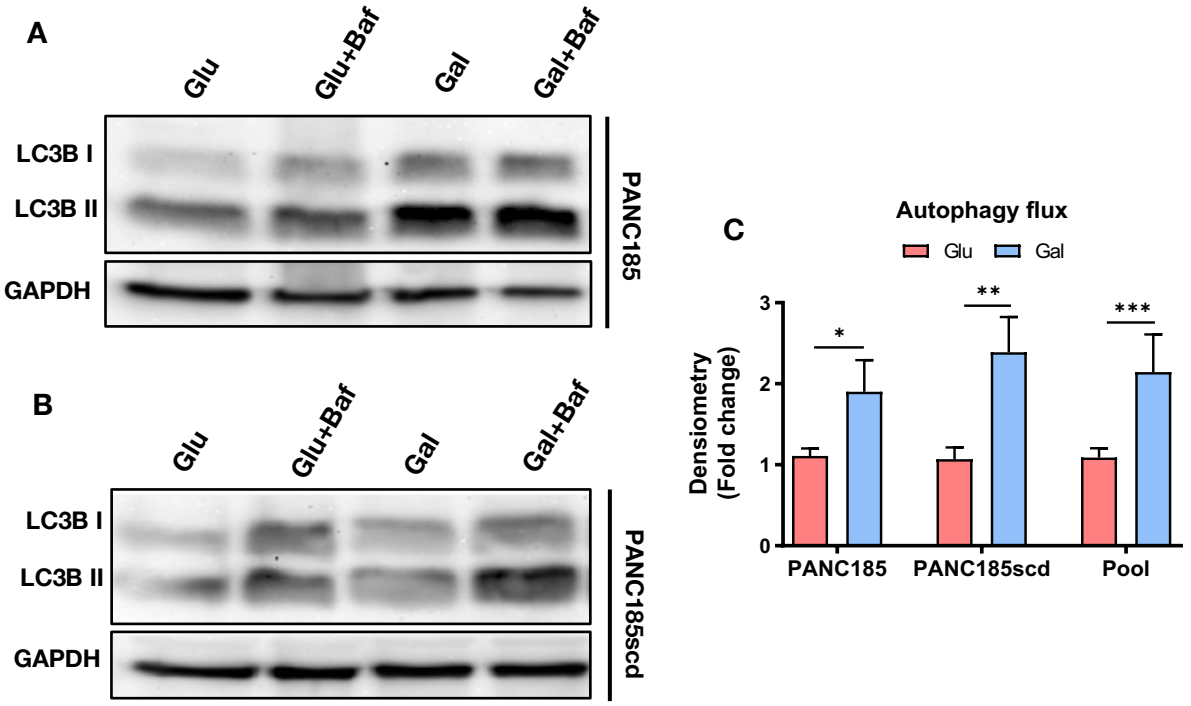

Figure 27. (A). WB analysis of LC3B I and LC3B II in Glu-CC and Gal-CC untreated (Glu, Gal) or treated with the autophagy inhibitor (Baf=Bafilomycin). GAPDH was used as loading control. (B) Autophagic flux determined by densitometric quantification of LC3B-II accumulation after autophagy inhibitor addition, subtracting their respective control expression levels, in 3 independent experiments. Data are presented as fold-change. Glu was set as 1.0. Holm-Sidak t-test statistical analysis: (*) = p< 0.05; (**) = p<0.01; (***) = p<0.001.

Taken together, these data demonstrated that Gal-CC contain more autophagic vesicles due to the presence of a higher autophagic flux compared to Glu-CC, suggesting is also likely an important mechanism used by OXPHOS-dependent cells to survive under metabolically restrictive conditions.

5. Mitochondrial-dependent metabolism (OXPHOS) causes an arrest in cell cycle and promotes cellular quiescence

Once confirmed that Gal-CC enriches for CSC with more mitochondria, enhanced mitochondrial function (increased OXPHOS) and increased autophagy, the next step was to evaluate the cell cycle and the senescence and quiescence status of Glu-CC versus Gal-CC.

Due to the proliferative differences observed between Glu-CC and the Gal-CC evaluated earlier using IncuCyte Zoom System in Figure 11A and the microscopy-based observations comparing the growth between Glu-CC and Gal-CC in Figure 23, we next evaluated the cell cycle profile of Glu-CC and Gal-CC. Numerous studies have described that CSCs are in a "slow-cycling" stage and that they proliferate slower than more differentiated tumor cells (non-CSCs)[182]. Therefore, a slow proliferation or quiescent stage is considered a CSC phenotype, essential to the metastatic potential of tumor cells. In this sense, to further asses proliferation, we analyzed the cell cycle of Glu-CC and Gal-CC by flow cytometry using Propidium Iodide (PI) dye. We found that Gal-CC were less proliferative compared to Glu-CC. Specifically, Gal-CC were arrested in G0/G1 and S phases whereas Glu-CC were in G2/M phase (Figure 28). As mentioned above, this difference is in line with the idea that CSCs are believed to have a slower cell cycle compared to non-CSCs.

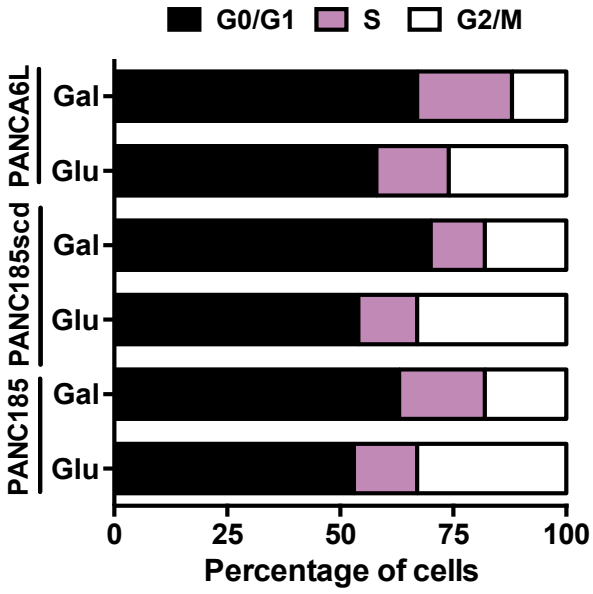

Figure 28. Cell cycle analysis of Glu-CC and Gal-CC PDAC cultures (PANC185, PANC185scd and PANCA6L) determined by flow cytometric analysis using Propidium Iodide (PI).

Importantly, contrary to quiescence, senescence is a degenerative process in which a cell can no longer proliferate ensuring a certain cell death; however, senescence and quiescence are frequently used interchangeably. Thus, a senescence assay was performed in order to determine if galactose was affecting cell proliferation by inducing cell senescence. Both Glu-CC and Gal-CC were labelled with β-galactosidase (**Figure 29A**), and we quantified the percentage of β-galactosidase positive area by ImageJ. The β-galactosidase positive area was significantly lower (approximately 2-fold) in Gal-CC compared to Glu-CC (**Figure 29B**), suggesting that Gal-CC are less senescent than Glu-CC.

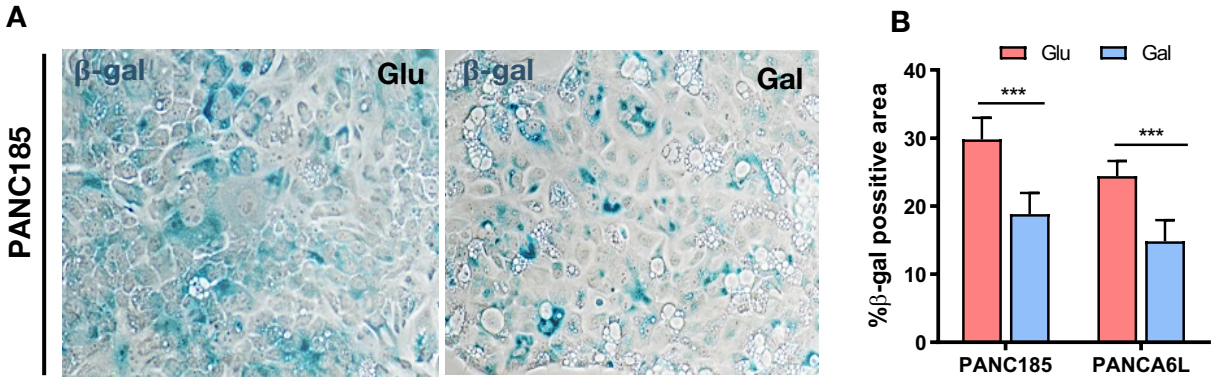

Figure 29. (**A**) Representative brightfield images by β-galactosidase staining of PANC185 Glu-CC and Gal-CC (blue). (**B**) Quantification of the percentage of β-galactosidase positive area in Glu-CC and Gal-CC, using ImageJ (n= 6 samples per group). Holm-Sidak t-test statistical analysis: (*) = p< 0.05; (**) = p<0.01; (***) = p<0.001.

Once senescence had been ruled out as a possible cause of the slow proliferative phenotype of Gal-CC, we performed a quiescence assay by labelling cultures with PKH26 dye (**Figure 30A**). PKH26 is a red fluorescent plasma membrane lipophilic dye, which was evaluated by flow cytometry at different time intervals (3, 7 and 14 days) in both Glu-CC and Gal-CC (**Figure 30B**).

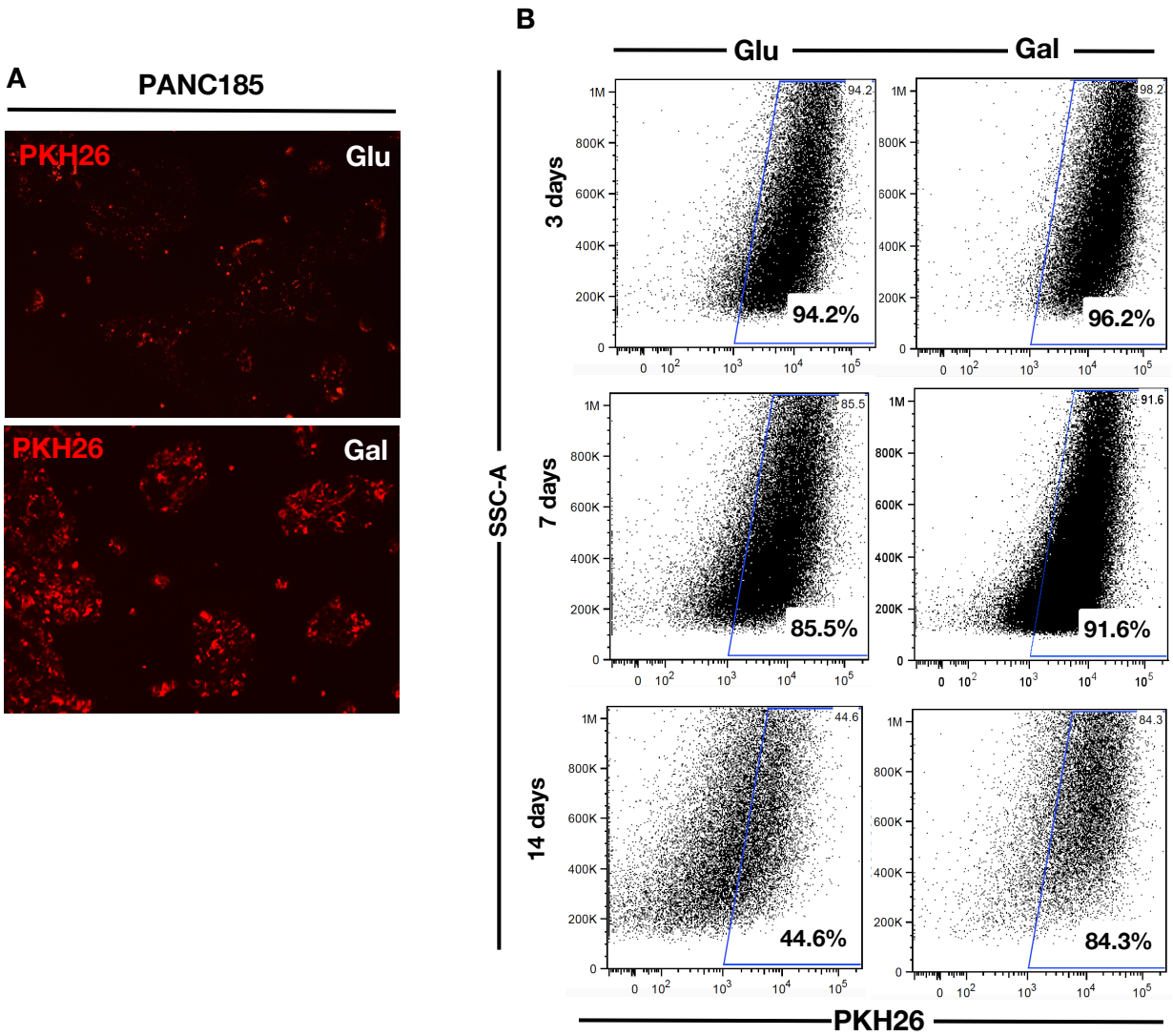

Figure 30. (A). Representative fluorescent images of PANC185 Glu-CC and Gal-CC stained with PKH26 (red) at 14 days. (B) Representative FACS dot plots of PKH26 staining in Glu-CC and Gal-CC at different times (3, 7 and 14 days).

At 3 days, flow cytometric analysis showed that in both Gal-CC and Glu-CC the percentage of PKH26 positive cells were very similar in all of PDAC primary cultures (Figures 31A-D). At 7 days, in most primary PDAC cultures, flow cytometric analysis showed a significant reduction of more than 15% in the percentage of PKH26 positive in Glu-CC, whereas in Gal-CC, the percentage of PKH26 positive cells did not significantly change (Figures 31A-D). Finally, at 14 days, more than a 50% significant reduction in the percentage of PKH26 positive in Glu-CC was observed, whereas in Gal-CC, the percentage of PKH26 positive cells were reduced between 10-15% (Figures 31A-D).

Importantly, to determine if 14-day Gal-CC were permanently fixed in a quiescent state or could recover their normal proliferation, the galactose medium was changed for glucose medium and the percentage of PKH26 positive cells was determined 7 days later. Interestingly, in as little as 7 days post medium change to glucose, all of the primary PDAC cultures showed a significant reduction in the percentage of PKH26 positive cells in approximately of 80% (Figure 31E). Of note, this decrease was much greater/faster than that observed in Gal-CC at 7 days post changing to Glu-containing media (Figures 31A-D).

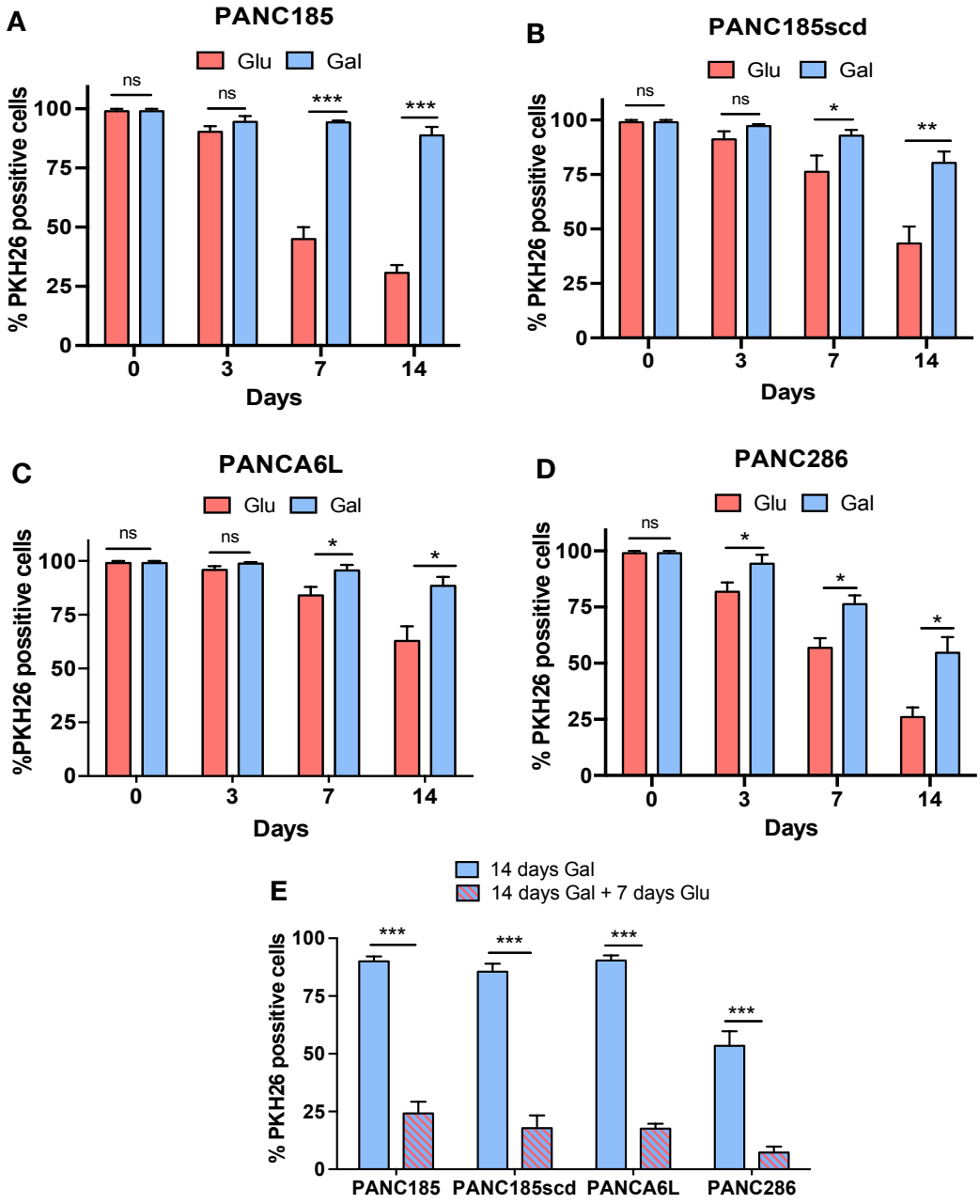

Figure 31. (A-D) Quantification of the percentage of PKH26 positive cells at different times (0, 3, 7 and 14 days) for Glu-CC to Gal-CC: (A) PANC185, (B) PANC185scd, (C) PANCA6L and (D) PANC286 (n= 3 samples per group). (E) Percentage of PKH26 positive cells in Gal-CC after 14 days in galactose-containing media and 7 days after substitution with glucose (n= 3 samples per group). Holm-Sidak t-test statistical analysis: (*) = p< 0.05; (**) = p<0.01; (***) = p<0.001.

Finally, to further evaluate the quiescence potential of Gal-CC compared to Glu-CC, WB analysis was performed to evaluate the levels of β-catenin (**Figure 32A**), a marker for canonical WNT pathway activation. Densitometric analysis revealed lower levels of active β-catenin in Gal-CC compared to Glu-CC (**Figure 32B**). To confirm these results, we performed immunofluorescence staining of β-catenin (**Figure 32C**), and images showed that the percentage of positive β-catenin area was significantly lower, approximately 4-fold, in Gal-CC compared to Glu-CC (**Figure 32D**). Interestingly, it had recently been demonstrated that dormant/quiescent tumor cells have reduced WNT signaling mediated by the WNT inhibitor dickkopf-related protein 1 (DKK-1), which is overexpressed in slow-cycling/quiescent tumor cells[183]. In line with this association, the expression of DKK-1 was evaluated by RT-qPCR, and its expression was significantly increased by more than 2-fold in all primary PDAC cells cultured in Gal-CC compared to Glu-CC (**Figure 32E**).

Taken together, these data suggested that Gal-CC are more quiescent than Glu-CC. However, this quiescence is not a permanent and/or irreversible state as Gal-CC can modulate their cellular proliferation and exit quiescence/dormancy in accordance to the carbon source available, thus adapting to their environment.

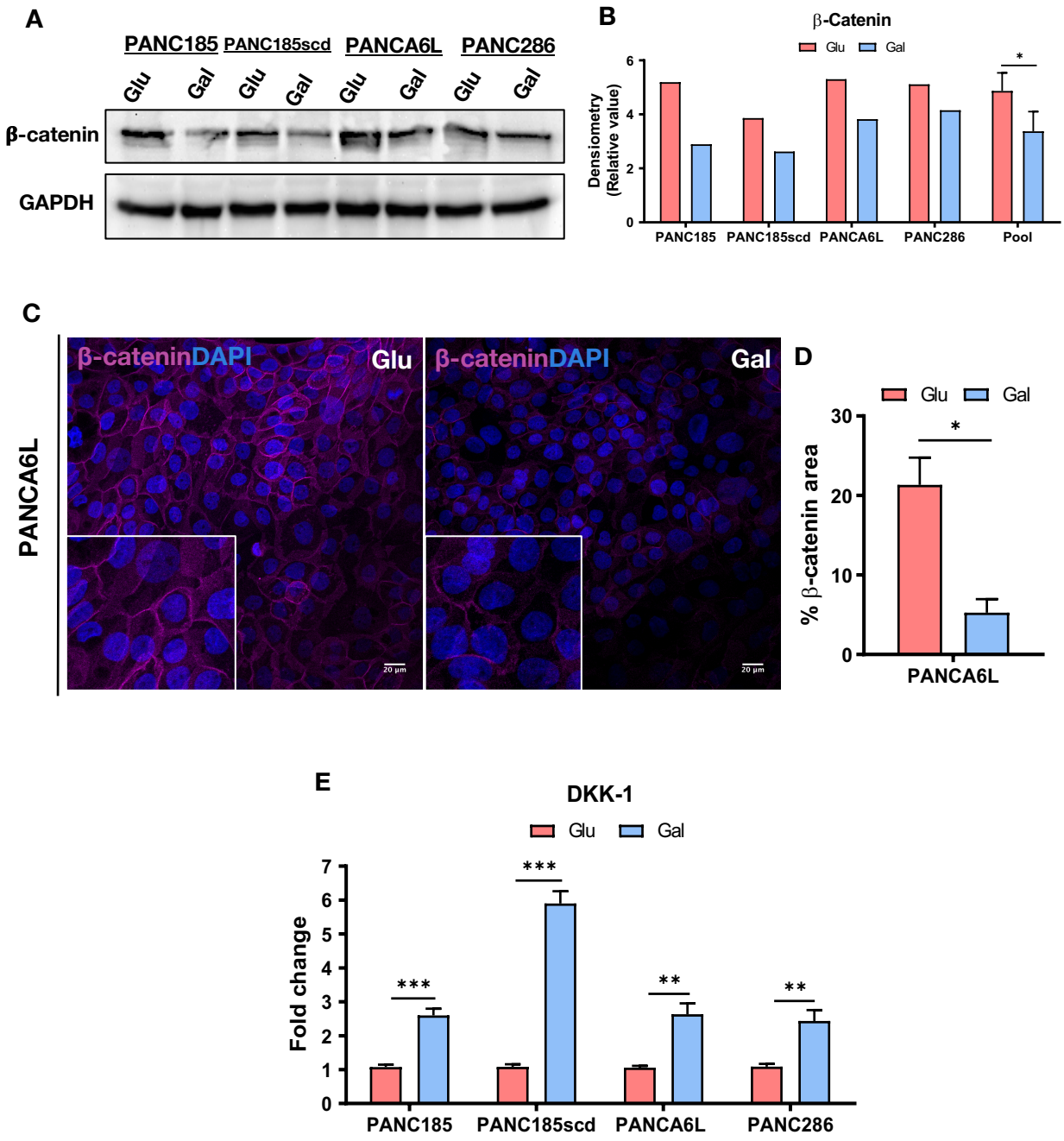

Figure 32. (A) WB analysis of β-catenin in PDAC Glu-CC and Gal-CC. GAPDH was used as a loading control. (B) Densitometric quantification of β-catenin expression normalized to GAPDH levels and expressed as relative values. (C) Representative immunofluorescence images of β-catenin (magenta) and DAPI (blue) staining in PANCA6L Glu-CC and Gal-CC. (D) Quantification of the percentage of fluorescent area for β-catenin in Glu-CC and Gal-CC, using ImageJ (n= 4 samples per group). (E) RT-qPCR analysis of relative mRNA expression levels for DKK-1 in PDAC Glu-CC to Gal-CC. mRNA expression levels were normalized to β-actin levels (n= 3 samples per group). Data are presented as fold-change. Glu was set as 1.0. Holm-Sidak t-test statistical analysis: (*) = p< 0.05; (**) = p<0.01; (***) = p<0.001.

6. Mitochondrial-dependent metabolism (OXPHOS) promotes PaCSCs chemoresistance

Once confirmed that Gal-CC enriches for CSC with more mitochondria, enhanced mitochondrial function (increased OXPHOS), a greater autophagy flux, less senescence and a quiescent phenotype compared to Glu-CC, we evaluated chemoresistance between Glu-CC and Gal-CC.

Chemoresistance is an inherent characteristic of CSCs[154,184]. In fact, chemoresistance, together with metastatic potential (*e.g.* quiescent stage), are the main clinical hallmarks of PaCSCs that can lead to disease relapse. PaCSCs present a series of mechanisms that make them highly chemoresistant, such as high autophagy, a low rate of proliferation, high levels of autofluorescence vesicles, the activation of CSCs-related signaling pathways, different levels of expression of chemotherapeutic transporters (e.g, Gemcitabine transporters) and over-expression of ATP-binding transporters (ABC transporters)[155,185,186]. ABC transporters, such as ABCG2, are known effectors of chemoresistance across multiple tumor types[187]. Over expression of these transporters in PaCSCs creates a highly efficient efflux pump system, resulting in efficient elimination of chemotoxic agents. Thus, we evaluated the expression of ABCG2 by RT-qPCR. ABCG2 transcript levels significantly increased 2-fold in Gal-CC compared to Glu-CC in all primary PDAC cultures (**Figure 33A**). In addition, we evaluated by RT-qPCR different genes related to the metabolism of Gemcitabine, one of the most used chemotherapeutics in the treatment of PDAC. In this sense, hENT1 and hENT2 express equilibrating transporters that mediate both the capture and exit of Gemcitabine according to their concentration gradient[186], in comparison with CNT1, which encodes for a gemcitabine entry transporter[185]. At the transcriptional levels, CNT1 was significantly lower in Gal-CC compared to Glu-CC, whereas hENT1 and hENT2 were significantly higher in Gal-CC (**Figure 33B**).

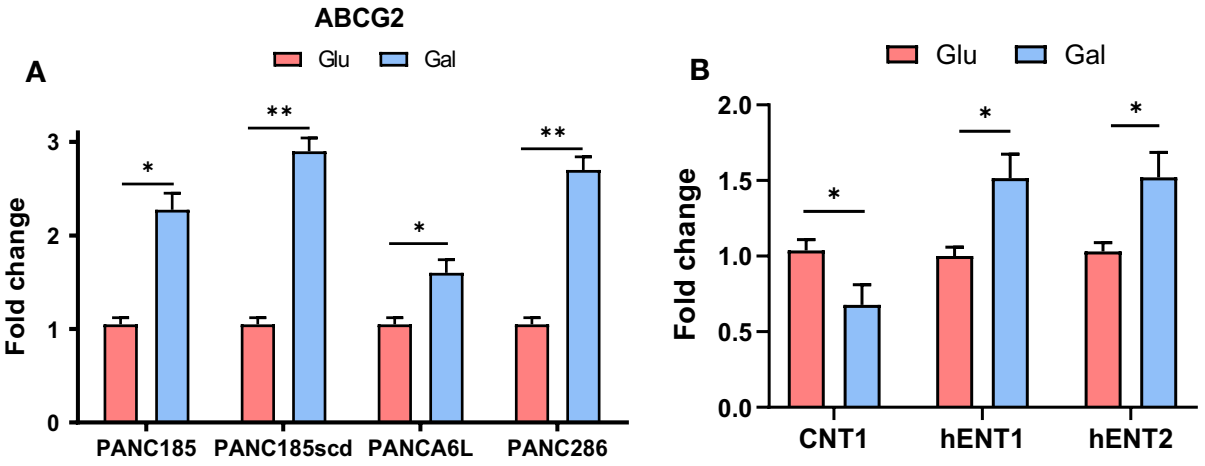

Figure 33. (A). RT-qPCR analysis of relative mRNA expression levels of ABCG2 in Glu-CC and Gal-CC PDAC cultures. mRNA expression levels are normalized to β-actin levels (n=3 biological replicates per tumor, 2 technical replicates). Data are presented as fold-change. Glu was set as 1.0. (B) RT-qPCR analysis of relative mRNA expression levels of CNT1, hENT1 and hENT2 genes in Glu-CC and Gal-CC PDAC cultures. mRNA expression levels for each target gene are normalized to β-actin levels (n=12 biological replicates, 2 technical replicates). Data are presented as fold-change. Glu was set as 1.0. Holm-Sidak t-test statistical analysis: (*) = p< 0.05; (**) = p<0.01; (***) = p<0.001.

In addition, we wanted to verify functionally if the differences found in the expression of the different transporters previously evaluated were linked to greater chemoresistance across our PDAC cells, particularly in Gal-CC. Likewise, we next evaluated the capacity of relapse/survival of the different Glu-CC and Gal-CC after treatment with different chemotherapeutics such as Mitoxantrone, Doxorrubicin and Gemcitabine for 48 hours. We chose Mitoxantrone and Doxorrubicin because both are specific substrates for ABCG2. After 48 hours post-treatment and recovery without drugs in basal culture media for 72 hours, we evaluated cell death by luminescence using the Toxilight cell cytotoxicity assay. We observed significantly less cell death for all of the different chemotherapeutics (Mitoxantrone, Doxorubicin and Gemcitabine) tested, and across all PDAC cultures in Gal-CC compared to Glu-CC (Figures 34A-C), indicating that Gal-CC are more inherently chemoresistant to different chemotherapeutics, including Gemcitabine.

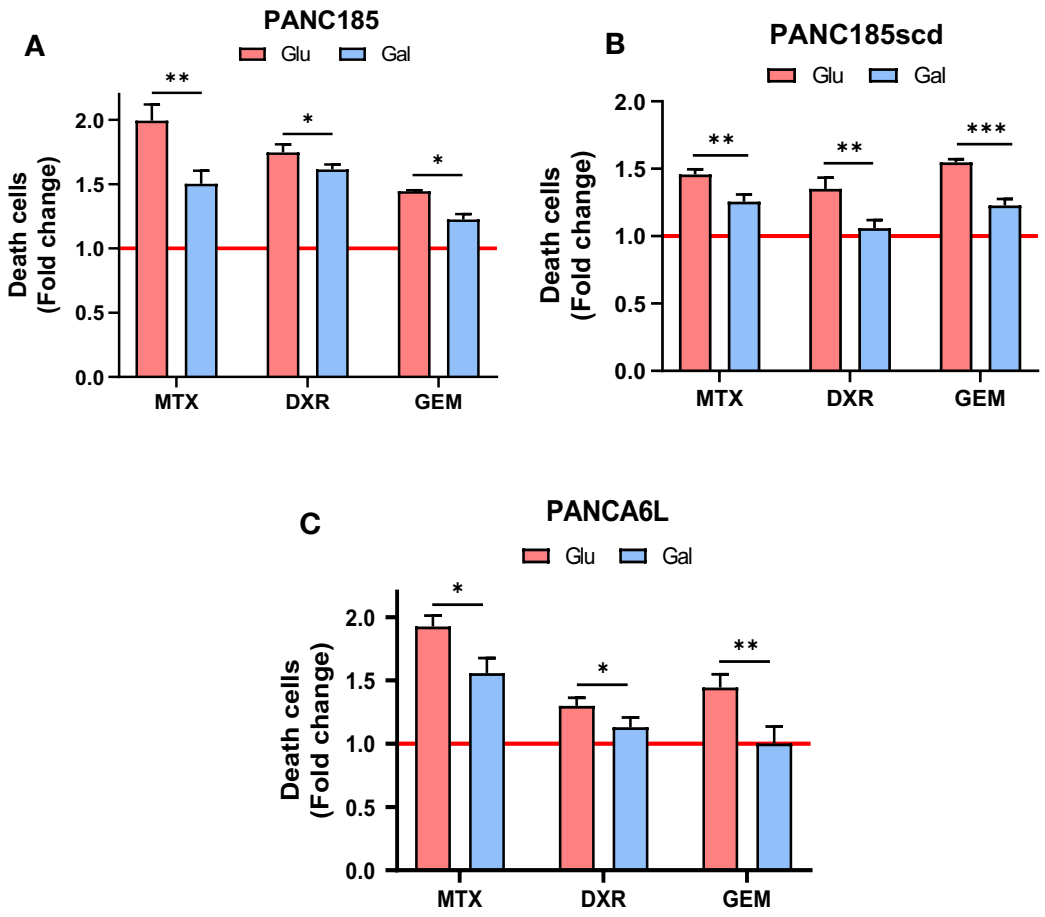

Figure 34. (A-C) Quantification of ToxiLight luminescence as a measure of cell death after 3 days of recovery from treatment with Mitoxantrone (MTX), Doxorubicin (DXR) and Gemcitabine (GEM) during 48 hours in Glu-CC and Gal-CC of (A) PANC185, (B) PANC185scd and (C) PANCA6L (n= 4 samples per group). Data are presented as fold-change in luminescence and compared to luminescence measured in untreated control cultures, set as 1.0 (red line=Control). Holm-Sidak t-test statistical analysis: (*) = p< 0.05; (**) = p<0.01; (***) = p<0.001.

In view of the results previously obtained at the level of OXPHOS metabolism, we performed a chemoresistance assay with different metabolic drugs, in order to evaluate the cell death of our PDAC cells in the presence of different OXPHOS metabolic drugs. Specifically, we tested Menadione, Rotenone, Resveratrol and Metformin and the glycolytic irreversible inhibitor, 2-Deoxy-Glucose (2DG), and evaluated cell death 72 hours post-treatment. Menadione triggers cell death via the over-production ROS; Rotenone, Resveratrol and Metformin block different electron transport chain (ETC) complexes and ATP production[159] and 2-Deoxy-Glucose (2DG), which is analog of glucose that can irreversibly inhibit the first glycolysis enzyme (glucokinase, GK), so that it cannot undergo further glycolysis[188].

As expected, we analyzed that the OXPHOS metabolic drugs caused significantly higher levels of cell death of approximately 2-fold in the majority of Gal-CC compared to Glu-CC whereas, 2DG had the opposite effect in all PDAC primary cultures that were evaluated (Figures 35A-D).

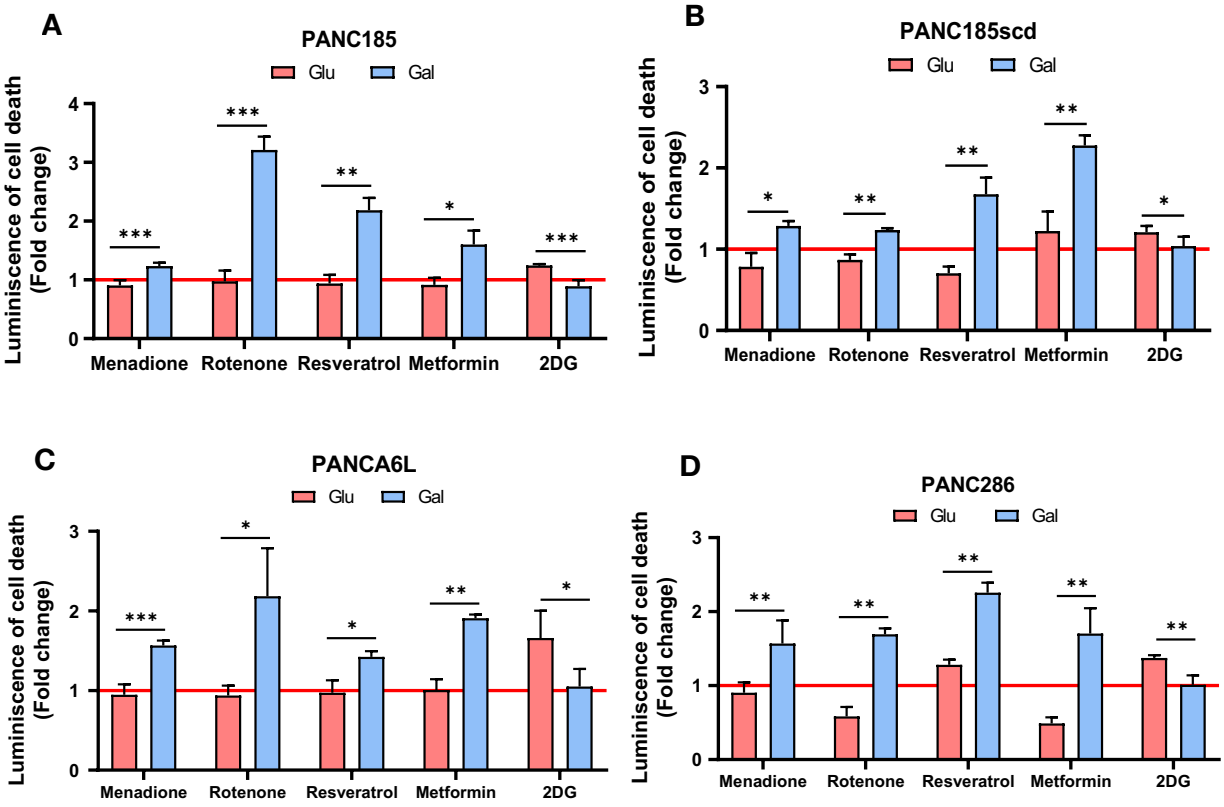

Figure 35. (A-D) Quantification of luminescence as a measure of cell death after 3 days of treatment with metabolic drugs comparing in Glu-CC and Gal-CC of (A) PANC185, (B) PANC185scd, (C) PANCA6L and (D) PANC286 (n= 4 samples per group). Data are presented as fold-change in luminescence and compared to luminescence measured in untreated control cultures, set as 1.0 (red line=Control). Holm-Sidak t-test statistical analysis: (*) = p< 0.05; (**) = p<0.01; (***) = p<0.001.

Taken together, these data indicated that Gal-CC are more chemoresistant to a panel of traditional chemotherapeutics than Glu-CC, largely due to the overexpression of the ABCG2 transporter and the different levels of expression of genes related to Gemcitabine metabolism. In contrast, and as expected, galactose-cultured cells are more sensitive to OXPHOS metabolic drugs, and less sensitive to the glycolysis inhibitor 2DG, strongly confirming the importance of OXPHOS metabolism in order to eliminate the PaCSCs population.

7. Mitochondrial-dependent metabolism (OXPHOS) induces PaCSCs immune evasion *in vitro*

Once confirmed that Gal-CC enriches for CSC with more mitochondria, enhanced mitochondrial function (increased OXPHOS), a greater autophagy flux, less senescence, a quiescent phenotype and enhanced chemoresistance compared to Glu-CC, we evaluated the immune evasive capacity of Glu-CC and Gal-CC.

Another important feature of CSCs is their inherent capacity to evade the immune system and metastasize to surrounding and distant organs. In this context, Gal-CC appears to recapitulate key features of the "latent" metastatic state of CSCs, which include increased autophagy, a propensity to enter proliferative quiescence, an ability to survive as latent entities in relevant organs for long-time periods, survive in the presence of chemotherapeutics and retain their metastasis-initiating potential[189]. Many studies have also shown that there is a clear relationship between tumor cell quiescence and immune evasion mechanisms[183,190–192], the latter of which are regulated by a balance between activating and inhibitory signals. In this sense, and based on the fact that little is known about PaCSC immune evasion, we evaluated different biomarkers and features related to immune evasion and metastasis in Glu-CC and Gal-CC.

We chose different receptors and ligands that were subsequently analyzed by flow cytometry in Gal-CC compared to Glu-CC in all PDAC primary cultures (**Figure 36A**). Ligands and receptors related to immune suppression of T lymphocytes (PD-L1), anti-phagocytic function (CD47 and CD206) and invasion, migration and metastasis (CD155 and CD206) were significantly overexpressed more than 2-fold in Gal-CC compared to Glu-CC (**Figure 36B**). Interestingly, ULBP2/5/6 ligands related to the activation of NK cells receptors were significant downregulated in Gal-CC compared to Glu-CC (**Figure 36B**). These results would suggest that Gal-CC would be more able to evade the immune system compared to Glu-CC.

At the transcriptional level, we evaluated different genes related to EMT in order to evaluate the epithelial or mesenchymal state of Glu-CC and Gal-CC by RT-qPCR. Importantly, ZEB1 is a key regulator of invasion and metastasis in many different cancer

types, particularly by coupling the activation of cellular motility with stemness and survival [193–197]. The expression levels of ZEB1, Slug and Snail were significant higher (approximately more than 2-fold) in Gal-CC compared to Glu-CC whereas, the expression levels of Cadherin1 (Cdh1) and Vimentin (Vim) were not significantly increased in Gal-CC compared to Glu-CC (**Figure 36C**). These results suggested that Gal-CC seem to be more mesenchymal compared to Glu-CC.

Moreover, we next evaluated the secretion levels of TGFβ by ELISA. TGFβ is one of the most important cytokines implicated in stemness, EMT, ECM regulation, B and T cell differentiation and immunological response, and activation of inflammatory cascades associated with cancer progression[198–201]. Our analysis showed that not only do Gal-CC modulate the expression of immune-related ligands and receptors related to immune suppression, but these cells secrete significantly higher levels of TGFβ compared to Glu-CC (**Figure 36D**).

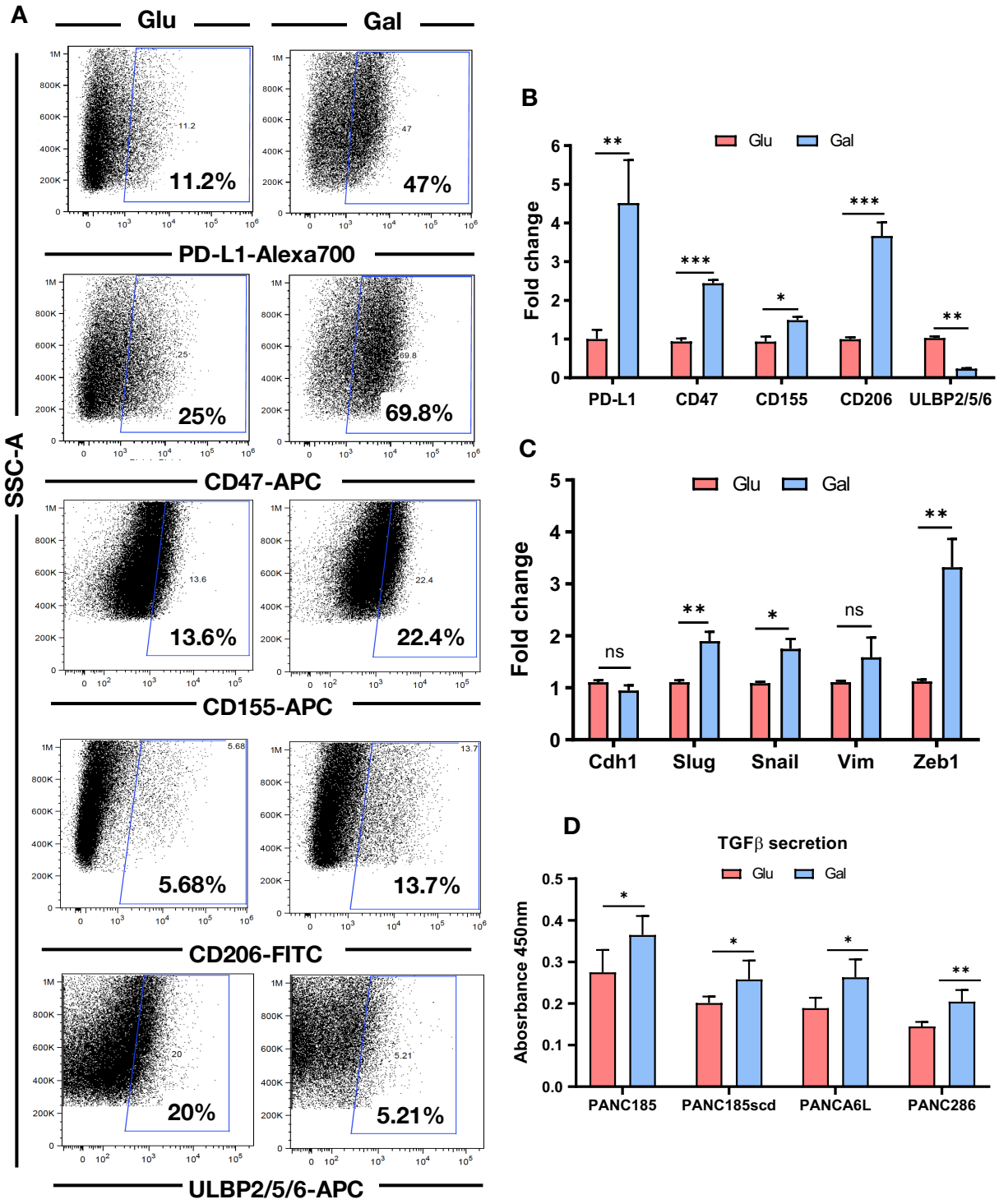

Figure 36. (A) Representative flow cytometric dot plots of the expression of different immune evasion/activation markers (PD-L1, CD47, CD155, CD206 and ULBP2/5/6) in Glu-CC and Gal-CC. (B) Quantification of the levels of the different markers in Glu-CC and Gal-CC (n=2-3 biological replicates per tumor). Data are presented as fold-change. Glu was set as 1.0. (C) RT-qPCR analysis of relative mRNA expression levels of different EMT-related genes in Glu-CC and Gal-CC. mRNA expression levels were normalized to β-actin levels (n=2-3 biological replicates per tumor). Data are presented as fold-change. Glu was set as 1.0. (D) Quantification of the levels of secreted TGFβ levels, by ELISA, from Glu-CC and Gal-CC, determined by absorbance spectrophotometry and normalized to total protein levels. Holm-Sidak t-test statistical analysis: (*) = p< 0.05; (**) = p<0.01; (***) = p<0.001; (ns)= not significant.

Continuing in this line, we next analyzed the expression of NFκB. In the context of CSCs, NFκB plays an important role in cell survival, proliferation, stemness, tumor formation and contributes to CSC invasiveness and metastasis[202]. NFκB is also an important transcription factor that mediates cytokine secretion, which is essential in modulating the microenvironment and the communication with immune cells within the tumor[202]. As expected, we found a significant overexpression of NFκB of more than 2-fold in Gal-CC compared to Glu-CC in all PDAC primary cultures (**Figure 37**).

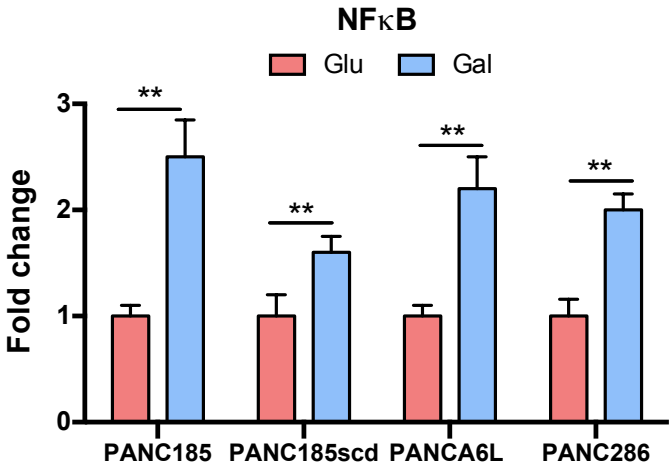

Figure 37. RT-qPCR analysis of relative mRNA expression levels for NFκB in Glu-CC and Gal-CC. mRNA expression levels were normalized to β-actin levels (n= 3 samples per group). Data are presented as fold-change. Glu was set as 1.0. Holm-Sidak t-test statistical analysis: (*) = p< 0.05; (**) = p<0.01; (***) = p<0.001.

Taking into account the results previously obtained, we performed a cytokine array to determine the secreted cytokine profile of Gal-CC compared to Glu-CC in PANC185 and PANCA6L (**Figure 38A**). Overall, we found differences in the expression levels of different cytokines in both culture conditions. Specifically, significant differences were found in CCL2, CXCL12, GM-CSF, and ICAM-1 (**Figure 38B**), as well as CCL5, CXCL1, Serpin E1 and IL-8 (**Figure 38C**). Interestingly, on the one hand the cytokines that increased in Gal-CC compared to Glu-CC have been associated to higher stemness (CCL2, IL-8), tumorigenesis (CCL2, CXCL12, IL-8), chemoresistance (CXCL12), metastasis, migration and invasion (CXCL12, IL-8) and quiescence (CXCL12). While on the other hand, the cytokines that decreased in Gal-CC compared to Glu-CC have been correlated with lower chemotaxis, communication and activation of immune cells like T-cells, basophils, neutrophils (ICAM-1, CCL5, CXCL1), higher quiescence of tumor cells and the infiltration

of pro-inflammatory macrophages (GM-CSF), higher metastasis and stemness (Serpin E1)[183,192,201,203–220].

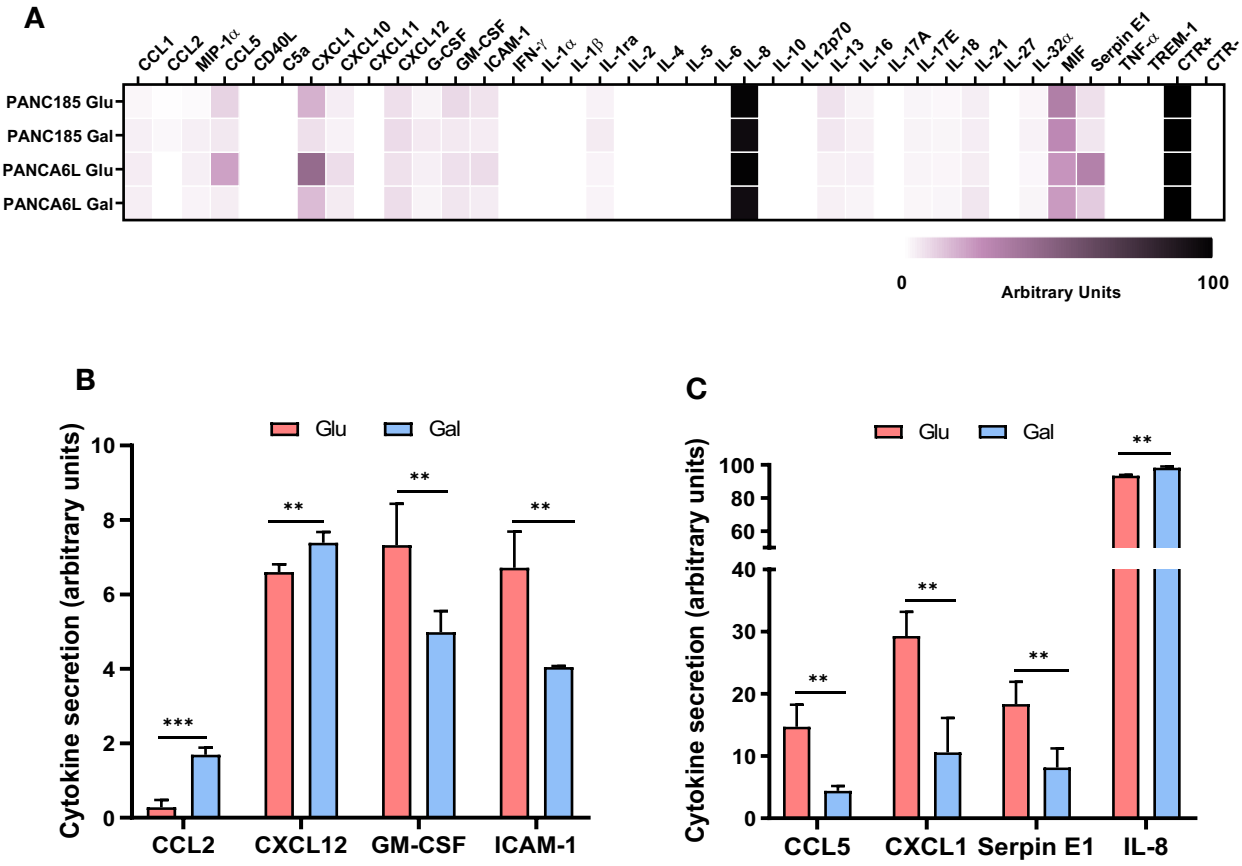

Figure 38. (A) Semi-quantification of the profile of cytokine secretion by pixel density of duplicated spots per sample comparing Glu-CC and Gal-CC. (B-C) Analysis of the secreted cytokines with significant changes in Glu-CC versus Gal-CC, normalized to positive control (CTR+) (n= 4 samples per group). Holm-Sidak t-test statistical analysis: (*) = p< 0.05; (**) = p<0.01; (***) = p<0.001.

The sum of the aforementioned experiments indicated that OXPHOS-dependent cells modulate their cell surface receptors/ligands and cytokine profile to possibly evade immune cell detection and/or elimination. To test this hypothesis, we performed functional *in vitro* immune evasion experiments with immune cells isolated from the blood (buffy coats) of three healthy donors. Firstly, we performed phagocytosis assays with monocyte-derived macrophages. Macrophages are distributed throughout every organ of the body and play a very important role in innate immune surveillance by eliminating pathogens via phagocytosis. For the phagocytosis assays, we stained macrophages and tumor cells PANC185, PANC185scd and PANCA6L (Glu- and Gal-CC) with the surface membrane

dyes DilC (red) and PKH67 (green), respectively. Next, we co-cultured both cell populations for 72 hours (Figure 39).

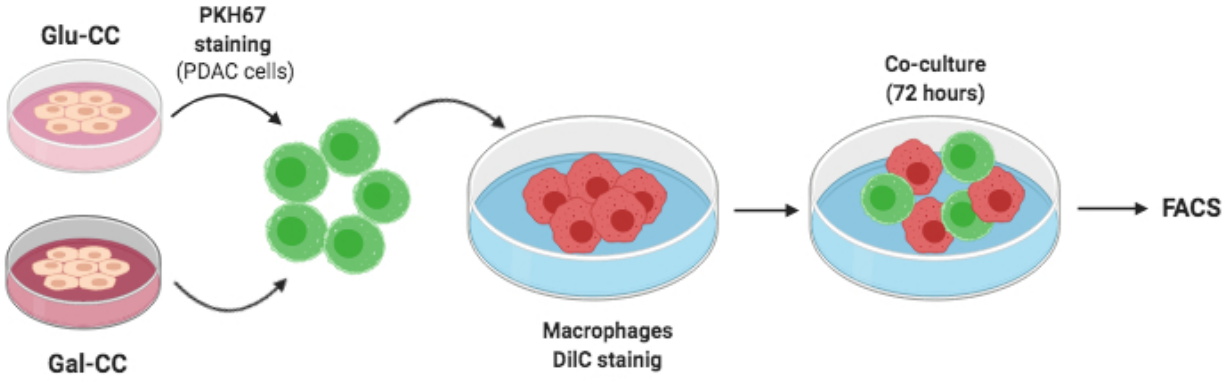

Figure 39. Representative scheme of phagocytosis assay. After 14d, Glu-CC and Gal-CC were stained with PKH67 dye (green) and were co-cultured with macrophages stained with DilC (red). After 72 hours, the percentage of phagocytosis ($PKH67^+/DilC^+$ population) were analyzed by FACS.

After 72 hours post co-culture, we evaluated the double-positive $DilC^+PKH67^+$ population (Figure 40A), which is indicative of macrophage-mediated phagocytosis. In line with an immune evasion profile, the double-positive $DilC^+PKH67^+$ population was significantly lower when macrophages were co-cultured with Gal-CC compared to Glu-CC for each donor tested (Figure 40B). These data strongly suggested that macrophages are more able to detect and phagocytose Glu-CC than Gal-CC, which we could attribute to the significant over-expression of the "don't eat me" CD47 and the CD206 receptor[203,221] on the surface of Gal-CC (Figures 36A-B).

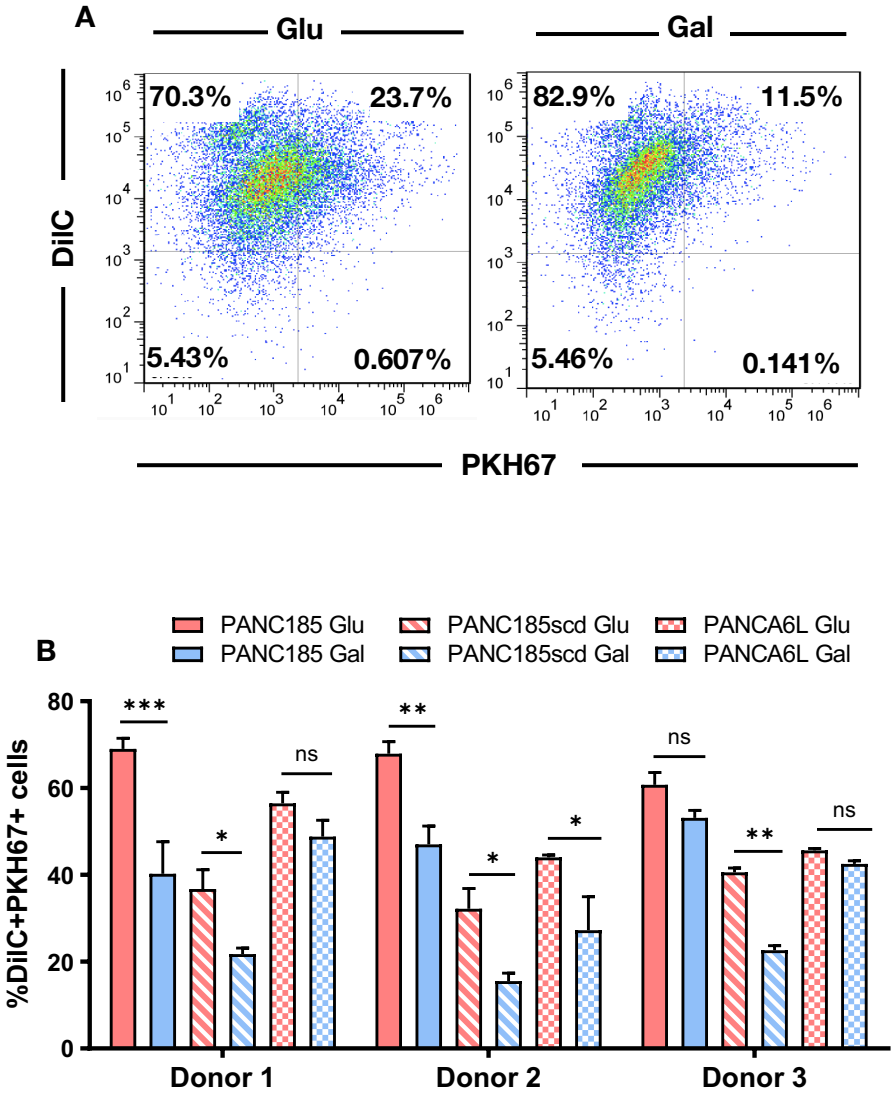

Figure 40. (A) Representative flow cytometric dot plots demonstrating DilC-stained macrophages and PKH67-stained Glu-CC to Gal-CC. $DilC^{+}PKH67^{+}$-double positive cells represent phagocytosis. (B) Quantification of the percentage of the $DilC^{+}PKH67^{+}$-double positive population in the phagocytosis assay, determined by FACS, using monocyte-derived macrophages from 3 different healthy donors incubated with Glu-CC or Gal-CC (PANC185, PANC185scd or PANCA6L) (n= 3 samples per group). 2-Way ANOVA statistical analysis: (*) = p< 0.05; (**) = p<0.01; (***) = p<0.001; (ns)= not significant.

Secondly, for the adaptive immune system, we performed assays with T-cells, which are able to recognize and kill target cells when activated by others immune cells and secreted cytokines. T-cells isolated from the blood of three healthy donors and subsequently activated were co-cultured with PANC185, PANC185scd and PANCA6L (Glu- and Gal-CC) for 10 days. After 10 days post co-culture, tumor cell death was subsequently assessed.

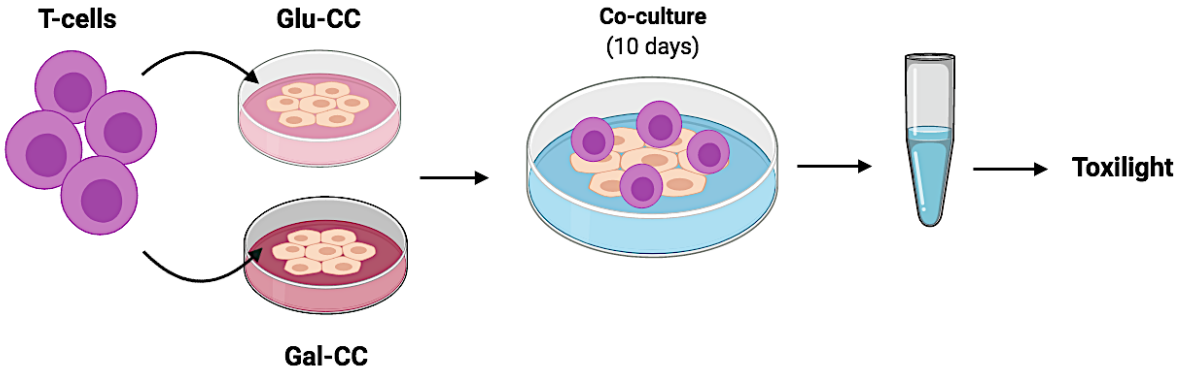

Figure 41. Representative scheme of toxicity assay. T-cells obtained from healthy donors were co-cultured with Gul-CC and Gal-CC during 10 days. Afterwards, supernatant was collected to perform the ToxiLight assay.

Regardless of the donor and PDAC cell line used, in general, T-cells were significantly less capable of eliminating Gal-CC compared to Glu-CC when co-cultivated (**Figures 42A-C**). Importantly, the levels of cell death detected in T-cell/Gal-CC was very similar to the control cultures (red line, without T-cells) for Donor 1 (**Figure 42A**) and Donor 3 (**Figure 42C**). T-cells from Donor 2, in general, displayed higher cytolytic capacity (**Figure 42B**).

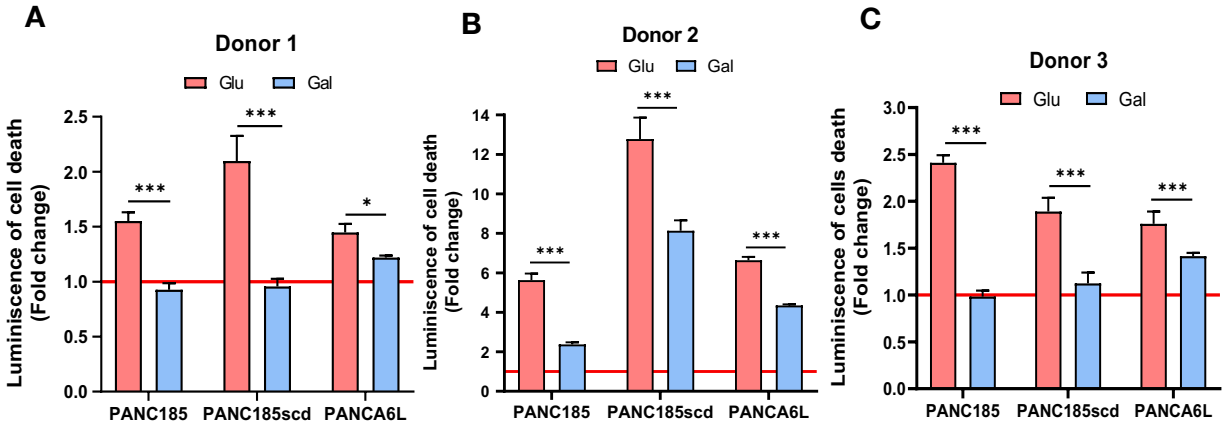

Figure 42. Fold change in cell death, detected using a ToxiLight luminescence-based cytotoxicity assay, after 10 days co-cultivating PDAC cells (PANC185, PANC185scd or PANCA6L) with activated T-cells isolated from healthy (**A**) Donor 1, (**B**) Donor 2 or (**C**) Donor 3 (n= 4 samples per group) (red line=Control (basal toxicity). Holm-Sidak t-test statistical analysis: (*) = p< 0.05; (**) = p<0.01; (***) = p<0.001.

Taken together, these data strongly suggested that T-cells are more able to detect and eliminate Glu-CC than Gal-CC, which we could attribute to the significant over-expression of PD-L1 ligand on the surface of Gal-CC (**Figures 36A-B**) and the lower secretion of some cytokines such as ICAM-1, CCL5, CXCL1 from Gal-CC compared to Glu-CC (**Figures 38A-C**).

8. Mitochondrial-dependent metabolism (OXPHOS) promotes immune evasion and metastasis of PaCSCs *in vivo*

Once confirmed that Gal-CC enriches for CSC with more mitochondria, enhanced mitochondrial function (increased OXPHOS), a greater autophagy flux, less senescence, enhanced quiescent phenotype, a higher chemoresistance to current chemotherapeutics and increased *in vitro* immune evasion compared to Glu-CC, we evaluated the immune evasive and invasive capacity Glu-CC and Gal-CC *in vivo*.

The immune evasion characteristics observed in the *in vitro* assays described above may be essential for CSCs to survive in the bloodstream and go unnoticed by the immune system, facilitating their eventual invasion and metastasis to distant organs. To functionally test the invasive capacity of Gal-CC and Glu-CC, zebrafish and NOD-SCID mouse models of cellular invasion were employed.

Firstly, the following zebrafish experiments we performed in collaboration with Dr. Laura Sánchez and Dr. Pablo Sáinz at the University of Santiago de Compostela in Lugo. Specifically, zebrafish embryos were microinjected in the caudal vein with mCherry H2B-labelled PANCA6L (**Figure 43A**) and PANC185scd (**Figure 44A**) cells cultured in glucose and galactose conditions, and the integrated density, based on mCherry fluorescence and indicative of in vivo cellular proliferation, was assessed 1, 4 and 6 day/s post-injection (dpi), as previously described in[153].

While at 1dpi the Glu-CC PANCA6L mCherry-H2B cells migrated more efficiently to the tail compared to Gal-CC (**Figure 43B**), Glu-CC were less viable at later time points, as evident by the loss in mCherry-H2B fluorescence observed at 4 and 6 dpi compared to Gal-CC, which had a more proliferative profile (**Figures 43C-D**). For PANC185scd cells, similar results were observed at the same time points evaluated for Glu-CC and Gal-CC (**Figures 44A-D**), although significance was not achieved.

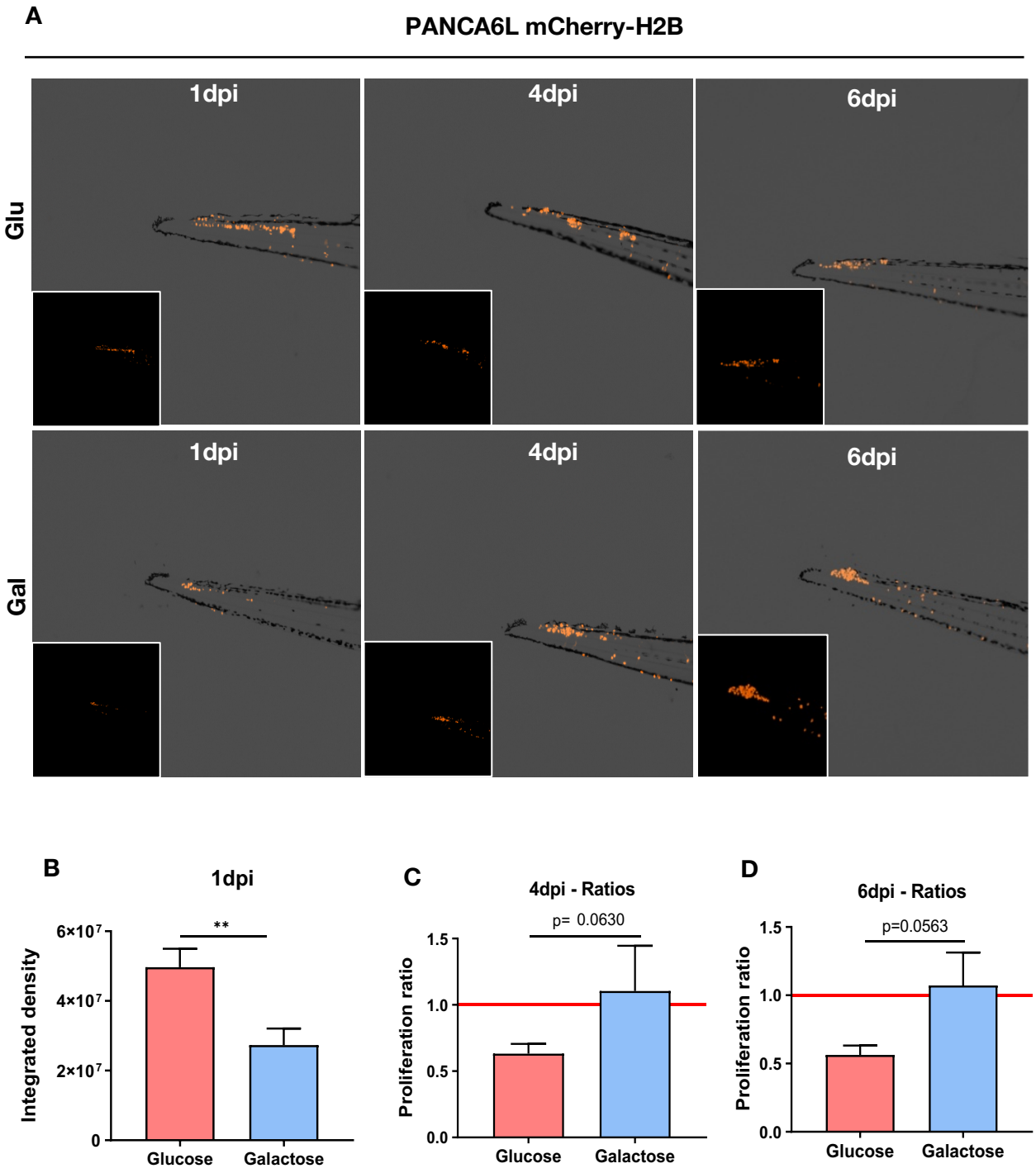

Figure 43. (A) Representative images of zebrafish embryo tails taken at 1-, 4- and 6-days post-injection (dpi) with mCherry-H2B-labeled PANCA6L Glu-CC or Gal-CC. (B) Quantification of the integrated density (fluorescence measure) between Glu-CC and Gal-CC 1-day post-injection (1dpi). (C-D) Quantification of the proliferation ratio observed between Glu-CC and Gal-CC at (C) 4dpi and (D) 6dpi. The proliferation ratios are represented in comparison to 1dpi (red line) for both conditions. Unpaired t-test statistical analysis: (*) = p< 0.05; (**) = p<0.01; (***) = p<0.001; (ns)= not significant; (nd)= not determined.

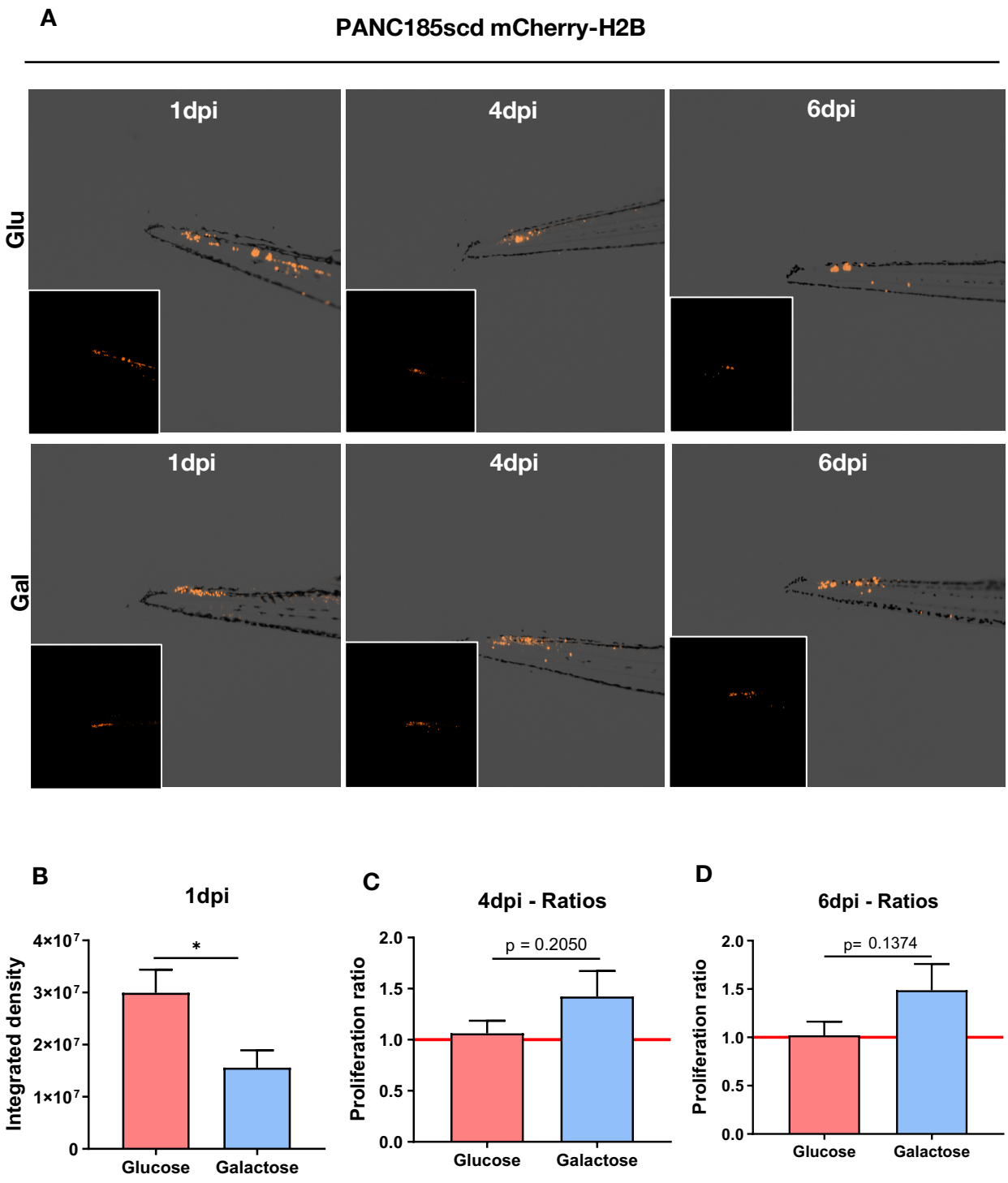

Figure 44. (A) Representative images of zebrafish embryo tails taken at 1-, 4- and 6-days post-injection (dpi) with mCherry-H2B-labeled PANC185scd Glu-CC or Gal-CC. (B) Quantification of the integrated density (fluorescence measure) between Glu-CC and Gal-CC 1-day post-injection (1dpi). (C-D) Quantification of the proliferation ratio observed between Glu-CC and Gal-CC at (C) 4dpi and (D) 6dpi. The proliferation ratios are represented in comparison to 1dpi (red line) for both conditions. Unpaired t-test statistical analysis: (*) = p< 0.05; (**) = p<0.01; (***) = p<0.001; (ns)= not significant; (nd)= not determined.

To extend these observations to other *in vivo* models, NOD-SCID mice were tail vein injected with PANCA6L mCherry-H2B cells cultured in glucose and galactose conditions and their capacity to disseminate and invade distant organs was assessed at different time points: 10 days post-injection (short time) and 3 months post-injection (long time) (Figure 45).

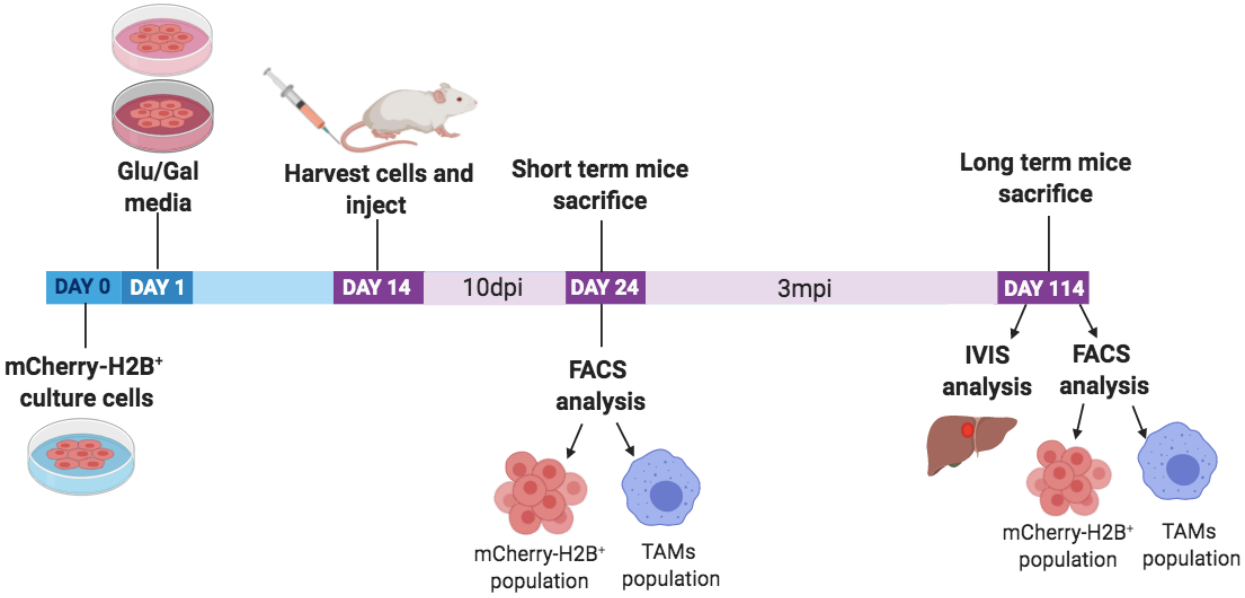

Figure 45. Representative scheme of the *in vivo* invasion assay in NOD-SCID mice.

Firstly, at 10-days post-injection, we digested different organs of mice and we analyzed the percentage of mCherry-H2B positive cells in these organs by flow cytometry. While there was no significant increase in mCherry-positive cells in the spleen, liver or lungs, there was a significant increase in mCherry-positive PDAC cells in the pancreas and blood in mice injected with Gal-CC compared to mice injected with Glu-CC (Figure 46A). In fact, at 3 months post-injection, in the organs digested we found by flow cytometry that mice injected with Gal-CC presented with significantly higher percentages of mCherry-H2B positive cells in all organs compared to mice injected with Glu-CC (Figure 46B). In other organs such as kidneys and thymus, no significant differences were observed. In the case of lymphatic nodes, mCherry-H2B positive nodes were only detected in mice injected with Gal-CC, whereas in Glu-CC the mCherry-H2B positive cells were not found in lymphatic nodes (Figure 46C).

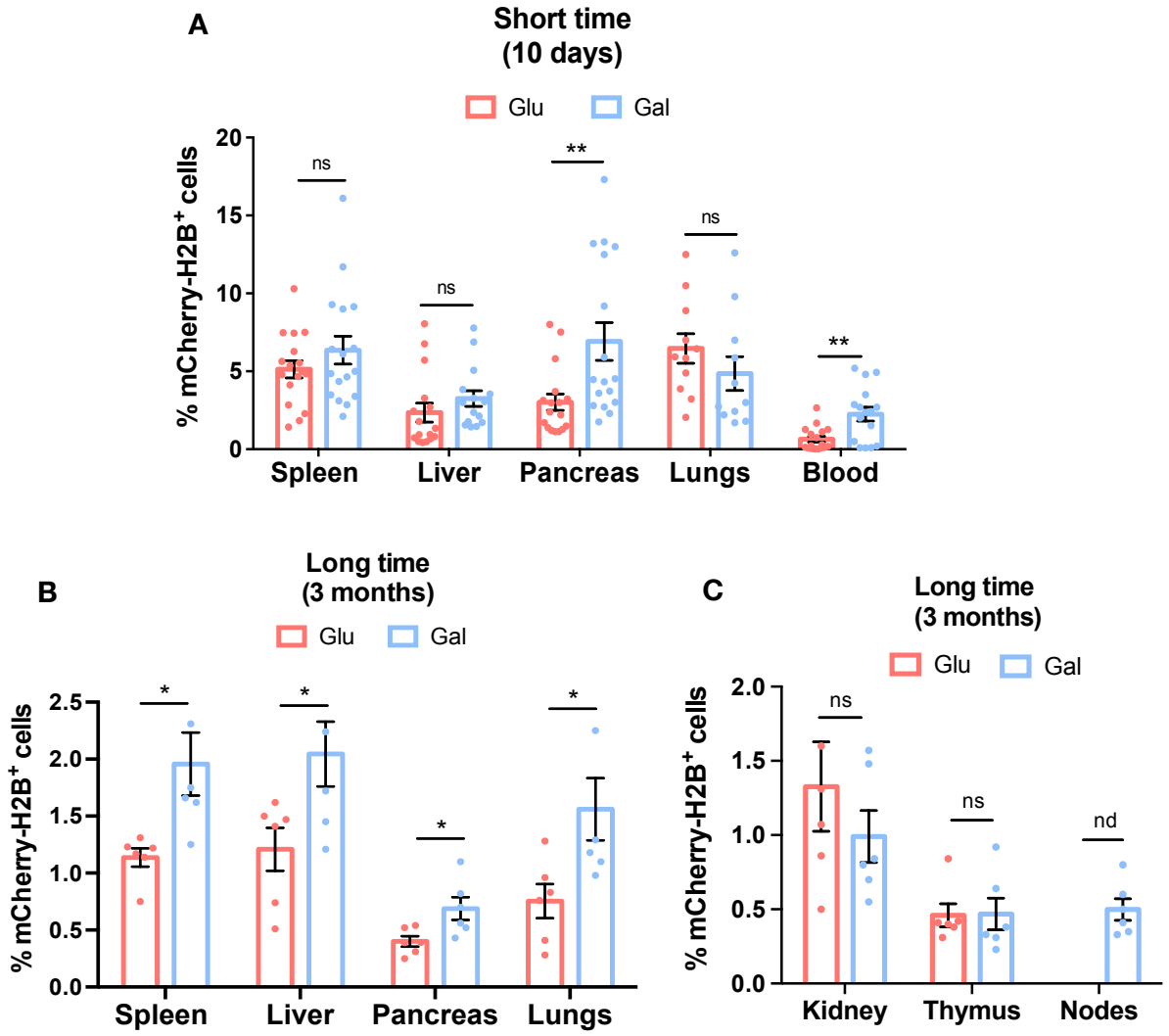

Figure 46. (A-B) Quantification of percentage of mCherry-H2B positive cells present in different organs analyzed by flow cytometry (spleen, liver, pancreas, lungs and blood) at (A) short time (10 days post-injection of PANCA6L mCherry-H2B cells) comparing Glu-CC with Gal-CC. (n= 16 mice per group) or at (B) long time (3 months post-injection of PANCA6L mCherry-H2B) comparing Glu-CC with Gal-CC (n= 6 mice per group).(C) Quantification of percentage of mCherry-H2B positive^{+} cells present in different organs analyzed by flow cytometry (kidney, thymus and nodes) at long time (3 months post-injection of PANCA6L mCherry-H2B) comparing Glu-CC with Gal-CC (n= 6 mice per group). Holm-Sidak t-test statistical analysis: (*) = p< 0.05; (**) = p<0.01; (***) = p<0.001; (ns)= not significant; (nd)= not determined.

For mice sacrificed 3 months post-injection with PANCA6L mCherry-H2B Gal-CC and Glu-CC organs were also validated *ex vivo* using IVIS imaging (Figures 47A-B). NOD-SCID mice injected with Gal-CC showed a higher radiance in all organs extracted and analyzed compared to the organs from NOD-SCID mice injected with Glu-CC. Interestingly, we found numerous and abnormally large lymphatic nodes in mice injected with Gal-CC, which were not detected in the mice injected with Glu-CC (Figure 47A, yellow squares).

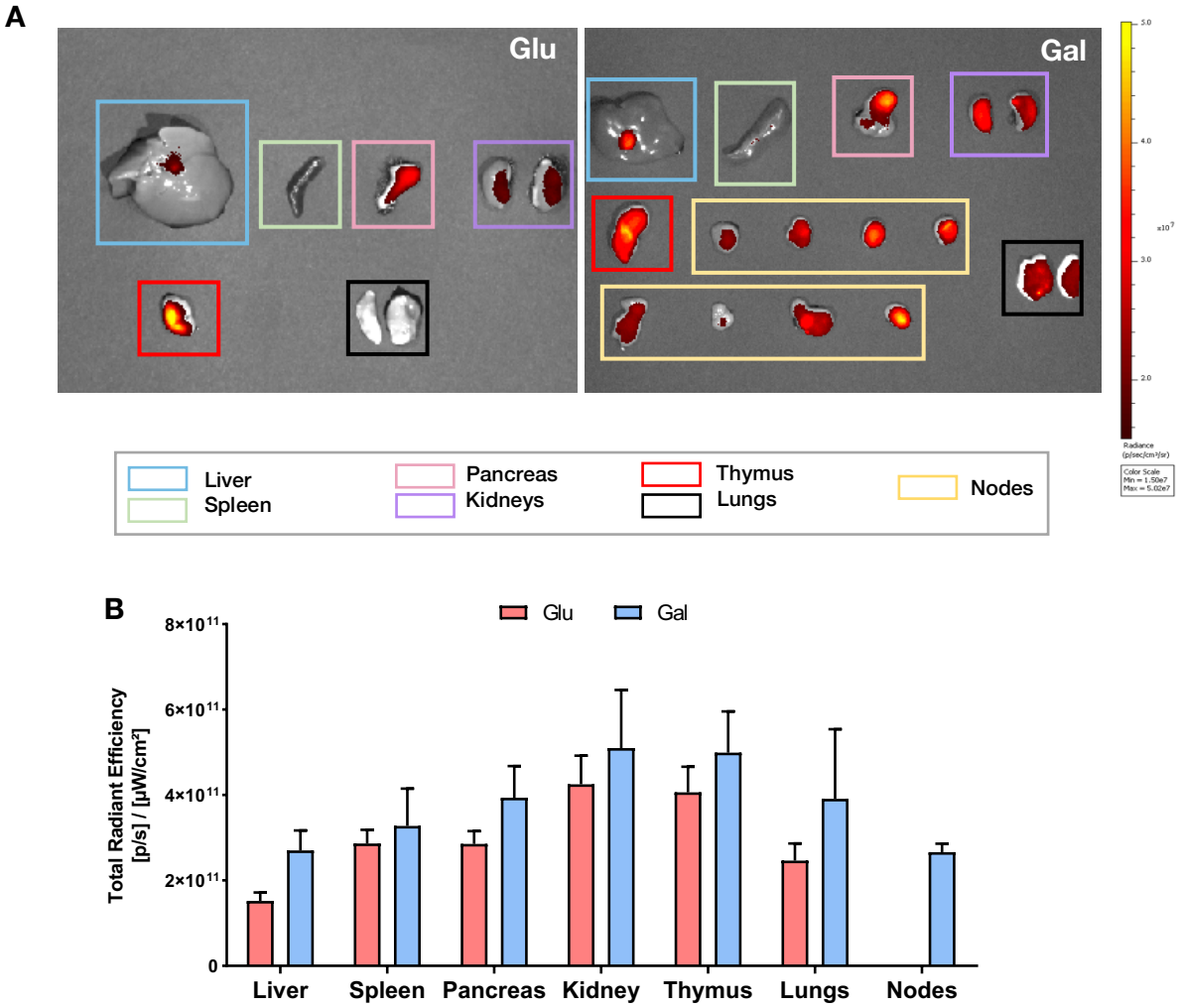

Figure 47. (A) Representative fluorescent IVIS images of different organs from NOD-SCID mice injected with Glu-CC and Gal-CC at long time (3 months post-injection of PANCA6L mCherry-H2B). (blue= liver, green= spleen, pink= pancreas, purple= kidneys, red= thymus, black= lungs and yellow=nodes). (B) Quantification of total radiant efficiency [p/s]/[µW/cm²] of different organs from mice injected with Glu-CC and Gal-CC at long time (3 months post-injection of PANCA6L mCherry-H2B). Holm-Sidak t-test statistical analysis: (ns)= not significant.

Lastly, because of the importance of the tumor-associated macrophage (TAM) population within the tumor and in the establishment and formation of pre-metastatic tumor niches during the process of dissemination of tumor cells (CSCs), we analyzed in each organ the percentage of TAMs population ($CD45^+CD11b^+F4\text{-}80^+$) by flow cytometry. In this sense, in mice 10 days post-injection with Gal-CC, we observed a significantly lower TAM population in the liver and pancreas compared to mice injected with Glu-CC (**Figure 48A**). However, at 3 months post-injection the population of TAMs increased significantly in all organs analyzed except in the kidneys of mice injected with Gal-CC compared to mice injected with Glu-CC (**Figures 48B-C**).

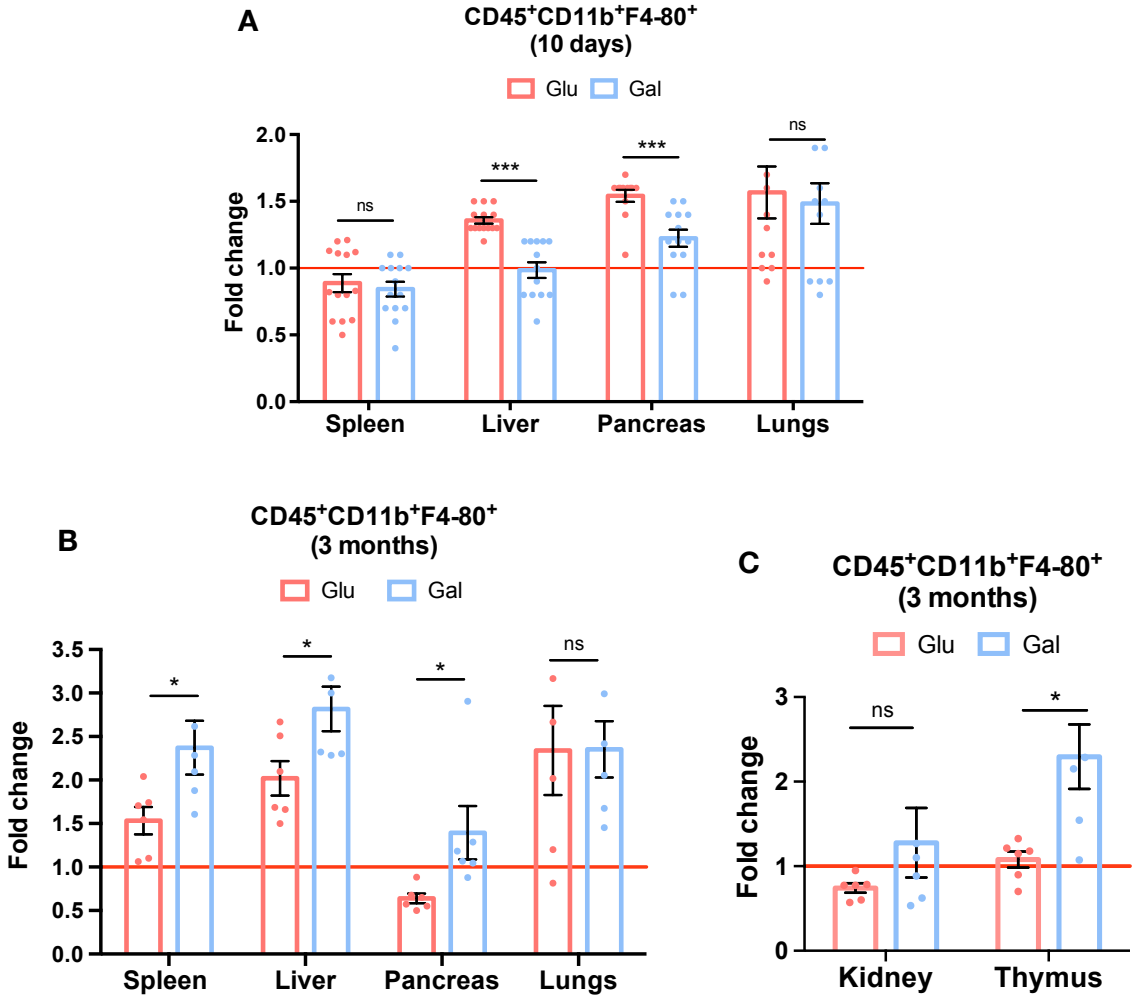

Figure 48. (A-B) Quantification of the CD45⁺CD11b⁺F4-80⁺ population present in the different organs analyzed by flow cytometry (spleen, liver, pancreas and lungs) at (A) short time or at (B) long time comparing Glu-CC with Gal-CC. (n= 6 mice per group). (C) Quantification of the CD45⁺CD11b⁺F4-80⁺ population present in the different organs analyzed (kidney and thymus) at long time (3 months post-injection of PANCA6L mCherry-H2B) comparing Glu-CC with Gal-CC. (n= 6 mice per group). Holm-Sidak t-test statistical analysis: (*) = p< 0.05; (**) = p<0.01; (***) = p<0.001; (ns)= not significant.

Taken together, Gal-CC were more invasiveness and metastatic in the two *in vivo* models utilized and were more able to modulate the immune infiltrating cell profile at early and late times points post-injection, attracting lower immune cells during the early stages, while at later times promoting the accumulation of pro-tumor immune cells in the different organs, which would facilitate establishment of the niche and tumor microenvironment.

DISCUSSION

At present, pancreatic cancer has become one of the most aggressive tumors with an extremely low life expectancy primarily due to the lack of early diagnostic symptoms and methods to predict non-advanced stages of the disease, coupled to the fact that pancreatic cancer has an extremely high invasive capacity to metastasize to surrounding organs[222]. Therefore, there exist numerous lines of research that focus on finding more efficient diagnostic models and new therapeutic targets for this disease[203]. Regarding the latter, our research group has based its efforts in investigating a small tumor cell subpopulation known as cancer stem cells (CSCs), which are responsible for the formation of the tumor, spread and resistance to current chemotherapies[223]. Based on previous work in our laboratory, specific PaCSCs characteristics/traits/properties have been discovered that allow for their separation from the rest of the cells (non-PaCSCs) present within a tumor. Notably, PaCSCs have a metabolism more dependent on mitochondrial respiration (OXPHOS)[168] as opposed to glycolysis, which is preferred by the rest of the tumor cells (non-PaCSCs)[155].

1. Overcoming challenges – Establishing a CSC-enriched long-term 2D culture

Current techniques based on the detection and separation of cell populations through the use of antibodies and flow cytometry-based separation techniques are not capable of maintaining a 2D culture enriched in CSCs (Figure 5). To overcome this issue, in this study, we developed a novel 2D *in vitro* system for long-term sustained enrichment of PaCSCs, which enabled us to recapitulate key features of CSCs, such as self-renewal and tumorigenesis, and at the same time better understand less studied properties such as quiescence, plasticity, metastasis and immune evasion. We took advantage of the inherent differences that exist between PaCSC and non-PaCSCs populations at the level of their mitochondria (Figures 6-7), and cultured our PDAC primary cultures with one of two carbon sources: glucose or galactose.

When glucose is no longer available in solid tumors, especially in pancreatic cancer, cancer cells are forced to use alternative energy substrates and/or metabolic pathways (e.g. oxidation of glutamine)[224] to survive in adverse conditions. Some cancer cells are able to switch their metabolism and under metabolic reprogramming with the goal of

producing sufficient energy to proliferate. In this regard, it has been proposed that oxidation of galactose to pyruvate through glycolysis yields no net production of ATP, forcing cells to rely on OXPHOS metabolism to generate enough ATP and proliferation products for cell survival[225,226]. Indeed, cancer cells grown in a medium where glucose was replaced with galactose showed an increase in oxygen consumption rate[227]. For these reasons, and taking into account the metabolic differences possessed by pancreatic cancer tumor cells, galactose was used as a tool to enhance OXPHOS metabolism that could alter or modified CSC features. Thus, by changing the carbon source from glucose to galactose, cancer cells (non-PaCSCs) that are exclusively dependent on aerobic glycolysis (Warburg effect) cannot survive due to metabolic rate differences with respect to obtaining ATP and proliferation products. That is, since ATP production from galactose is slower, only cancer cells (PaCSCs) that do not have strict ATP requirements, possess functional mitochondria and can obtain ATP via OXPHOS (or that are metabolically plastic and shift between metabolic states) will survive and proliferate in the presence of galactose. Of note, adapting cancer cells to a carbon source other than glucose has been previously applied *in vitro* to breast cancer cells[228]. Specifically, Banerjee et al. induced glycolytic restriction in breast cancer cell lines using 10mM fructose, which significantly reduces the rate of glycolysis, as cells are only able to import and retain fructose at approximately 100 times reduced rates compared to glucose[226,228]. Under these glucose-restrictive conditions, the authors observed a modest enrichment in breast CSC markers and functional properties (e.g. sphere and colony formation and tumorigenesis); however, their study only assessed classic CSC properties and did not consider the system as a method for dissecting CSC OXPHOS-dependence, understanding CSC plasticity or discovering new CSC properties such as those described in this study. Also, although other metabolites such as fructose or glutamine can be used to partially force cells in culture to use OXPHOS, it is known that culturing cells in galactose forces cells to use OXPHOS[225,227,229] and for this reason we chose galactose as our metabolic substrate for this project.

While more studies are still needed to definitively determine how galactose promotes PaCSC enrichment, the results presented in this thesis conclude that Gal-CC initially present higher levels of apoptotic cells compared to Glu-CC. However, the ratio of CSC enrichment (percentage of autofluorescent cells / percentage of apoptotic cells) was

higher in all the primary PDAC cultures that were analyzed at 14 days (**Figure 9**), indicating that while there is an initial wave of cell death, the cells that survive are enriched in CSCs. After developing the culture methods, we determined that 14 days was the minimum time necessary to see clear differences between Glu-CC and Gal-CC. Both Glu-CC and Gal-CC maintained these differential characteristics/properties for up to a month in culture (maximum time maintained in culture), showing similar parameters of growth and enrichment in CSCs to those evaluated at day 14. Although further analyses are necessary we suggest that PaCSC enrichment in Gal-CC may be a consequence of two reasons: 1) the first one is that non-PaCSCs, which base their metabolism on aerobic glycolysis, cannot obtain ATP and proliferation products quickly and efficiently to survive in galactose and/or 2) the second reason is that some subpopulations of non-PaCSCs are able to dedifferentiate (move from non-CSCs to CSCs) and acquire CSC metabolic features and survive along with hybrid-CC and PaCSCs present in the culture. The concept that the CSC subpopulation can be replenished by non-CSCs was experimentally proven in two recent studies targeting the LGR5^{+} CSC population in colon cancer organoid cultures[158,230]. In both studies, once the LGR5^{+} population had been eliminated, tumors regrew and the *LGR5*$^{+}$ population re-emerged, indicative of cellular plasticity driven by a non-CSC (or quiescent CSC) transient population. For this reason we believe that plasticity may also be playing a role in our system, but further analyses are still needed to understand the real dynamic that occurs with cell cultured in galactose, which could also be of great help towards understanding the biological behavior of PDAC.

Once the culture conditions were established, the results presented in this thesis conclude that our galactose-based OXPHOS-promoting system results in a profound increase in traditional CSC features, including a two to four-fold increase in the expression of multiple pancreatic CSC biomarkers (including autofluorescence and TEM8) (**Figures 10A-B**), over-expression of pluripotency-associated genes (such as OCT3/4 and KLF4) (**Figure 14A**), increase in Nanog-positive cells (YFP positive population by FACS analysis) (**Figure 14B**), enhanced self-renewal capacity (**Figure 12A**) and, most notably, significantly increased *in vivo* tumorigenicity using an ELDA approach (**Figures 16D,F**). Thus, all of the established CSC hallmarks are satisfied in our system; however, some specific results deserve further discussion. For example, while we observed a clear enrichment in CSCs, we did not obtain 100% CSC biomarker staining in Gal-CC. We reconcile this issue by

acknowledging that heterogeneity exists within the CSC population(s), making it impossible to detect all CSC clones as not all CSCs will express the same single biomarker, or combinations of different biomarkers. In addition, it is important to note that the cultures derived from PDAC patient tumors used in this study also have differences between them, including intertumoral heterogeneity (further discussed below). Thus, it is not surprising that the expression level of CSC biomarkers can also vary or may not be exactly the same at the level of identifying subpopulations of CSCs. Therefore, the two to four-fold increase in the percentage of CSC populations in galactose, at the level of cell-surface marker expression, may be an underestimate of the true enrichment obtained. Moreover, we propose that hybrid cancer cell (hybrid-CC) populations also exist in Gal-CC (as described above), and these cells are also able to survive under OXPHOS-promoting conditions and maintain CSC intrinsic features, but they may not express the biomarkers traditionally used to detect PaCSCs. Consequently, we are currently unable to identify/isolate these cells using current biomarker methodologies (**Figure 49**). Nonetheless, this system affords the possibility for studying this previously unappreciated hybrid-CC population, and could facilitate the identification of markers that could one day discriminate these cells from fully dedifferentiated CSCs and differentiated non-CSCs. This possibility would definitely improve our ability to monitor treatment response and disease relapse, where hybrid-CC play an important role[231].

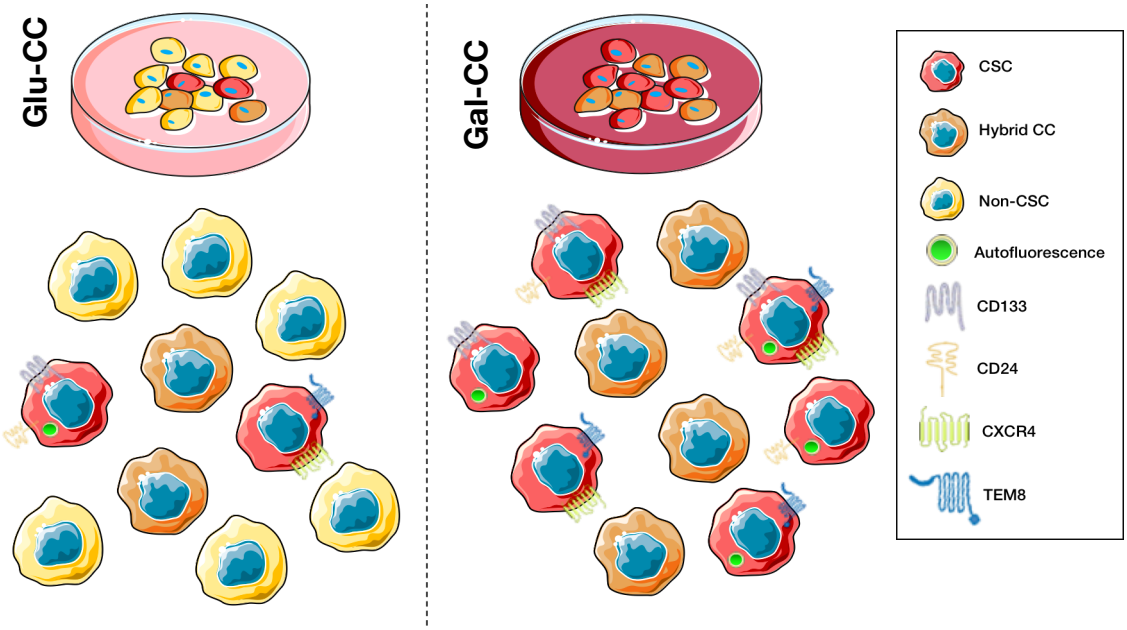

Figure 49. Different pancreatic cancer cell populations found in glucose and galactose cell culture conditions. On the left, in Glu-CC there is little enrichment in PaCSCs, the majority of cancer cells are both glycolytic and more differentiated (non-CSC). Whereas, on the right, in Gal-CC there is an enrichment in PaCSC and hybrid-CC populations, thus the majority of cells have an OXPHOS-dependent metabolism. Each CSC clone expresses different combinations of PaCSC biomarkers.

Secondly, while we did observe significantly more *in vivo* tumorigenicity with Gal-CC using an ELDA approach, further *in vivo* experiments would be necessary to verify that the tumorigenic capacity and enrichment in CSC population within the tumors are also applicable and extrapolated to the rest of PDAC primary tumors that we have used in the remaining experiments.

1.1. Mitochondrial metabolism

It is not surprising that mitochondria are important mediators of cancer "stemness"[171]. While we have previously shown that PaCSCs use OXPHOS to meet their energy requirements[168], the extent to which CSC mitochondria, mitochondrial biogenesis and OXPHOS favor and promote CSC properties, functional characteristics, quiescence, chemoresistance, invasion, migration and most importantly immune evasion could not be fully studied or appreciated prior to the development of this system[171,232]. In this line, Gal-CC showed higher mitochondrial mass (related to mitochondrial biogenesis) and more functional mitochondria compared to glycolytic cells (non-PaCSCs) (**Figures 17, 20-21**). Moreover, the mitochondria network in Gal-CC was denser and more extensive than the observed in Glu-CC (**Figures 21A, D**). Several reports have suggested that CSCs with fused mitochondrial networks rely more on OXPHOS as they have increased membrane potential, enhanced oxygen consumption rates, and increased mitochondrial biogenesis though expression of PGC-1α[233,234]. Indeed, Gal-CC over-express mitochondrial-associated genes like the master gene PGC-1α, which promotes mitochondrial biogenesis and OXPHOS and these processes are linked to cancer cell migration, epithelial-mesenchymal plasticity (EMP) and immune evasion[171]. Of interest was the observation that Gal-CC formed tight clones with the highest mitochondrial mass and membrane potential observed in cells of the borders, suggesting a possible hierarchical organization of clones with border cells having the highest migratory capacity. Likewise, it has been shown in other systems that the aberrant expression of immune evasion receptors (e.g. PD-L1) is metabolically controlled[235], and in cancer, correlations between metabolic alterations, EMT and PD-L1 upregulation have been demonstrated[236]. Thus, it could be hypothesized that PaCSC mitochondria and OXPHOS represent a master regulator of previously known and yet to be discovered key CSC features. More experiments are still needed to definitely prove this hypothesis, but below we discuss results that currently support this concept.

1.2. Quiescence

Apart from traditional CSC features, we also observed that Gal-CC were significantly less proliferative than Glu-CC, indicating that OXPHOS-dependent cells are more quiescent (i.e. dormant) (**Figures 29A,B**), a feature typically-associated with a CSC´s capacity to 1) survive in hostile environments (i.e. chemotherapy treatments), 2) stay latent for long periods of time and 3) to metastasize to distant organs when conditions become favorable[183]. Indeed, OXPHOS metabolism may be favored by quiescent CSCs as a means of maintaining mitochondrial membrane potential, ATP production and mtDNA content[171]. Whether metabolic reprogramming induces CSC dormancy or whether quiescent CSCs favor OXPHOS metabolism is still a black box. In this study, we observed that WNT signaling, which induces glycolysis[237,238], was reduced in Gal-CC compared to Glu-CC. We attribute this to the overexpression of the WNT inhibitor DKK-1, which has also been shown to be overexpressed in slow-cycling/quiescent latency competent breast and lung cancer cells[183]. Thus, metabolic reprogramming might be affecting WNT activity via upregulation of DKK-1. However, this is in contrast to a recent report by Shares et al., where they showed that culturing mesenchymal stem cells with galactose induced rather than inhibited β-catenin activity[239]. DKK-1 expression was not measured in their study; therefore, the reduced β-catenin activity we observe might be cell (cancer) type- and DKK-1-specific. Importantly though, OXPHOS-mediated CSC quiescence is not a permanent and/or irreversible state, as Gal-CC are highly plastic and can modulate their cellular proliferation and exit quiescence/dormancy in accordance to the carbon source available, thus adapting to their environment as shown in **Figure 30D**. Results after 14 days in galactose showed that Gal-CC were able to proliferate (even more than Glu-CC) when they were changed to medium containing glucose in only 7 days (Gal-CC + Glu).

1.3. Immune evasion

Novel to this study and to the PaCSC field, we show for the first time that OXPHOS-driven PaCSCs exhibit phenotypic characteristics and functional properties related to immune evasion as we mentioned above. Indeed, several studies have speculated that CSCs may maintain only limited antigen presentation levels and hence are invisible to the immune system, but it is also possible that CSCs possess antigen editing-independent molecular features that may endow them with the capacity to evade immune recognition and elimination[119,201,240]. In this sense, TGF-β has been described as a crucial player in the

cancer immune landscape, activating transcriptional cascades that can dramatically change CSC "behavior" by adjusting their metabolism, stress responses, immune evasion properties as well as their interactions with the microenvironment, to survive in adverse conditions (e.g. chemotherapy treatments)[159,160,201]. Specific to our system, Gal-CC secreted more TGF-β compared to Glu-CC (**Figure 35D**) and acquired an immune evasive molecular signature, enabling them to evade immune innate cells (i.e. macrophages and NK cells) and adaptive immune cells (T-cells) thanks to the modulation of different immune-associated receptors, ligands and secreted cytokines. As a consequence, Gal-CC were more invasive and metastatic in the two *in vivo* models utilized (i.e. zebra fish and NOD-SCID mice) (**Figures 40-44**). In this sense, Gal-CC were able to modulate the immune infiltrating cell profile at early and late times points post-injection in NOD-SCID mice, attracting fewer immune cells during the early stages of extravasation, thus allowing for greater invasion, while at later times promoting the accumulation of pro-tumor immune cells (e.g. TAMs) in the different organs analyzed, which would facilitate establishment of the niche and tumor microenvironment (**Figures 43, 45**).

1.4. Heterogeneity

It is important to note that in this study we used 4 primary PDX-derived PDAC lines with varying degrees of heterogeneity, which have been previously established and described[241,242]. Two heterogenous primary pancreatic tumors (PANC286 and PAN185), a liver metastasis (PANCA6L), and the PANC185 single cell-derived (scd) tumor that was generated by injecting a single autofluorescent-positive CSC isolated from PANC185 into an immunocompromised mouse[243]. As we have previously shown, the heterogeneity should be higher in the primary tumors, lower in the metastatic tumor and homogenous in the scd tumor[243]. In fact, the 185scd culture allows for the study of multilineage differentiation, plasticity and CSC fate at the level of a single CSC clone, and allows one to ask the question of whether specific CSC features, such as metabolic plasticity, are a consequence of tumor heterogeneity where multiple different CSCs concomitantly contribute to the specific phenotype or an intrinsic property of CSCs independent of the degree of CSC heterogeneity[244]. Since similar effects were seen between the 185scd clone and the other three cell lines, we can conclude that single-cell-cloned PaCSCs have the same plastic capacity and multilineage differentiation potential as cultures with more or less heterogenous CSC subpopulations. Thus, in theory, our 2D OXPHOS-based

system could be applied to any primary PDAC culture regardless of the degree of CSC heterogeneity. The latter is important when contemplating the applicability or translatability of this culture system to personalized medicine or screening platforms that use cultures derived from PDXs or directly from CSCs isolated from freshly resected tumors. In both cases, the methodologies employed do not capture the complete heterogeneity of the original tumor, and this has created a debate as to whether *ex vivo* systems are biologically or clinically relevant. We can conclude from our studies that the metabolic plasticity of PaCSCs and the role of mitochondria in PaCSC stemness is recapitulated across tumors of differing heterogeneity. It appears that mitochondria are one key feature that is homogenous and conserved across all CSC clones. Therefore, in theory, this system could be applied to any primary PDAC culture that contains CSCs; however, more experiments are still necessary. As future perspectives we should, 1) expand these studies to a larger number of PDX-derived cultures, 2) establish Glu-CC and Gal-CC cultures directly from digested PDXs, and 3) establish Glu-CC and Gal-CC cultures from tumor cells isolated directly from resected patient tumors.

2. Future applicability of the CSC-enriched long-term 2D culture

Regarding current treatments for PDAC, the standard of care is mainly based on surgery and/or chemotherapy. PDAC is a deadly disease with an OS (overall survival) rate of less than 6%[245]. Although current treatments like nab-paclitaxel (Abraxane) plus gemcitabine therapy (GnP therapy), and 5-FU, leucovin, irinotecan and oxaliplatin (FOLFIRINOX) therapy can improve the clinical outcome of unresectable PDAC, surgery is the only way to achieve a greater long-term survival, especially in early stages of the disease. Unfortunately, most PDAC patients remain asymptomatic until the disease develops to more advanced stages[246], thus, surgical intervention is often complicated and not possible when PDAC is detected at such late stages. Many times, these complications are due to the fact that the tumor has metastasized to areas close to important blood vessels, which makes its removal very risky and the life of patients is compromised. However, even in patients who undergo surgery, 5-year survival is poor at <30%[247–249]. This fact indicates that surgery alone is insufficient and the poor survival characteristic of PDAC is attributable to early metastatic spread as most patients have metastatic foci at the time of surgery[245]. A preclinical study using a mouse model of PDAC indicated that early metastasis might possibly be detected even when there is no primary

tumor found in the pancreas and is associated with EMT and local inflammation[250]. Therefore, the design of new therapies that include early treatment of micrometastases would help to reduce the risk of tumor spread at the time of surgery and improve the tolerance of postoperative therapies. In this sense, neoadjuvant chemotherapy (NAC) with GnP protocol is being investigated as a possible treatment for resectable PDAC since it has managed to reduce the stroma in most patients[245,251].

Although these advances in PDAC therapy have afforded a modest benefit to patients, more research is urgently needed to achieve more effective treatments, as well as more accurate diagnostic and prognostic markers for this deadly disease. In this sense, it is essential to consider the nature of PaCSCs when designing novel therapeutic strategies, because they are the promoters of tumor initiation, progression and metastatic dissemination. Essentially, CSCs represent the seed of the tumor and, from a clinical perspective, only elimination of the PaCSCs population will ensure tumor eradication.

Unfortunately, standard chemotherapy either does not reach the CSC population, or is ineffective against them. A significant factor driving the inherent chemoresistance of CSCs is their slow-cycling or quiescent state. In fact, chemotherapy can even induce quiescence as a mechanism of resistance to therapy (when the cell cycle is stopped, chemotherapy does not affect them). In addition, the upregulation of drug efflux pumps represents another important factor that promotes drug resistance in CSCs. Regarding quiescence, multiple studies have described that slow-cycling/dormant tumor cells are more chemoresistant, show EMP and are more immunoevasive, which enable these cells to drive post-treatment relapse, tumor cell dissemination and cell survival in hostile environments[182,252–254]. Along these lines, Gal-CC were more chemoresistant when treated with a panel of traditional chemotherapeutics than Glu-CC, largely due to the overexpression of the ABCG2 transporter and the different levels of expression of genes related to Gemcitabine metabolism (**Figures 32-33**). In contrast, and as expected, Gal-CC were more sensitive to OXPHOS-targeting metabolic drugs and less sensitive to the glycolysis inhibitor 2DG (**Figure 34**). Thus, cytotoxic/genotoxic agents targeting high-proliferative cells (non-CSCs), such as Gemcitabine, are not able to effectively target CSCs, and often lead to relapse (**Figure 33**). For this reason, combinatory treatments like

surgery plus standard chemotherapy and metabolic drugs would be an interesting option to get rid of the circulating and metastatic PaCSCs in this type of tumor.

2.1. Autophagy

PaCSC-targeting strategies are based on differential features of PaCSCs compared to non-CSCs, healthy cells and normal stem cells and seem to be highly promising for PDAC treatment. Thus, numerous studies have tried to identify novel drugs to disrupt the biology of these cells. In recent years, it has been reported that both the use of inhibitors and activators of autophagy can promote apoptosis in CSCs and decreasing tumorigenic potential in mice[108]. Therefore, modulation of autophagy in CSCs through activating or inhibiting drugs is able to disrupt their autophagic physiological balance, which sensitizes them to antitumor drugs[255].

In this sense, several autophagy inhibitors have been explored to target PaCSCs. For example, it has been shown that Alisertib, an inhibitor of Aurora kinase A, induces cell cycle arrest and promotes autophagy in PDAC cells[256]. Also, chloroquine and BAY 1170-82, an inhibitor of NF-κB activation, succeed in suppressing autophagy in PaCSCs and rendered them more susceptible to treatment with the chemotherapeutic Gemcitabine. In light of these findings, it seems that the combinatory therapy of both drugs is a promising therapeutic strategy for this disease[45]. In addition, it has been recently described that combined use of Deguelin and Doxorubicin potentiates the anticancer effects against PDAC cells. Deguelin is an organic compound that exerts a potent antiproliferative effect by blocking autophagy and inducing apoptosis in PDAC cells *in vitro*. Accordingly, the use of Deguelin as an autophagy inhibitor resulted in the chemosensitization of PDAC cell lines against Doxorubicin[257]. Also, the inhibition of casein kinase 2 (CK2) has been reported as a novel therapeutic strategy for many cancers, including PDAC. CX-4945, a novel CK2 inhibitor, induced significant inhibition of proliferation and resulted in an induction of autophagy in PDAC cells[258]. Taking into account our results, we observed an increase in amount of cytoplasmic vesicles in the majority of Gal-CC compared to Glu-CC (**Figure 23**) due to their higher levels of autophagy (**Figures 23-26**). This result suggests that autophagy could play an important protective role in PaCSCs and is also very likely an important mechanism used by OXPHOS-dependent cells to survive under chemotherapeutic stress and metabolically restrictive

conditions, such as those faced by CSCs in the PDAC microenvironment where oxygen and nutrients supply is reduced[156,259]. Moreover, it was observed that autophagic processes are strongly linked to quiescent/dormant states in cancer cells[260,261]. In summary, the significant increase of the autophagic vesicles and, likewise, the autophagic flux in Gal-CC could be another mechanism of resistance against the chemotherapeutic agents used in our experiments (Gemcitabine, Doxorubicin and Mitoxantrone). As future perspectives, the autophagy-modulating drugs mentioned above (e.g. Deguelin) in combination with chemotherapeutic agents (i.e. Doxorubicin) or OXPHOS-targeting metabolic drugs could be an interesting option to be tested in our 2D *in vitro* platform.

2.2. EMT, MET and EMP

Interestingly, the observed increase in autophagy supports recent reports linking autophagy with EMP, which is termed as the ability of cells to maintain their plasticity and transit between EMT and MET states[262]. In fact, tumor cells that are able to co-express epithelial and mesenchymal markers (hybrid E/M cells) are more aggressive and responsible for the migration of tumor cell clusters in bloodstream[262–264]. Two recent reports in breast and lung cancer demonstrate that autophagy is intimately linked to EMP, specifically the capacity of cancer cells to transition between epithelial and mesenchymal states[252,265]. EMP is now considered a critical process for tumor cell dissemination, metastatic colonization, chemoresistance, and is also intimately associated with a CSC phenotype. When EMT is in progress, cells will lose their adhesion and polarity characteristics, characterized by reduced expression of E-Cadherin and increased expression of mesenchymal markers and EMT factors, such as Snail, Slug and ZEB1[266]. The ZEB1 transcription factor is strongly associated with the EMP process and is largely responsible for driving EMP in genetically engineered mouse models (GEMM) of PDAC development[267,268]. Likewise, ZEB1 has been recently linked with PDAC metabolic plasticity *in vivo*[268]. Interestingly, we observed that not only were Gal-CC were more chemoresistant, but we also observed increased expression of different EMT transcription factors, with ZEB1 showing the highest induction (**Figure 31C**), suggesting Gal-CC cells would have a hybrid E/M (EMP) phenotype because, apart from presenting differences in EMT factors, they have been shown to have a greater invasive capacity *in vivo* (**Figures 46-47**). In fact, biological associations between EMT and metabolic reprogramming in cancer have been described and shown to be a consequence of EMT transcription factor

signaling[269]. Thus, it is not surprising to observe the overexpression of ZEB1 in cultures enriched in CSCs and other OXPHOS-dependent cells (hybrid-CC), but it rather validates the system and its biological relevance.

2.3. Immunotherapies

Propelling comprehensive research on identifying, isolating, and dissecting the PaCSC subpopulations within the tumor is of the utmost importance. The identification of cytokines secreted by PaCSCs and their impact on the anti-tumor immune response is comparable to the identification of PaCSCs by cell-surface biomarkers, in terms of diagnosis and prognosis in PDAC. In this study, we showed that the profile of immunoevasive cytokines secreted by PDAC cells is notably different between Glu-CC and Gal-CC. The cytokine secretion profile of Gal-CC is dramatically more immunoevasive than the observed in Glu-CC (**Figure 37A-C**). Therefore, it could be possible that Gal-CC may also secrete other relevant factors for the development and establishment of the tumor both in the early and later stages of the disease. This could explain the differences we observed in the populations of TAMs (at short and long times) in the *in vivo* invasion assay (**Figure 48**). Therefore, our 2D cell culture system could also be useful as a possible screening method for the detection of new PaCSC-specific secreted proteins that could be evaluated as possible diagnostic markers. Likewise, our system could also be useful to study the role of immune checkpoint receptors/ligands and to test new immunotherapies against PaCSCs in combination with current therapies.

The PDAC stroma is highly desmoplastic and represents more than 90% of the tumor composition; thus, research focused on therapies directed against the cells that make up the stromal tissue (e.g. tumor-associated macrophages, TAMs) could be an interesting strategy to fight the tumor. As already mentioned above, we showed that Gal-CC had a higher expression of receptors that enable them to evade the anti-tumor action of TAMs, including CD206 and CD47 (“don’t-eat-me” receptor) (**Figure 35B**). Consequently, Gal-CC were not as efficiently phagocytosed as Glu-CC when co-cultured with macrophages derived from healthy donors (**Figure 38C**), indicating that these immunoevasive receptors were functionally protecting Gal-CCs from TAM killing, while Glu-CC were unprotected.

Moreover, PDAC has been described as a poorly immunogenic tumor, since the T-cell population is mainly found in the periphery of the tumor or otherwise isolated from the tumor niche/TME, in contrast to the location of the rest of cells that make up the TME. Interestingly, Gal-CC showed higher expression of the immunoevasive ligand PD-L1 for the receptor PD-1 present in T-cells and downregulated expression of the immune activation ligands ULBP2/5/6 for the receptor NKG2D present in NK cells and T-cells (**Figure 35B**), clearly indicating that Gal-CC have an immunosuppressive profile. Therefore, treatments with immunotherapies seem to be quite complicated for this type of tumor. However, despite the great challenges that stand in the way of achieving effective immunotherapy against PDAC, great advances are currently under research in the field like immunotherapies based on T-cells. A recent study based on CAR-T cells showed that CAR-T cells directed against prostate stem cell antigen (PSCA) present in PDAC tumors achieved specific tumor cell lysis. Nonetheless, the TME and CSCs can create a highly immunosuppressive environment to reduce T-cell killing through the secretion of IL-4[270], which inhibits the cytolytic activity of T-cells, thus highlighting the importance of the immunomodulation induced by secreted cytokines in the success of immunotherapies. To surpass this restriction, these CAR T-cells were modified by transgenic expression to express a custom inverted cytokine receptor (ICR) encoding the cytokine-binding portion of the IL-4 receptor exodomain linked to the immunostimulatory IL-7 receptor signaling endodomain, thus protecting CAR T-cells from IL-4 immunosuppressive effect, and enabling this approach to achieve better results both *in vitro* and *in vivo*[271]. In this sense, our 2D *in vitro* platform could be a useful tool to discover new immune checkpoints against CSCs to test and improve new approaches in the field of immunotherapies.

2.4. Personalized medicine

CSCs represent an emerging field in therapeutic research. In this sense, it is important to highlight the initial model that provided the necessary cell cultures to develop this novel 2D culture platform. PDAC tumors derived from patients were used to generate patient-derived xenografts (PDXs). The PDX models are created by engrafting tumor tissues from patients in immunodeficient mice. Since a PDX model retains the characteristics of the primary tumor of patients, including gene expression profiles and responses to medications, it has become the most reliable *in vivo* human cancer model[272]. PDX models

allow for the isolation and culture of cells from PDAC patients, thus facilitating 1) the obtention of different tumor populations within the tumor, including CSCs populations, 2) the obtention of a molecular profile of the tumor through the corresponding analyses, 3) *in vitro* preclinical drug testing for the response to different treatments and 4) the selection of the optimal treatment for each patient and tumor, opening the way to a possible personalized medicine in the future (**Figure 50**).

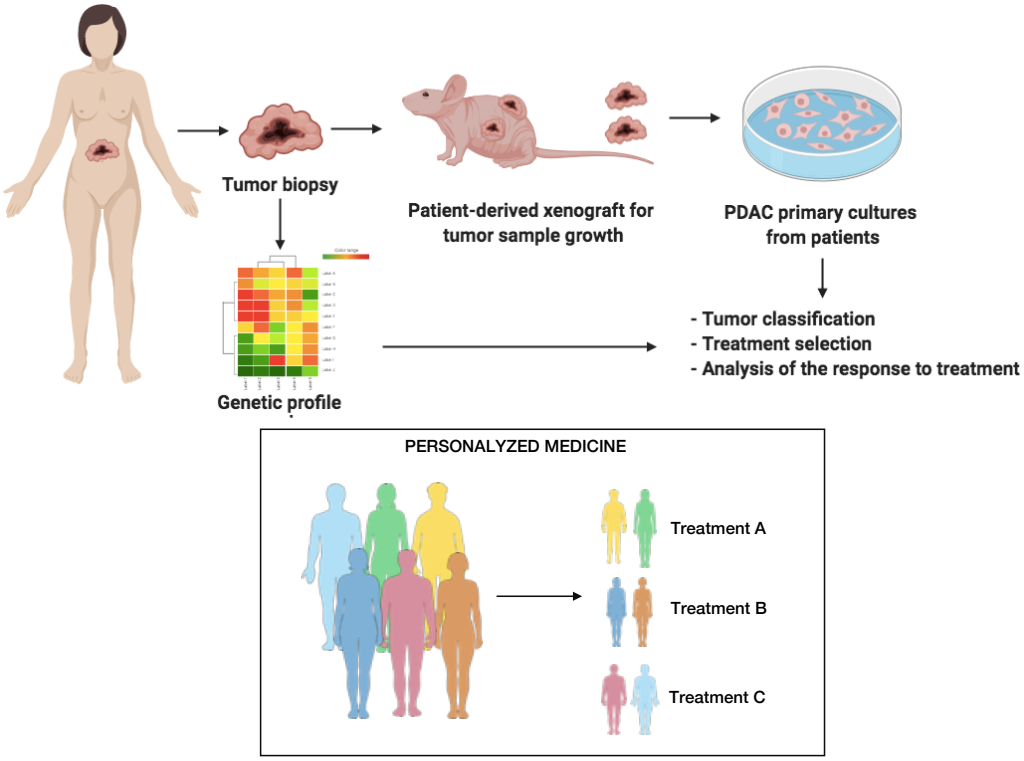

Figure 50. Representative scheme of the protocol for obtaining cancer cells using the PDX technique and its 2D primary cultures and its potential application for the development of a personalized medicine.

Thus, although there are limitations in the different preclinical models currently used in PDAC research, the combination of these different models strengthens the options for a new therapy to be successful in a clinical trial, which represents the real definitive test for future therapeutic use in patients. PDX models have been used for decades to increase our understanding of factors affecting tumor growth; however, they also show some disadvantages[273]. Recent information regarding the key influence of the TME on tumor progression and tumor growth has led to greater reliance on GEMM tumor models using immunocompetent mice, specially the commonly used KPC model ($Kras^{G12D}$; Trp53 mutant; Cre)[274]. Although GEMM are highly useful for evaluating the effects of mutations during murine tumor progression, they usually cannot fully reproduce the genetic complexity of human tumors[272,273].

In summary, in a novel way, our study demonstrates that the metabolism of PaCSCs is intimately linked to their quiescent, metastatic and immuno-evasive capacities (**Figure 51**). The plasticity of PaCSCs and their relative dependence on mitochondrial dynamics may offer new therapeutics avenues for cancer treatments, particularly as CSCs display extreme resistance to most conventional chemotherapeutics. Thus, our data also highlight the potential applicability of this platform to screen for novel CSC-specific inhibitors, discover features related to hybrid-CC population, as well as new compounds directed towards cancer cell metabolism and metabolic reprogramming, an area of research that is gaining considerable attention. Moreover, based on the correlation observed with immune evasion, this metabolic platform may synergize with immunotherapeutic approaches for improved and long-lasting antitumor outcomes.

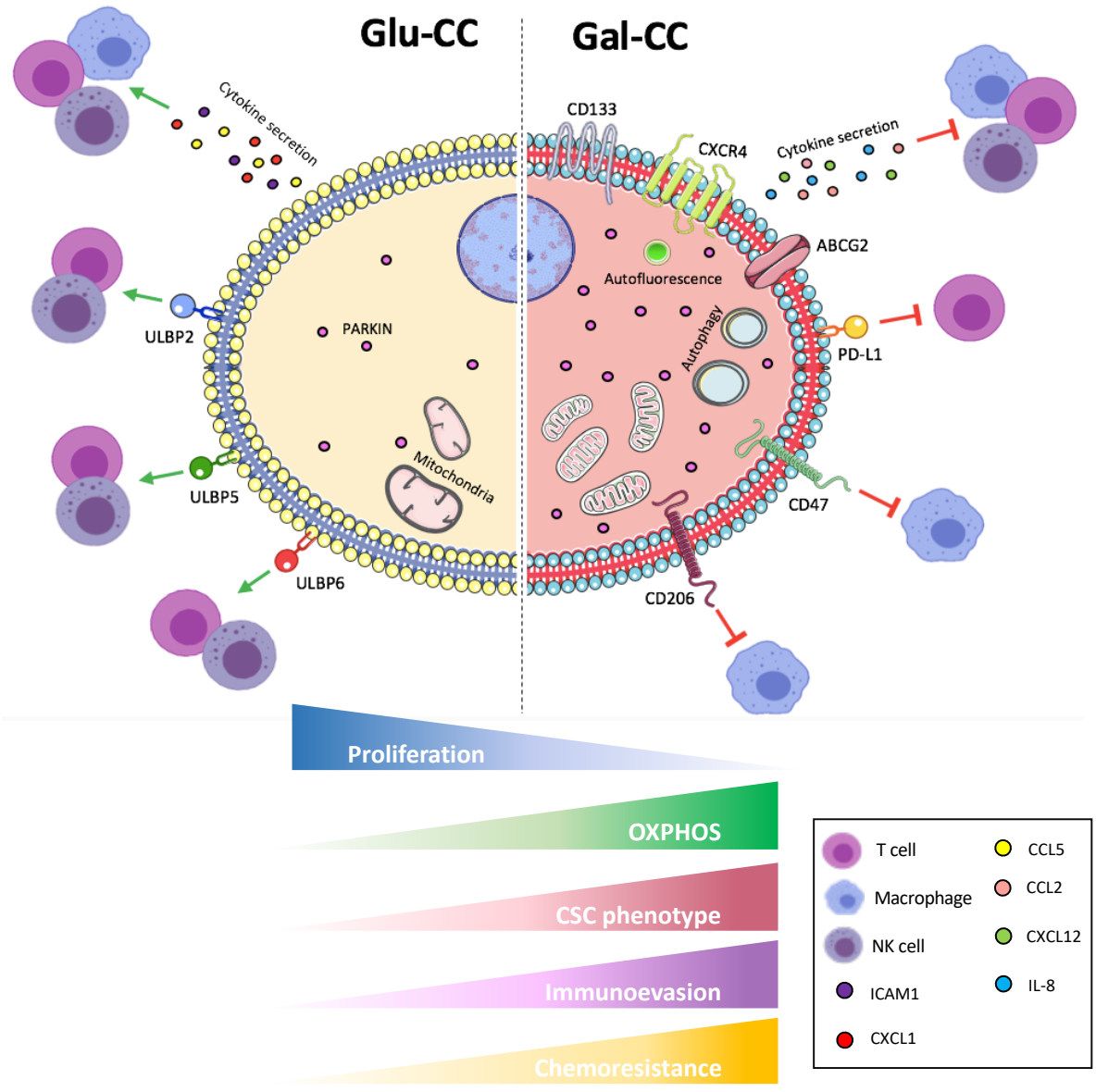

Figure 51. Representative summary scheme of the biological and molecular differences found between Glu-CC and Gal-CC.

CONCLUSIONS / CONCLUSIONES

The following conclusions can be drawn from the results presented in this doctoral thesis:

1. The mitochondria of PaCSCs are morphologically and functionally different from the mitochondria of non-PaCSCs cells. Mitochondria of PaCSCs seem to be better structurally defined and present higher mitochondrial membrane potential, which would imply that based their metabolism on OXPHOS system.

2. Culturing primary PDAC cells in carbon sources other than glucose (galactose in this case) is technically feasible; however, media with galactose must be supplemented with FBS. While initial cell death is observed under galactose culture conditions (Gal-CC), a stable culture that can be maintained indefinitely is obtained.

3. Galactose promotes an enrichment in CSCs, at the level of the expression of CSC cell surface markers (e.g. autofluorescence, CD133, CXCR4), at the molecular level (e.g. increase in the expression of pluripotency-associated genes) and at the functional level (e.g. increased sphere formation and tumor formation capacity) compared to glycolysis metabolism (Glu-CC).

4. Compared to Glu-CC, which are more glycolytic and less dependent on functional mitochondria, Gal-CC have increased mitochondrial mass, increased mitochondrial membrane potential (i.e. increased functional mitochondria), increased ROS levels and increased markers of mitochondria recycling and maintenance.

5. Gal-CC contain more autophagic vesicles due to the presence of a higher autophagic flux compared to Glu-CC, suggesting that autophagy is also likely an important mechanism that also participates in cell adaptation or quality control of mitochondria used by OXPHOS-dependent cells to survive under metabolically restrictive conditions.

6. Gal-CC seem to enter into a more quiescent / slow-cycling state compared to Glu-CC. However, this quiescence is not a permanent and/or irreversible state as

Gal-CC can modulate their cellular proliferation and exit quiescence/dormancy in accordance to the carbon source available, thus adapting to their environment.

7. Gal-CC are more resistant to a panel of traditional chemotherapeutics than Glu-CC. This is due, in part, to the modulation of multidrug resistant and gemcitabine-specific cell membrane transporters. In contrast, and as expected, Gal-CC are more sensitive to OXPHOS metabolic drugs and less sensitive to inhibitors of glycolysis compared to Glu-CC.

8. Gal-CC modulate their cell surface receptors and ligands and cytokine profile to possibly evade immune cell detection and/or elimination. Moreover, this was strongly confirmed in functional assays performed with macrophages and T-cells derived from healthy donors, in which Gal-CC were more resistant to immune cell phagocytosis or lysis, respectively.

9. Injected Gal-CC are more invasiveness and metastatic in both zebrafish and mouse *in vivo* models. In mice model, they were able to modulate the TAM infiltrating cell profile at early and late times points post-injection, facilitating the establishment of the niche and tumor microenvironment.

10. The Gal-CC system described demonstrates that the metabolism of PaCSCs is intimately linked to their stem, quiescent, metastatic and immuno-evasive capacities. This system could be potentially used to screen for novel CSC-specific inhibitors as well as new compounds directed towards cancer cell metabolism and metabolic reprogramming, an area of research that is gaining considerable attention, and based on the correlation observed with immune evasion, may synergize with immunotherapeutic approaches for improved and long-lasting antitumor outcomes.

De los resultados recogidos en la presente tesis doctoral se pueden extraer las siguientes conclusiones:

1. Las mitocondrias de las PaCSCs son morfológica y funcionalmente diferentes de las mitocondrias de las no PaCSCs. Las mitocondrias de PaCSCs parecen estar mejor definidas estructuralmente y presentan un mayor potencial de membrana mitocondrial, lo que sugiere que presentan un metabolismo energético basado en el sistema OXPHOS.

2. El cultivo de células primarias de PDAC en fuentes de carbono distintas a la glucosa (en este caso galactosa) es técnicamente factible; sin embargo, los medios con galactosa deben complementarse con FBS. Si bien al utilizar galactosa como única fuente de carbono se observa cierto nivel de muerte celular inicial, se puede obtener un cultivo estable que puede mantenerse indefinidamente.

3. El cultivo con galactosa promueve un enriquecimiento en CSCs, a nivel de expresión de marcadores de superficie celular de CSCs (por ejemplo, autofluorescencia, CD133, CXCR4), a nivel molecular (por ejemplo, aumento en la expresión de genes asociados a pluripotencia) y a nivel funcional (p. ej., aumento de la formación de esferas y capacidad de formación de tumores) en comparación con las células con metabolismo glucolítico (Glu-CC).

4. En comparación con las Glu-CC, las cuáles son más glucolíticas y menos dependientes de las mitocondrias funcionales, las Gal-CC han aumentado la masa mitocondrial, el potencial de membrana mitocondrial (es decir, el aumento de las mitocondrias funcionales), los niveles de ROS y de los marcadores de reciclaje y mantenimiento de las mitocondrias.

5. Las Gal-CC contienen más vesículas autofágicas debido a la presencia de un mayor flujo autofágico en comparación con las Glu-CC, lo que sugiere que la autofagia también es un mecanismo importante que participa en la adaptación celular y control de calidad de las mitocondrias de las células dependientes de OXPHOS para sobrevivir en condiciones metabólicamente restrictivas.

6. Las Gal-CC parecen entrar en un estado de reposo/ciclo lento en comparación con las Glu-CC. Sin embargo, esta inactividad no es un estado permanente o irreversible ya que las Gal-CC pueden modular su proliferación celular y salir de la inactividad/latencia de acuerdo con la fuente de carbono disponible, adaptándose así a su entorno.

7. Las Gal-CC son más resistentes a un panel de quimioterapia tradicional que las Glu-CC. Esto se debe, en parte, a la modulación de transportadores de membrana celular resistentes a múltiples fármacos y específicos a la gemcitabina. Por el contrario, y como se esperaba, las Gal-CC son más sensibles a los fármacos metabólicos OXPHOS y menos sensibles a los inhibidores de la glucólisis que las Glu-CC.

8. Las Gal-CC modulan sus receptores y ligandos de la superficie celular y el perfil de secreción de citoquinas para, posiblemente, evadir su detección y/o eliminación por parte de las células inmunes. Además, esto se confirmó mediante ensayos funcionales realizados con macrófagos y células T derivadas de donantes sanos, en los que las Gal-CC eran más resistentes a la fagocitosis y lisis de las células inmunes, respectivamente.

9. Las Gal-CC inyectadas son más invasivas y metastásicas en los modelos *in vivo* tanto de pez zebra como en ratón. En este último, pudieron modular el perfil de TAMs infiltrados en los tiempos tempranos y tardíos posteriores a la inyección, lo que facilita el establecimiento del nicho y el microambiente tumoral.

10. El sistema Gal-CC descrito demuestra que el metabolismo de las PaCSCs está íntimamente relacionado con sus características de *stem*, quiescencia, metástasis e inmunoevasivas. Este sistema podría usarse potencialmente para detectar nuevos inhibidores específicos de CSCs, así como nuevos compuestos dirigidos hacia el metabolismo de las células tumorales y la reprogramación metabólica, un área de investigación que está ganando considerable atención y, según la correlación observada con la evasión inmune, puede sinergizar con enfoques inmunoterapéuticos para resultados antitumorales mejorados y duraderos.

REFERENCES

1. Torres, C. & Grippo, P. J. Pancreatic cancer subtypes: a roadmap for precision medicine. Ann. Med. 50, 277–287 (2018).
2. Gleeson, F. C. et al. Targeted next generation sequencing of endoscopic ultrasound acquired cytology from ampullary and pancreatic adenocarcinoma has the potential to aid patient stratification for optimal therapy selection. Oncotarget 7, 54526–54536 (2016).
3. Hidalgo, M. Pancreatic cancer. N. Engl. J. Med. 362, 1605–1617 (2010).
4. Bray, F. et al. Global cancer statistics 2018: GLOBOCAN estimates of incidence and mortality worldwide for 36 cancers in 185 countries. CA. Cancer J. Clin. 68, 394–424 (2018).
5. Rahib, L. et al. Projecting cancer incidence and deaths to 2030: the unexpected burden of thyroid, liver, and pancreas cancers in the United States. Cancer Res. 74, 2913–2921 (2014).
6. Scarà, S., Bottoni, P. & Scatena, R. CA 19-9: Biochemical and Clinical Aspects. Adv. Exp. Med. Biol. 867, 247–260 (2015).
7. Haab, B. B. et al. Definitive Characterization of CA 19-9 in Resectable Pancreatic Cancer Using a Reference Set of Serum and Plasma Specimens. PloS One 10, e0139049 (2015).
8. Kim, J. et al. Detection of early pancreatic ductal adenocarcinoma with thrombospondin-2 and CA19-9 blood markers. Sci. Transl. Med. 9, (2017).
9. Capello, M. et al. Sequential Validation of Blood-Based Protein Biomarker Candidates for Early-Stage Pancreatic Cancer. J. Natl. Cancer Inst. 109, (2017).
10. Dunne, R. F. & Hezel, A. F. Genetics and Biology of Pancreatic Ductal Adenocarcinoma. Hematol. Oncol. Clin. North Am. 29, 595–608 (2015).
11. Greer, J. B. & Brand, R. E. Screening for pancreatic cancer: current evidence and future directions. Gastroenterol. Hepatol. 3, 929–938 (2007).
12. Hassan, M. M. et al. Risk factors for pancreatic cancer: case-control study. Am. J. Gastroenterol. 102, 2696–2707 (2007).
13. Berrington de Gonzalez, A., Sweetland, S. & Spencer, E. A meta-analysis of obesity and the risk of pancreatic cancer. Br. J. Cancer 89, 519–523 (2003).
14. Kamarajah, S. K., Burns, W. R., Frankel, T. L., Cho, C. S. & Nathan, H. Validation of the American Joint Commission on Cancer (AJCC) 8th Edition Staging System for Patients with Pancreatic Adenocarcinoma: A Surveillance, Epidemiology and End

Results (SEER) Analysis. Ann. Surg. Oncol. (2017) doi:10.1245/s10434-017-5810-x.

15. Conlon, K. C., Klimstra, D. S. & Brennan, M. F. Long-term survival after curative resection for pancreatic ductal adenocarcinoma. Clinicopathologic analysis of 5-year survivors. Ann. Surg. 223, 273–279 (1996).
16. Hartwig, W. et al. Pancreatic cancer surgery in the new millennium: better prediction of outcome. Ann. Surg. 254, 311–319 (2011).
17. Garrido-Laguna, I. & Hidalgo, M. Pancreatic cancer: from state-of-the-art treatments to promising novel therapies. Nat. Rev. Clin. Oncol. 12, 319–334 (2015).
18. Visvader, J. E. & Lindeman, G. J. Cancer stem cells in solid tumours: accumulating evidence and unresolved questions. Nat. Rev. Cancer 8, 755–768 (2008).
19. Sancho, P., Alcala, S., Usachov, V., Hermann, P. C. & Sainz, B. The ever-changing landscape of pancreatic cancer stem cells. Pancreatology 16, 489–496 (2016).
20. Rich, J. N. Cancer stem cells: understanding tumor hierarchy and heterogeneity. doi:10.1097/MD.0000000000004764.
21. Kreso, A. & Dick, J. E. Evolution of the cancer stem cell model. Cell Stem Cell 14, 275–91 (2014).
22. Bonnet, D. & Dick, J. E. Human acute myeloid leukemia is organized as a hierarchy that originates from a primitive hematopoietic cell. Nat. Med. 3, 730–737 (1997).
23. Song, L. L. & Miele, L. Cancer stem cells--an old idea that's new again: implications for the diagnosis and treatment of breast cancer. Expert Opin. Biol. Ther. 7, 431–438 (2007).
24. Dieter, S. M. et al. Distinct types of tumor-initiating cells form human colon cancer tumors and metastases. Cell Stem Cell 9, 357–65 (2011).
25. Wang, J., Ma, Y. & Cooper, M. K. Cancer stem cells in glioma: challenges and opportunities. Transl. Cancer Res. 2, 429–441 (2013).
26. Nguyen, L. V, Vanner, R., Dirks, P. & Eaves, C. J. Cancer stem cells: an evolving concept. Nat. Rev. Cancer 12, 133–143 (2012).
27. Vermeulen, L., Sprick, M. R., Kemper, K., Stassi, G. & Medema, J. P. Cancer stem cells--old concepts, new insights. Cell Death Differ. 15, 947–958 (2008).
28. Lonardo, E. et al. Nodal/Activin signaling drives self-renewal and tumorigenicity of pancreatic cancer stem cells and provides a target for combined drug therapy. Cell Stem Cell 9, 433–446 (2011).
29. O'Brien-Ball, C. & Biddle, A. Reprogramming to developmental plasticity in cancer

stem cells. Dev. Biol. (2017) doi:10.1016/j.ydbio.2017.07.025.

30. Virchow, R. An Address on the Value of Pathological Experiments. Br. Med. J. 2, 198–203 (1881).
31. Lapidot, T. et al. A cell initiating human acute myeloid leukaemia after transplantation into SCID mice. Nature 367, 645–648 (1994).
32. Li, C. et al. Identification of pancreatic cancer stem cells. Cancer Res. 67, 1030–1037 (2007).
33. Hermann, P. C. et al. Distinct populations of cancer stem cells determine tumor growth and metastatic activity in human pancreatic cancer. Cell Stem Cell 1, 313–323 (2007).
34. Plaks, V., Kong, N. & Werb, Z. The Cancer Stem Cell Niche: How Essential Is the Niche in Regulating Stemness of Tumor Cells? Cell Stem Cell 16, 225–238 (2015).
35. Albini, A. et al. Cancer stem cells and the tumor microenvironment: interplay in tumor heterogeneity. Connect. Tissue Res. 56, 414–425 (2015).
36. Nguyen, P. H. et al. Characterization of Biomarkers of Tumorigenic and Chemoresistant Cancer Stem Cells in Human Gastric Carcinoma. Clin. Cancer Res. Off. J. Am. Assoc. Cancer Res. (2016) doi:10.1158/1078-0432.CCR-15-2157.
37. Rasheed, Z. A. et al. Prognostic significance of tumorigenic cells with mesenchymal features in pancreatic adenocarcinoma. J. Natl. Cancer Inst. 102, 340–351 (2010).
38. Miranda-Lorenzo, I. et al. Intracellular autofluorescence: a biomarker for epithelial cancer stem cells. Nat. Methods 11, 1161–1169 (2014).
39. Alcalá, S., Martinelli, P., Hermann, P. C., Heeschen, C. & Sainz, B. The Anthrax Toxin Receptor 1 (ANTXR1) Is Enriched in Pancreatic Cancer Stem Cells Derived from Primary Tumor Cultures. Stem Cells International https://www.hindawi.com/journals/sci/2019/1378639/ (2019) doi:10.1155/2019/1378639.
40. Wang, V. M.-Y. et al. CD9 identifies pancreatic cancer stem cells and modulates glutamine metabolism to fuel tumour growth. Nat. Cell Biol. 21, 1425–1435 (2019).
41. Gottesman, M. M. Mechanisms of cancer drug resistance. Annu. Rev. Med. 53, 615–627 (2002).
42. Abdullah, L. N. & Chow, E. K.-H. Mechanisms of chemoresistance in cancer stem cells. Clin. Transl. Med. 2, 3 (2013).
43. Sun, Y.-L., Patel, A., Kumar, P. & Chen, Z.-S. Role of ABC transporters in cancer

chemotherapy. Chin. J. Cancer 31, 51–7 (2012).

44. Duong, H.-Q. et al. Aldehyde dehydrogenase 1A1 confers intrinsic and acquired resistance to gemcitabine in human pancreatic adenocarcinoma MIA PaCa-2 cells. Int. J. Oncol. 41, 855–861 (2012).
45. Yang, M.-C. et al. Blockade of autophagy reduces pancreatic cancer stem cell activity and potentiates the tumoricidal effect of gemcitabine. Mol. Cancer 14, 179 (2015).
46. Cochrane, C. R., Szczepny, A., Watkins, D. N. & Cain, J. E. Hedgehog Signaling in the Maintenance of Cancer Stem Cells. Cancers 7, 1554–85 (2015).
47. Zhang, Z. et al. Gemcitabine treatment promotes pancreatic cancer stemness through the Nox/ROS/NF-κB/STAT3 signaling cascade. Cancer Lett. 382, 53–63 (2016).
48. Yeh, D.-W., Huang, L.-R., Chen, Y.-W., Huang, C.-Y. F. & Chuang, T.-H. Interplay between Inflammation and Stemness in Cancer Cells: The Role of Toll-Like Receptor Signaling. J. Immunol. Res. 2016, 4368101 (2016).
49. Wang, J., Sullenger, B. A. & Rich, J. N. Notch Signaling in Cancer Stem Cells. in Advances in experimental medicine and biology vol. 727 174–185 (2012).
50. Ip, C. K. M. et al. Stemness and chemoresistance in epithelial ovarian carcinoma cells under shear stress. Sci. Rep. 6, 26788 (2016).
51. Xia, P. & Xu, X.-Y. PI3K/Akt/mTOR signaling pathway in cancer stem cells: from basic research to clinical application. Am. J. Cancer Res. 5, 1602–9 (2015).
52. Ikushima, H. et al. Autocrine TGF-β Signaling Maintains Tumorigenicity of Glioma-Initiating Cells through Sry-Related HMG-Box Factors. Cell Stem Cell 5, 504–514 (2009).
53. Bae, W.-J., Lee, S.-H., Rho, Y.-S., Koo, B.-S. & Lim, Y.-C. Transforming growth factor β1 enhances stemness of head and neck squamous cell carcinoma cells through activation of Wnt signaling. Oncol. Lett. 12, 5315–5320 (2016).
54. Mohammed, M. K. et al. Wnt/β-catenin signaling plays an ever-expanding role in stem cell self-renewal, tumorigenesis and cancer chemoresistance. Genes Dis. 3, 11–40 (2016).
55. Kalluri, R. & Weinberg, R. A. The basics of epithelial-mesenchymal transition. J. Clin. Invest. 119, 1420–1428 (2009).
56. Zheng, X. et al. Epithelial-to-mesenchymal transition is dispensable for metastasis but induces chemoresistance in pancreatic cancer. Nature 527, 525–530 (2015).

57. Krebs, A. M. et al. The EMT-activator Zeb1 is a key factor for cell plasticity and promotes metastasis in pancreatic cancer. Nat. Cell Biol. (2017) doi:10.1038/ncb3513.
58. Storz, P. Acinar cell plasticity and development of pancreatic ductal adenocarcinoma. Nat. Rev. Gastroenterol. Hepatol. 14, 296–304 (2017).
59. Voon, D. C.-C. et al. Runx3 Protects Gastric Epithelial Cells Against Epithelial-Mesenchymal Transition-Induced Cellular Plasticity and Tumorigenicity. STEM CELLS 30, 2088–2099 (2012).
60. Lee, E. et al. DNMT1 Regulates Epithelial-Mesenchymal Transition and Cancer Stem Cells, Which Promotes Prostate Cancer Metastasis. Neoplasia N. Y. N 18, 553–66 (2016).
61. Yang, Y. et al. Epithelial-mesenchymal transition and cancer stem cell-like phenotype induced by Twist1 contribute to acquired resistance to irinotecan in colon cancer. Int. J. Oncol. 51, 515–524 (2017).
62. Pan, J.-J. & Yang, M.-H. The role of epithelial-mesenchymal transition in pancreatic cancer. J. Gastrointest. Oncol. 2, 151–6 (2011).
63. Jolly, M. K. et al. Implications of the Hybrid Epithelial/Mesenchymal Phenotype in Metastasis. Front. Oncol. 5, 155 (2015).
64. Mandal, M. et al. Modeling continuum of epithelial mesenchymal transition plasticity. Integr. Biol. Quant. Biosci. Nano Macro 8, 167–76 (2016).
65. Grillet, F. et al. Circulating tumour cells from patients with colorectal cancer have cancer stem cell hallmarks in ex vivo culture. doi:10.1136/gutjnl-2016-311447.
66. Aktas, B. et al. Stem cell and epithelial-mesenchymal transition markers are frequently overexpressed in circulating tumor cells of metastatic breast cancer patients. Breast Cancer Res. 11, R46 (2009).
67. Poruk, K. E. et al. Circulating Tumor Cells Expressing Markers of Tumor-Initiating Cells Predict Poor Survival and Cancer Recurrence in Patients with Pancreatic Ductal Adenocarcinoma. Clin. Cancer Res. Off. J. Am. Assoc. Cancer Res. (2016) doi:10.1158/1078-0432.CCR-16-1467.
68. Garg, M. Epithelial, mesenchymal and hybrid epithelial/mesenchymal phenotypes and their clinical relevance in cancer metastasis. Expert Rev. Mol. Med. 19, e3 (2017).
69. Sainz, B., Martín, B., Tatari, M., Heeschen, C. & Guerra, S. ISG15 is a critical microenvironmental factor for pancreatic cancer stem cells. Cancer Res. 74, 7309–

7320 (2014).

70. Sainz, B., Carron, E., Vallespinós, M. & Machado, H. L. Cancer Stem Cells and Macrophages: Implications in Tumor Biology and Therapeutic Strategies. Mediators Inflamm. 2016, (2016).
71. Stanger, B. Z. Cellular homeostasis and repair in the mammalian liver. Annu. Rev. Physiol. 77, 179–200 (2015).
72. Reddy, J. K. et al. Induction and origin of hepatocytes in rat pancreas. J. Cell Biol. 98, 2082–90 (1984).
73. Dabeva, M. D., Hurston, E. & Shafritz, D. A. Transcription factor and liver-specific mRNA expression in facultative epithelial progenitor cells of liver and pancreas. Am. J. Pathol. 147, 1633–48 (1995).
74. Martinelli, P. et al. The acinar regulator Gata6 suppresses KrasG12V-driven pancreatic tumorigenesis in mice. Gut 65, 476–86 (2016).
75. Bonal, C. et al. Pancreatic inactivation of c-Myc decreases acinar mass and transdifferentiates acinar cells into adipocytes in mice. Gastroenterology 136, 309-319.e9 (2009).
76. Chaffer, C. L. et al. Normal and neoplastic nonstem cells can spontaneously convert to a stem-like state. Proc. Natl. Acad. Sci. 108, 7950–7955 (2011).
77. Biddle, A. et al. Cancer Stem Cells in Squamous Cell Carcinoma Switch between Two Distinct Phenotypes That Are Preferentially Migratory or Proliferative. Cancer Res. 71, 5317–5326 (2011).
78. Kreso, A. et al. Variable Clonal Repopulation Dynamics Influence Chemotherapy Response in Colorectal Cancer. Science 339, 543–548 (2013).
79. Shimokawa, M. et al. Visualization and targeting of LGR5(+) human colon cancer stem cells. Nature 545, 187–192 (2017).
80. Melo, F. de S. e et al. A distinct role for Lgr5+ stem cells in primary and metastatic colon cancer. Nature 543, 676–680 (2017).
81. Hay, E. D. The mesenchymal cell, its role in the embryo, and the remarkable signaling mechanisms that create it. Dev. Dyn. 233, 706–720 (2005).
82. Yang, M.-H. et al. Direct regulation of TWIST by HIF-1alpha promotes metastasis. Nat. Cell Biol. 10, 295–305 (2008).
83. Grosse-Wilde, A. et al. Stemness of the hybrid Epithelial/Mesenchymal State in Breast Cancer and Its Association with Poor Survival. PLOS ONE 10, e0126522

(2015).

84. Jolly, M. K. et al. Implications of the Hybrid Epithelial/Mesenchymal Phenotype in Metastasis. Front. Oncol. 5, 155 (2015).
85. Andriani, F. et al. Conversion to stem-cell state in response to microenvironmental cues is regulated by balance between epithelial and mesenchymal features in lung cancer cells. Mol. Oncol. 10, 253–271 (2016).
86. Thiery, J. P., Acloque, H., Huang, R. Y. J. & Nieto, M. A. Epithelial-mesenchymal transitions in development and disease. Cell 139, 871–890 (2009).
87. Biddle, A., Gammon, L., Liang, X., Costea, D. E. & Mackenzie, I. C. Phenotypic Plasticity Determines Cancer Stem Cell Therapeutic Resistance in Oral Squamous Cell Carcinoma. EBioMedicine 4, 138–145 (2016).
88. Chen, W., Dong, J., Haiech, J., Kilhoffer, M.-C. & Zeniou, M. Cancer Stem Cell Quiescence and Plasticity as Major Challenges in Cancer Therapy. Stem Cells Int. 2016, 1–16 (2016).
89. Rhim, A. D. et al. EMT and dissemination precede pancreatic tumor formation. Cell 148, 349–61 (2012).
90. Malladi, S. et al. Metastatic Latency and Immune Evasion through Autocrine Inhibition of WNT. Cell 165, 45–60 (2016).
91. Cioffi, M. et al. Inhibition of CD47 Effectively Targets Pancreatic Cancer Stem Cells via Dual Mechanisms. Clin. Cancer Res. Off. J. Am. Assoc. Cancer Res. 21, 2325–37 (2015).
92. Brown, J. M. & Giaccia, A. J. The unique physiology of solid tumors: opportunities (and problems) for cancer therapy. Cancer Res. 58, 1408–1416 (1998).
93. Michalopoulou, E., Bulusu, V. & Kamphorst, J. J. Metabolic scavenging by cancer cells: when the going gets tough, the tough keep eating. Br. J. Cancer 115, 635–40 (2016).
94. Wang, G. L., Jiang, B. H., Rue, E. A. & Semenza, G. L. Hypoxia-inducible factor 1 is a basic-helix-loop-helix-PAS heterodimer regulated by cellular O2 tension. Proc. Natl. Acad. Sci. U. S. A. 92, 5510–5514 (1995).
95. Akakura, N. et al. Constitutive expression of hypoxia-inducible factor-1alpha renders pancreatic cancer cells resistant to apoptosis induced by hypoxia and nutrient deprivation. Cancer Res. 61, 6548–6554 (2001).
96. Rausch, V. et al. Synergistic activity of sorafenib and sulforaphane abolishes

pancreatic cancer stem cell characteristics. Cancer Res. 70, 5004–5013 (2010).

97. Kim, J., Tchernyshyov, I., Semenza, G. L. & Dang, C. V. HIF-1-mediated expression of pyruvate dehydrogenase kinase: a metabolic switch required for cellular adaptation to hypoxia. Cell Metab. 3, 177–85 (2006).
98. Vadde, R. et al. Role of hypoxia-inducible factors (HIF) in the maintenance of stemness and malignancy of colorectal cancer. Crit. Rev. Oncol. Hematol. 113, 22–27 (2017).
99. Erkan, M., Kurtoglu, M. & Kleeff, J. The role of hypoxia in pancreatic cancer: a potential therapeutic target? Expert Rev. Gastroenterol. Hepatol. 10, 301–16 (2016).
100. Peng, G. & Liu, Y. Hypoxia-inducible factors in cancer stem cells and inflammation. Trends Pharmacol. Sci. 36, 374–83 (2015).
101. Rausch, V. et al. Autophagy mediates survival of pancreatic tumour-initiating cells in a hypoxic microenvironment. J. Pathol. 227, 325–35 (2012).
102. Levine, B. & Kroemer, G. Autophagy in the pathogenesis of disease. Cell 132, 27–42 (2008).
103. Yang, A. et al. Autophagy is critical for pancreatic tumor growth and progression in tumors with p53 alterations. Cancer Discov. 4, 905–13 (2014).
104. Apel, A., Zentgraf, H., Büchler, M. W. & Herr, I. Autophagy-A double-edged sword in oncology. Int. J. Cancer 125, 991–995 (2009).
105. Mizushima, N., Yoshimori, T. & Levine, B. Methods in mammalian autophagy research. Cell 140, 313–326 (2010).
106. Fujii, S. et al. Autophagy is activated in pancreatic cancer cells and correlates with poor patient outcome. Cancer Sci. 99, 1813–1819 (2008).
107. Marcucci, F., Ghezzi, P. & Rumio, C. The role of autophagy in the cross-talk between epithelial-mesenchymal transitioned tumor cells and cancer stem-like cells. Mol. Cancer 16, 3 (2017).
108. Rausch, V. et al. Autophagy mediates survival of pancreatic tumour-initiating cells in a hypoxic microenvironment. J. Pathol. 227, 325–335 (2012).
109. Zhu, H. et al. Role of the Hypoxia-inducible factor-1 alpha induced autophagy in the conversion of non-stem pancreatic cancer cells into CD133+ pancreatic cancer stem-like cells. Cancer Cell Int. 13, 119 (2013).
110. Pan, H., Cai, N., Li, M., Liu, G.-H. & Izpisua Belmonte, J. C. Autophagic control of cell 'stemness'. EMBO Mol. Med. 5, 327–31 (2013).

111. Sharif, T. et al. Autophagic homeostasis is required for the pluripotency of cancer stem cells. Autophagy 13, 264–284 (2017).

112. Perusina Lanfranca, M. et al. Metabolism and epigenetics of pancreatic cancer stem cells. Semin. Cancer Biol. 57, 19–26 (2019).

113. White, E. Exploiting the bad eating habits of Ras-driven cancers. Genes Dev. 27, 2065–2071 (2013).

114. Sancho, P. et al. MYC/PGC-1α Balance Determines the Metabolic Phenotype and Plasticity of Pancreatic Cancer Stem Cells. Cell Metab. 22, 590–605 (2015).

115. Shyh-Chang, N., Daley, G. Q. & Cantley, L. C. Stem cell metabolism in tissue development and aging. Dev. Camb. Engl. 140, 2535–2547 (2013).

116. Vlashi, E. et al. Metabolic state of glioma stem cells and nontumorigenic cells. Proc. Natl. Acad. Sci. U. S. A. 108, 16062–16067 (2011).

117. Fasih, A., Elbaz, H. A., Hüttemann, M., Konski, A. A. & Zielske, S. P. Radiosensitization of pancreatic cancer cells by metformin through the AMPK pathway. Radiat. Res. 182, 50–59 (2014).

118. Krebs, A. M. et al. The EMT-activator Zeb1 is a key factor for cell plasticity and promotes metastasis in pancreatic cancer. Nat. Cell Biol. (2017) doi:10.1038/ncb3513.

119. Ilmer, M. & Horst, D. Pancreatic CSCs and microenvironment. Genes Cancer 6, 365–366 (2015).

120. Waghray, M., Yalamanchili, M., di Magliano, M. P. & Simeone, D. M. Deciphering the role of stroma in pancreatic cancer. Curr. Opin. Gastroenterol. 29, 537–543 (2013).

121. Zhan, H., Xu, J., Wu, D., Zhang, T. & Hu, S. Pancreatic cancer stem cells: new insight into a stubborn disease. Cancer Lett. 357, 429–437 (2015).

122. Masamune, A. & Shimosegawa, T. Signal transduction in pancreatic stellate cells. J. Gastroenterol. 44, 249–260 (2009).

123. Erkan, M. et al. Cancer-stellate cell interactions perpetuate the hypoxia-fibrosis cycle in pancreatic ductal adenocarcinoma. Neoplasia N. Y. N 11, 497–508 (2009).

124. Murakami, T. et al. Role of the tumor microenvironment in pancreatic cancer. Ann. Gastroenterol. Surg. 3, 130–137 (2019).

125. Amedei, A., Niccolai, E. & Prisco, D. Pancreatic cancer: role of the immune system in cancer progression and vaccine-based immunotherapy. Hum. Vaccines

Immunother. 10, 3354–3368 (2014).

126. Alguacil-Núñez, C. et al. Current perspectives on the crosstalk between lung cancer stem cells and cancer-associated fibroblasts. Crit. Rev. Oncol. Hematol. 125, 102–110 (2018).

127. Laplagne, C. et al. Latest Advances in Targeting the Tumor Microenvironment for Tumor Suppression. Int. J. Mol. Sci. 20, 4719 (2019).

128. Dougan, S. K. The Pancreatic Cancer Microenvironment: Cancer J. 23, 321–325 (2017).

129. Nielsen, S. R. et al. Macrophage-secreted granulin supports pancreatic cancer metastasis by inducing liver fibrosis. Nat. Cell Biol. 18, 549–560 (2016).

130. Sainz, B., Carron, E., Vallespinós, M. & Machado, H. L. Cancer Stem Cells and Macrophages: Implications in Tumor Biology and Therapeutic Strategies. Mediators Inflamm. 2016, (2016).

131. Sainz, B. et al. Microenvironmental hCAP-18/LL-37 promotes pancreatic ductal adenocarcinoma by activating its cancer stem cell compartment. Gut 64, 1921–1935 (2015).

132. D'Errico, G. et al. Tumor-associated macrophage-secreted 14-3-3ζ signals via AXL to promote pancreatic cancer chemoresistance. Oncogene 38, 5469–5485 (2019).

133. Ireland, L. et al. Chemoresistance in Pancreatic Cancer Is Driven by Stroma-Derived Insulin-Like Growth Factors. Cancer Res. 76, 6851–6863 (2016).

134. Ludwig, K. F. et al. Small-Molecule Inhibition of Axl Targets Tumor Immune Suppression and Enhances Chemotherapy in Pancreatic Cancer. Cancer Res. 78, 246–255 (2018).

135. Weizman, N. et al. Macrophages mediate gemcitabine resistance of pancreatic adenocarcinoma by upregulating cytidine deaminase. Oncogene 33, 3812–3819 (2014).

136. Zhang, X. et al. Macrophages induce resistance to 5-fluorouracil chemotherapy in colorectal cancer through the release of putrescine. Cancer Lett. 381, 305–313 (2016).

137. Clawson, G. A. et al. 'Stealth dissemination' of macrophage-tumor cell fusions cultured from blood of patients with pancreatic ductal adenocarcinoma. PloS One 12, e0184451 (2017).

138. Adams, D. L. et al. Circulating giant macrophages as a potential biomarker of solid tumors. Proc. Natl. Acad. Sci. U. S. A. 111, 3514–3519 (2014).

139. Carstens, J. L. et al. Spatial computation of intratumoral T cells correlates with survival of patients with pancreatic cancer. Nat. Commun. 8, 15095 (2017).

140. Peng, W. et al. PD-1 blockade enhances T-cell migration to tumors by elevating IFN-γ inducible chemokines. Cancer Res. 72, 5209–5218 (2012).

141. Macherla, S. et al. Emerging Role of Immune Checkpoint Blockade in Pancreatic Cancer. Int. J. Mol. Sci. 19, (2018).

142. Wang, X., Teng, F., Kong, L. & Yu, J. PD-L1 expression in human cancers and its association with clinical outcomes. OncoTargets Ther. 9, 5023–5039 (2016).

143. Knudsen, E. S. et al. Stratification of Pancreatic Ductal Adenocarcinoma: Combinatorial Genetic, Stromal, and Immunologic Markers. Clin. Cancer Res. Off. J. Am. Assoc. Cancer Res. 23, 4429–4440 (2017).

144. Hou, Y.-C. et al. Low CD8+ T Cell Infiltration and High PD-L1 Expression Are Associated with Level of CD44+/CD133+ Cancer Stem Cells and Predict an Unfavorable Prognosis in Pancreatic Cancer. Cancers 11, 541 (2019).

145. Sultan, M. et al. Hide-and-seek: the interplay between cancer stem cells and the immune system. Carcinogenesis 38, 107–118 (2017).

146. Bruttel, V. S. & Wischhusen, J. Cancer stem cell immunology: key to understanding tumorigenesis and tumor immune escape? Front. Immunol. 5, 360 (2014).

147. Di Tomaso, T. et al. Immunobiological characterization of cancer stem cells isolated from glioblastoma patients. Clin. Cancer Res. Off. J. Am. Assoc. Cancer Res. 16, 800–813 (2010).

148. Lee, Y. et al. CD44+ Cells in Head and Neck Squamous Cell Carcinoma Suppress T-Cell-Mediated Immunity by Selective Constitutive and Inducible Expression of PD-L1. Clin. Cancer Res. Off. J. Am. Assoc. Cancer Res. 22, 3571–3581 (2016).

149. Morrison, A. H., Byrne, K. T. & Vonderheide, R. H. Immunotherapy and Prevention of Pancreatic Cancer. Trends Cancer 4, 418–428 (2018).

150. Ram Makena, M. et al. Wnt/β-Catenin Signaling: The Culprit in Pancreatic Carcinogenesis and Therapeutic Resistance. Int. J. Mol. Sci. 20, 4242 (2019).

151. Gallmeier, E. et al. Inhibition of ataxia telangiectasia- and Rad3-related function abrogates the in vitro and in vivo tumorigenicity of human colon cancer cells through

depletion of the CD133(+) tumor-initiating cell fraction. Stem Cells Dayt. Ohio 29, 418–429 (2011).

152. Hotta, A. et al. Isolation of human iPS cells using EOS lentiviral vectors to select for pluripotency. Nat. Methods 6, 370–376 (2009).

153. Cabezas-Sainz, P. et al. Improving zebrafish embryo xenotransplantation conditions by increasing incubation temperature and establishing a proliferation index with ZFtool. BMC Cancer 18, 3 (2018).

154. Valle, S., Martin-Hijano, L., Alcalá, S., Alonso-Nocelo, M. & Sainz Jr., B. The Ever-Evolving Concept of the Cancer Stem Cell in Pancreatic Cancer. Cancers 10, 33 (2018).

155. Miranda-Lorenzo, I. et al. Intracellular autofluorescence: a biomarker for epithelial cancer stem cells. Nat. Methods 11, 1161–1169 (2014).

156. Hidalgo, M. et al. Addressing the challenges of pancreatic cancer: future directions for improving outcomes. Pancreatol. Off. J. Int. Assoc. Pancreatol. IAP Al 15, 8–18 (2015).

157. Hermann, P. C. et al. Distinct populations of cancer stem cells determine tumor growth and metastatic activity in human pancreatic cancer. Cell Stem Cell 1, 313–323 (2007).

158. de Sousa e Melo, F. et al. A distinct role for Lgr5+ stem cells in primary and metastatic colon cancer. Nature 543, 676–680 (2017).

159. (PDF) Metabolism-Based Therapeutic Strategies Targeting Cancer Stem Cells. https://www.researchgate.net/publication/331955309_Metabolism-Based_Therapeutic_Strategies_Targeting_Cancer_Stem_Cells.

160. Peiris-Pagès, M., Martinez-Outschoorn, U. E., Pestell, R. G., Sotgia, F. & Lisanti, M. P. Cancer stem cell metabolism. Breast Cancer Res. BCR 18, 55 (2016).

161. Hermann, P. C. et al. Distinct populations of cancer stem cells determine tumor growth and metastatic activity in human pancreatic cancer. Cell Stem Cell 1, 313–323 (2007).

162. Frey, P. A. The Leloir pathway: a mechanistic imperative for three enzymes to change the stereochemical configuration of a single carbon in galactose. FASEB J. Off. Publ. Fed. Am. Soc. Exp. Biol. 10, 461–470 (1996).

163. Zagorac, S., Garcia-Bermejo, L. & Sainz, B. The Epigenetic Landscape of Pancreatic Cancer Stem Cells. Epigenomes 2, 10 (2018).

164. Guttman, M. et al. lincRNAs act in the circuitry controlling pluripotency and differentiation. Nature 477, 295–300 (2011).

165. Yu, X., Lin, Y., Sui, W., Zou, Y. & Lv, Z. Analysis of distinct long noncoding RNA transcriptional fingerprints in pancreatic ductal adenocarcinoma. Cancer Med. (2017) doi:10.1002/cam4.1027.

166. Non-coding RNAs in cancer stem cells | Elsevier Enhanced Reader. https://reader.elsevier.com/reader/sd/pii/S0304383518300491?token=0F91F648C877CCD6A5331A16DA9E948FBBB5A9ED6B1B14DEEEB30C809833F6F581DFDEC4019F58E552E436EC83E5A357 doi:10.1016/j.canlet.2018.01.027.

167. Yu, L., Chen, X., Sun, X., Wang, L. & Chen, S. The Glycolytic Switch in Tumors: How Many Players Are Involved? J. Cancer 8, 3430–3440 (2017).

168. Sancho, P. et al. MYC/PGC-1α Balance Determines the Metabolic Phenotype and Plasticity of Pancreatic Cancer Stem Cells. Cell Metab. 22, 590–605 (2015).

169. Wu, S., Lu, H. & Bai, Y. Nrf2 in cancers: A double-edged sword. Cancer Med. 8, 2252–2267 (2019).

170. Narendra, D., Tanaka, A., Suen, D.-F. & Youle, R. J. Parkin is recruited selectively to impaired mitochondria and promotes their autophagy. J. Cell Biol. 183, 795–803 (2008).

171. De Luca, A. et al. Mitochondrial biogenesis is required for the anchorage-independent survival and propagation of stem-like cancer cells. Oncotarget 6, 14777–14795 (2015).

172. Zhao, J. et al. Mitochondrial dynamics regulates migration and invasion of breast cancer cells. Oncogene 32, 4814–4824 (2013).

173. Zhang, Z.-L. et al. Somatic and germline mutations in the tumor suppressor gene PARK2 impair PINK1/Parkin-mediated mitophagy in lung cancer cells. Acta Pharmacol. Sin. (2019) doi:10.1038/s41401-019-0260-6.

174. Sharif, T. et al. Autophagic homeostasis is required for the pluripotency of cancer stem cells. Autophagy 13, 264–284 (2017).

175. Fujii, S. et al. Autophagy is activated in pancreatic cancer cells and correlates with poor patient outcome. Cancer Sci. 99, 1813–1819 (2008).

176. Levine, B. & Kroemer, G. Autophagy in the pathogenesis of disease. Cell 132, 27–42 (2008).

177. Hwang, D. W. et al. Autophagy Induced by CX-4945, a Casein Kinase 2 Inhibitor,

Enhances Apoptosis in Pancreatic Cancer Cell Lines. Pancreas (2017) doi:10.1097/MPA.0000000000000780.

178. Rausch, V. et al. Autophagy mediates survival of pancreatic tumour-initiating cells in a hypoxic microenvironment. J. Pathol. 227, 325–335 (2012).

179. Apel, A., Zentgraf, H., Büchler, M. W. & Herr, I. Autophagy-A double-edged sword in oncology. Int. J. Cancer 125, 991–995 (2009).

180. Yang, M.-C. et al. Blockade of autophagy reduces pancreatic cancer stem cell activity and potentiates the tumoricidal effect of gemcitabine. Mol. Cancer 14, 179 (2015).

181. Mauvezin, C. & Neufeld, T. P. Bafilomycin A1 disrupts autophagic flux by inhibiting both V-ATPase-dependent acidification and Ca-P60A/SERCA-dependent autophagosome-lysosome fusion. Autophagy 11, 1437–1438 (2015).

182. Takeishi, S. & Nakayama, K. I. To wake up cancer stem cells, or to let them sleep, that is the question. Cancer Sci. 107, 875–881 (2016).

183. Malladi, S. et al. Metastatic Latency and Immune Evasion through Autocrine Inhibition of WNT. Cell 165, 45–60 (2016).

184. Nguyen, P. H. et al. Characterization of Biomarkers of Tumorigenic and Chemoresistant Cancer Stem Cells in Human Gastric Carcinoma. Clin. Cancer Res. Off. J. Am. Assoc. Cancer Res. (2016) doi:10.1158/1078-0432.CCR-15-2157.

185. Ding, X., Chen, W., Fan, H. & Zhu, B. Cytidine deaminase polymorphism predicts toxicity of gemcitabine-based chemotherapy. Gene 559, 31–37 (2015).

186. Spratlin, J. L. & Mackey, J. R. Human Equilibrative Nucleoside Transporter 1 (hENT1) in Pancreatic Adenocarcinoma: Towards Individualized Treatment Decisions. Cancers 2, 2044–2054 (2010).

187. Peña-Solórzano, D., Stark, S. A., König, B., Sierra, C. A. & Ochoa-Puentes, C. ABCG2/BCRP: Specific and Nonspecific Modulators. Med. Res. Rev. 37, 987–1050 (2017).

188. Zhang, D. et al. 2-Deoxy-D-glucose targeting of glucose metabolism in cancer cells as a potential therapy. Cancer Lett. 355, 176–183 (2014).

189. Massagué, J. & Obenauf, A. C. Metastatic colonization by circulating tumour cells. Nature 529, 298–306 (2016).

190. Dunn, G. P., Old, L. J. & Schreiber, R. D. The immunobiology of cancer immunosurveillance and immunoediting. Immunity 21, 137–148 (2004).

191. Eyles, J. et al. Tumor cells disseminate early, but immunosurveillance limits metastatic outgrowth, in a mouse model of melanoma. J. Clin. Invest. 120, 2030–2039 (2010).

192. Kitamura, T., Qian, B.-Z. & Pollard, J. W. Immune cell promotion of metastasis. Nat. Rev. Immunol. 15, 73–86 (2015).

193. Chaffer, C. L. et al. Poised Chromatin at the ZEB1 Promoter Enables Breast Cancer Cell Plasticity and Enhances Tumorigenicity. Cell 154, 61–74 (2013).

194. Lee, S. Y. et al. Induction of metastasis, cancer stem cell phenotype, and oncogenic metabolism in cancer cells by ionizing radiation. Mol. Cancer 16, (2017).

195. Lehmann, W. et al. ZEB1 turns into a transcriptional activator by interacting with YAP1 in aggressive cancer types. Nat. Commun. 7, 10498 (2016).

196. Kowalski-Chauvel, A. et al. Alpha6-Integrin Regulates FGFR1 Expression through the ZEB1/YAP1 Transcription Complex in Glioblastoma Stem Cells Resulting in Enhanced Proliferation and Stemness. Cancers 11, (2019).

197. Wellner, U. et al. The EMT-activator ZEB1 promotes tumorigenicity by repressing stemness-inhibiting microRNAs. Nat. Cell Biol. 11, 1487–1495 (2009).

198. Brown, J. A. et al. TGFβ-induced quiescence mediates chemoresistance of tumor propagating cells in squamous cell carcinoma. Cell Stem Cell 21, 650-664.e8 (2017).

199. David, C. J. et al. TGF-β Tumor Suppression through a Lethal EMT. Cell 164, 1015–1030 (2016).

200. Oshimori, N., Oristian, D. & Fuchs, E. TGF-β promotes heterogeneity and drug resistance in squamous cell carcinoma. Cell 160, 963–976 (2015).

201. Miao, Y. et al. Adaptive Immune Resistance Emerges from Tumor-Initiating Stem Cells. Cell 177, 1172-1186.e14 (2019).

202. Rinkenbaugh, A. L. & Baldwin, A. S. The NF-κB Pathway and Cancer Stem Cells. Cells 5, (2016).

203. Cioffi, M. et al. Inhibition of CD47 Effectively Targets Pancreatic Cancer Stem Cells via Dual Mechanisms. Clin. Cancer Res. Off. J. Am. Assoc. Cancer Res. 21, 2325–2337 (2015).

204. D'Errico, G. et al. Tumor-associated macrophage-secreted 14-3-3ζ signals via AXL to promote pancreatic cancer chemoresistance. Oncogene 1 (2019) doi:10.1038/s41388-019-0803-9.

205. Sierra-Filardi, E. et al. CCL2 Shapes Macrophage Polarization by GM-CSF and M-

CSF: Identification of CCL2/CCR2-Dependent Gene Expression Profile. J. Immunol. 192, 3858–3867 (2014).

206. Research, A. A. for C. CXCL12 Has Niche-Specific Roles in Leukemia Stem Cell Function. Cancer Discov. (2019) doi:10.1158/2159-8290.CD-RW2019-044.

207. Li, X. et al. CXCL12/CXCR4 pathway orchestrates CSC-like properties by CAF recruited tumor associated macrophage in OSCC. Exp. Cell Res. (2019) doi:10.1016/j.yexcr.2019.03.013.

208. Sato, M. et al. Decreased expression of the plasminogen activator inhibitor type 1 is involved in degradation of extracellular matrix surrounding cervical cancer stem cells. Int. J. Oncol. 48, 829–835 (2016).

209. Maeda, S. et al. Duffy antigen receptor for chemokines (DARC) expressing in cancer cells inhibits tumor progression by suppressing CXCR2 signaling in human pancreatic ductal adenocarcinoma. Cytokine 95, 12–21 (2017).

210. GM-CSF in inflammation and autoimmunity. - PubMed - NCBI. https://www.ncbi.nlm.nih.gov/pubmed/12133803.

211. Jin, F., Miao, Y., Xu, P. & Qiu, X. IL-8 regulates the stemness properties of cancer stem cells in the small-cell lung cancer cell line H446. OncoTargets Ther. 11, 5723–5731 (2018).

212. Chen, Y. et al. Interleukin-8, a promising predictor for prognosis of pancreatic cancer. World J. Gastroenterol. 18, 1123–1129 (2012).

213. Agarwal, P. et al. Mesenchymal Niche-Specific Expression of Cxcl12 Controls Quiescence of Treatment-Resistant Leukemia Stem Cells. Cell Stem Cell (2019) doi:10.1016/j.stem.2019.02.018.

214. Wang, Z. et al. Oncogenic roles and drug target of CXCR4/CXCL12 axis in lung cancer and cancer stem cell. Tumour Biol. J. Int. Soc. Oncodevelopmental Biol. Med. 37, 8515–8528 (2016).

215. Jaguin, M., Houlbert, N., Fardel, O. & Lecureur, V. Polarization profiles of human M-CSF-generated macrophages and comparison of M1-markers in classically activated macrophages from GM-CSF and M-CSF origin. Cell. Immunol. 281, 51–61 (2013).

216. Badrinath, N. & Yoo, S. Y. Recent Advances in Cancer Stem Cell-Targeted Immunotherapy. Cancers 11, (2019).

217. Jinushi, M. Role of cancer stem cell-associated inflammation in creating pro-

inflammatory tumorigenic microenvironments. Oncoimmunology 3, (2014).

218. Heissig, B. et al. Role of mesenchymal stem cell-derived fibrinolytic factor in tissue regeneration and cancer progression. Cell. Mol. Life Sci. 72, 4759–4770 (2015).

219. Wang, X. et al. Stem cell autocrine CXCL12/CXCR4 stimulates invasion and metastasis of esophageal cancer. Oncotarget 8, 36149–36160 (2017).

220. Chen, L. et al. The IL-8/CXCR1 axis is associated with cancer stem cell-like properties and correlates with clinical prognosis in human pancreatic cancer cases. Sci. Rep. 4, 5911 (2014).

221. Alvey, C. & Discher, D. E. Engineering macrophages to eat cancer: from 'marker of self' CD47 and phagocytosis to differentiation. J. Leukoc. Biol. 102, 31–40 (2017).

222. Hidalgo, M. Pancreatic cancer. N. Engl. J. Med. 362, 1605–1617 (2010).

223. Hanahan, D. & Weinberg, R. A. Hallmarks of cancer: the next generation. Cell 144, 646–674 (2011).

224. Rossignol, R. et al. Energy substrate modulates mitochondrial structure and oxidative capacity in cancer cells. Cancer Res. 64, 985–993 (2004).

225. Aguer, C. et al. Galactose Enhances Oxidative Metabolism and Reveals Mitochondrial Dysfunction in Human Primary Muscle Cells. PLoS ONE 6, (2011).

226. Reitzer, L. J., Wice, B. M. & Kennell, D. Evidence that glutamine, not sugar, is the major energy source for cultured HeLa cells. J. Biol. Chem. 254, 2669–2676 (1979).

227. Kase, E. T. et al. Remodeling of Oxidative Energy Metabolism by Galactose Improves Glucose Handling and Metabolic Switching in Human Skeletal Muscle Cells. PLoS ONE 8, (2013).

228. Banerjee, A. et al. The effects of restricted glycolysis on stem-cell like characteristics of breast cancer cells. Oncotarget 9, 23274–23288 (2018).

229. Marroquin, L. D., Hynes, J., Dykens, J. A., Jamieson, J. D. & Will, Y. Circumventing the Crabtree Effect: Replacing Media Glucose with Galactose Increases Susceptibility of HepG2 Cells to Mitochondrial Toxicants. Toxicol. Sci. 97, 539–547 (2007).

230. Shimokawa, M. et al. Visualization and targeting of LGR5+ human colon cancer stem cells. Nature 545, 187–192 (2017).

231. Batlle, E. & Clevers, H. Cancer stem cells revisited. Nat. Med. 23, 1124–1134 (2017).

232. Vyas, S., Zaganjor, E. & Haigis, M. C. Mitochondria and Cancer. Cell 166, 555–566 (2016).

233. De Francesco, E. M., Sotgia, F. & Lisanti, M. P. Cancer stem cells (CSCs): metabolic strategies for their identification and eradication. Biochem. J. 475, 1611–1634 (2018).

234. Trotta, A. P. & Chipuk, J. E. Mitochondrial Dynamics As Regulators Of Cancer Biology. Cell. Mol. Life Sci. CMLS 74, 1999–2017 (2017).

235. Watanabe, R. et al. Pyruvate controls the checkpoint inhibitor PD-L1 and suppresses T cell immunity. J. Clin. Invest. 127, 2725–2738 (2017).

236. Wangpaichitr, M. et al. Relationship of Metabolic Alterations and PD-L1 Expression in Cisplatin Resistant Lung Cancer. Cell Dev. Biol. 6, (2017).

237. El-Sahli, S., Xie, Y., Wang, L. & Liu, S. Wnt Signaling in Cancer Metabolism and Immunity. Cancers 11, (2019).

238. Deshmukh, A., Arfuso, F., Newsholme, P. & Dharmarajan, A. Regulation of Cancer Stem Cell Metabolism by Secreted Frizzled-Related Protein 4 (sFRP4). Cancers 10, (2018).

239. Shares, B. H., Busch, M., White, N., Shum, L. & Eliseev, R. A. Active mitochondria support osteogenic differentiation by stimulating β-catenin acetylation. J. Biol. Chem. 293, 16019–16027 (2018).

240. Chen, W., Dong, J., Haiech, J., Kilhoffer, M.-C. & Zeniou, M. Cancer Stem Cell Quiescence and Plasticity as Major Challenges in Cancer Therapy. Stem Cells Int. 2016, 1740936 (2016).

241. Mueller, M.-T. et al. Combined targeted treatment to eliminate tumorigenic cancer stem cells in human pancreatic cancer. Gastroenterology 137, 1102–1113 (2009).

242. Lonardo, E. et al. Nodal/Activin signaling drives self-renewal and tumorigenicity of pancreatic cancer stem cells and provides a target for combined drug therapy. Cell Stem Cell 9, 433–446 (2011).

243. Zagorac, S. et al. DNMT1 Inhibition Reprograms Pancreatic Cancer Stem Cells via Upregulation of the miR-17-92 Cluster. Cancer Res. 76, 4546–4558 (2016).

244. Liu, H. et al. Single-cell clones of liver cancer stem cells have the potential of differentiating into different types of tumor cells. Cell Death Dis. 4, e857–e857 (2013).

245. Tajima, H. et al. Neoadjuvant chemotherapy with gemcitabine-based regimens improves the prognosis of node positive resectable pancreatic head cancer. Mol. Clin. Oncol. 11, 157–166 (2019).

246. Von Hoff, D. D. et al. Gemcitabine Plus nab-Paclitaxel Is an Active Regimen in

Patients With Advanced Pancreatic Cancer: A Phase I/II Trial. J. Clin. Oncol. 29, 4548–4554 (2011).

247. Burris, H. A. et al. Improvements in survival and clinical benefit with gemcitabine as first-line therapy for patients with advanced pancreas cancer: a randomized trial. J. Clin. Oncol. Off. J. Am. Soc. Clin. Oncol. 15, 2403–2413 (1997).

248. Spitz, F. R. et al. Preoperative and postoperative chemoradiation strategies in patients treated with pancreaticoduodenectomy for adenocarcinoma of the pancreas. J. Clin. Oncol. 15, 928–937 (1997).

249. Yeo, C. J. et al. Pancreaticoduodenectomy for pancreatic adenocarcinoma: postoperative adjuvant chemoradiation improves survival. A prospective, single-institution experience. Ann. Surg. 225, 621–636 (1997).

250. Rhim, A. D. et al. EMT and dissemination precede pancreatic tumor formation. Cell 148, 349–361 (2012).

251. Miyashita, T. et al. Neoadjuvant Chemotherapy with Gemcitabine Plus Nab-paclitaxel Reduces the Number of Cancer-associated Fibroblasts Through Depletion of Pancreatic Stroma. Anticancer Res. 38, 337–343 (2018).

252. Vera-Ramirez, L., Vodnala, S. K., Nini, R., Hunter, K. W. & Green, J. E. Autophagy promotes the survival of dormant breast cancer cells and metastatic tumour recurrence. Nat. Commun. 9, 1944 (2018).

253. Visvader, J. E. & Lindeman, G. J. Cancer stem cells in solid tumours: accumulating evidence and unresolved questions. Nat. Rev. Cancer 8, 755–768 (2008).

254. Kreso, A. et al. Variable Clonal Repopulation Dynamics Influence Chemotherapy Response in Colorectal Cancer. Science 339, 543–548 (2013).

255. Rothe, K. et al. The core autophagy protein ATG4B is a potential biomarker and therapeutic target in CML stem/progenitor cells. Blood 123, 3622–3634 (2014).

256. Wang, F. et al. Alisertib induces cell cycle arrest and autophagy and suppresses epithelial-to-mesenchymal transition involving PI3K/Akt/mTOR and sirtuin 1-mediated signaling pathways in human pancreatic cancer cells. Drug Des. Devel. Ther. 9, 575–601 (2015).

257. Xu, X. D. et al. Inhibition of Autophagy by Deguelin Sensitizes Pancreatic Cancer Cells to Doxorubicin. Int. J. Mol. Sci. 18, (2017).

258. Hwang, D. W. et al. Autophagy Induced by CX-4945, a Casein Kinase 2 Inhibitor, Enhances Apoptosis in Pancreatic Cancer Cell Lines. Pancreas (2017)

doi:10.1097/MPA.0000000000000780.

259. Hidalgo, M. Pancreatic cancer. N. Engl. J. Med. 362, 1605–1617 (2010).

260. Sosa, M. S., Bragado, P. & Aguirre-Ghiso, J. A. Mechanisms of disseminated cancer cell dormancy: an awakening field. Nat. Rev. Cancer 14, 611–622 (2014).

261. Wang, F. et al. Alisertib induces cell cycle arrest and autophagy and suppresses epithelial-to-mesenchymal transition involving PI3K/Akt/mTOR and sirtuin 1-mediated signaling pathways in human pancreatic cancer cells. Drug Des. Devel. Ther. 9, 575–601 (2015).

262. Chin, V. L. & Lim, C. L. Epithelial-mesenchymal plasticity—engaging stemness in an interplay of phenotypes. Stem Cell Investig. 6, (2019).

263. Yu, M. et al. Circulating breast tumor cells exhibit dynamic changes in epithelial and mesenchymal composition. Science 339, 580–584 (2013).

264. Grosse-Wilde, A. et al. Stemness of the hybrid Epithelial/Mesenchymal State in Breast Cancer and Its Association with Poor Survival. PLOS ONE 10, e0126522 (2015).

265. Shinde, A. et al. Spleen Tyrosine Kinase-Mediated Autophagy Is Required for Epithelial-Mesenchymal Plasticity and Metastasis in Breast Cancer. Cancer Res. 79, 1831–1843 (2019).

266. Adhikary, A. et al. Inhibition of epithelial to mesenchymal transition by E-cadherin up-regulation via repression of slug transcription and inhibition of E-cadherin degradation: dual role of scaffold/matrix attachment region-binding protein 1 (SMAR1) in breast cancer cells. J. Biol. Chem. 289, 25431–25444 (2014).

267. Monkman, J. H., Thompson, E. W. & Nagaraj, S. H. Targeting Epithelial Mesenchymal Plasticity in Pancreatic Cancer: A Compendium of Preclinical Discovery in a Heterogeneous Disease. Cancers 11, (2019).

268. Krebs, A. M. et al. The EMT-activator Zeb1 is a key factor for cell plasticity and promotes metastasis in pancreatic cancer. Nat. Cell Biol. 19, 518–529 (2017).

269. Sciacovelli, M. & Frezza, C. Metabolic reprogramming and epithelial-to-mesenchymal transition in cancer. FEBS J. 284, 3132–3144 (2017).

270. LIU, C.-T. et al. Production of interleukin-4 in CD133+ cervical cancer stem cells promotes resistance to apoptosis and initiates tumor growth. Mol. Med. Rep. 13, 5068–5076 (2016).

271. Mohammed, S. et al. Improving Chimeric Antigen Receptor-Modified T Cell

Function by Reversing the Immunosuppressive Tumor Microenvironment of Pancreatic Cancer. Mol. Ther. J. Am. Soc. Gene Ther. 25, 249–258 (2017).

272. Okada, S., Vaeteewoottacharn, K. & Kariya, R. Application of Highly Immunocompromised Mice for the Establishment of Patient-Derived Xenograft (PDX) Models. Cells 8, (2019).

273. Richmond, A. & Su, Y. Mouse xenograft models vs GEM models for human cancer therapeutics. Dis. Model. Mech. 1, 78–82 (2008).

274. Lee, J. W., Komar, C. A., Bengsch, F., Graham, K. & Beatty, G. L. Genetically Engineered Mouse Models of Pancreatic Cancer: The KPC Model (LSL-KrasG12D/+;LSL-Trp53R172H/+;Pdx-1-Cre), Its Variants and Their Application in Immuno-oncology Drug Discovery. Curr. Protoc. Pharmacol. Editor. Board SJ Enna Ed.--Chief Al 73, 14.39.1-14.39.20 (2016).